

Dissertation zur Erlangung des Doktorgrades
der Fakultät für Chemie und Pharmazie
der Ludwig-Maximilians-Universität München

Inhibition of the V-ATPase

–

A novel strategy to prevent epithelial-mesenchymal transition and cancer stem cell formation

Henriette Merk

aus

Sathmar, Rumänien

2016

Erklärung

Diese Dissertation wurde im Sinne von § 7 der Promotionsordnung vom 28. November 2011 von Frau Prof. Dr. Angelika M. Vollmar betreut.

Eidesstattliche Versicherung

Diese Dissertation wurde eigenständig und ohne unerlaubte Hilfe erarbeitet.

München, den _____

Henriette Merk

Dissertation eingereicht am	17.03.2016
1. Gutachterin	Prof. Dr. Angelika M. Vollmar
2. Gutachter	Prof. Dr. Stefan Zahler
Mündliche Prüfung am	22.04.2016

meinen Eltern

CONTENTS

CONTENTS

CONTENTS	I
SUMMARY	VI
1 INTRODUCTION	2
1.1 Metastatic cancer	2
1.1.1 Metastatic breast cancer	2
1.1.2 Cancer stem cells	2
1.2 Epithelial-mesenchymal transition – A hallmark of cancer	4
1.2.1 Epithelial-mesenchymal transition	4
1.2.2 EMT in physiological and pathological events	5
1.2.3 Regulation of EMT.....	6
1.2.3.1 EMT induction.....	6
1.2.3.2 The major player in EMT: E-cadherin	7
1.3 V-ATPase - A potential target for EMT	10
1.3.1 Physiological function and structure	10
1.3.2 Role of V-ATPase in cancer and metastasis	11
1.3.3 The V-ATPase inhibitor: Archazolid A	12
1.4 Aim of the study	13
2 MATERIALS AND METHODS	15
2.1 Materials	15
2.1.1 Compound.....	15
2.1.2 Reagents and technical equipment	15
2.2 Methods	19
2.2.1 Cell culture	19
2.2.2 Freezing and thawing.....	19
2.2.3 Transduction of HMLE Twist1-ER cells with lentiviral V-ATPase shRNA	20
2.2.4 V-ATPase inhibition and EMT induction in HMLE Twist1-ER cells and in HMLE Twist1-ER shRNA clones.....	21
2.2.4.1 Pharmacological V-ATPase inhibition with Archazolid A and EMT induction in HMLE Twist1-ER cells	21

2.2.4.2 Genetic V-ATPase knockdown and EMT induction in HMLE Twist1-ER shRNA clones	21
2.2.4.3 Induction of Notch1 with EGTA	21
2.2.5 Immunoblotting	22
2.2.6 Quantitative real-time PCR analysis	25
2.2.7 Immunostaining	26
2.2.8 LysoTracker® staining	27
2.2.9 E-cadherin internalization assay	27
2.2.10 Mammosphere assay	28
2.2.11 Boyden chamber assay.....	28
2.2.12 Cell viability assay.....	29
2.2.12.1 Fluorescence activated cell sorting	29
2.2.12.2 Cell viability in mammosphere assays.....	29
2.2.13 Statistics	29
3 RESULTS	31
3.1 Characterization of EMT in HMLE Twist1-ER cells	31
3.1.1 4-OH-TX induces EMT in HMLE Twist1-ER cells	31
3.1.2 4-OH-TX induces translocation of Twist1-ER into the nucleus.....	32
3.2 Role of V-ATPase in HMLE Twist1-ER cells during EMT	34
3.2.1 Archazolid A inhibits V-ATPase activity in HMLE Twist1-ER cells during EMT.....	34
3.2.2 Archazolid A treatment during EMT impedes migration and mammosphere formation of HMLE cells.....	35
3.2.2.1 Archazolid A treatment during EMT inhibits migration	35
3.2.2.2 Archazolid A inhibits mammosphere formation	36
3.2.2.3 Archazolid A sustainably prevents mammosphere formation.....	38
3.2.3 Archazolid A preserves an epithelial phenotype during EMT	39
3.2.4 TGF- β -induced EMT is inhibited by Archazolid A.....	41
3.2.5 Archazolid A impedes Notch1-induced signaling	43
3.2.6 V-ATPase knockdown inhibits EMT	45
3.2.7 E-cadherin internalization is repressed by Archazolid A	47
3.2.8 E-cadherin recycling is inhibited upon V-ATPase inhibition	49
3.3 Archazolid A reduces migration and mammosphere formation of mesenchymal HMLE cells.....	52
3.3.1 Archazolid A reduces migration of mesenchymal HMLE cells.....	52
3.3.2 Archazolid A reduces mammosphere formation in mesenchymal HMLE cells.....	53

4	DISCUSSION.....	55
4.1	EMT, CSCs and the relevance of V-ATPase in this context.....	55
4.2	V-ATPase inhibition diminishes cancer stem cell-like traits and promotes epithelial characteristics	56
4.3	E-cadherin: the major player in V-ATPase-related EMT	57
4.4	Archazolid A inhibits preexisting mesenchymal traits.....	60
4.5	Targeting of EMT in clinic: advantages and limitations	60
4.6	Conclusion and further perspectives	62
5	REFERENCES	64
6	APPENDIX.....	71
6.1	Abbreviations.....	71
6.2	Publications	73
6.2.1	Articles	73
6.2.2	Oral presentations	73
6.2.3	Poster presentations.....	73
6.3	Original article	75
6.4	Danksagung	94

SUMMARY

SUMMARY

Breast cancer is the leading cause for cancer deaths among females worldwide and its incidence is growing. The high rate of relapse and metastatic spread is attributed to breast cancer stem cells (CSCs) (1). Of note, CSC formation is closely linked to epithelial-mesenchymal transition (EMT), a process which confers mesenchymal properties on epithelial cells (2). Hence, the pharmacological targeting of EMT may represent a new strategy to overcome tumor progression. Recent reports showed that targeting the endolysosomal machinery is a promising approach to overcome EMT (3). To this end, the vacuolar H⁺-ATPase (V-ATPase) represents an attractive target. V-ATPases are ubiquitous expressed, multimeric ATP-dependent proton pumps, essential for ligand internalization, endosomal recycling and lysosomal degradation (4). Although V-ATPase has been linked with the recycling of E-cadherin, a crucial player in EMT, detailed information about a potential role of V-ATPase in EMT and CSCs is still missing.

In fact, we introduce V-ATPase as a promising target affecting EMT and breast CSC formation. By using Archazolid A, a myxobacteria-derived V-ATPase inhibitor, we show that V-ATPase is pharmacologically accessible. The approach to mimic EMT was accomplished by utilizing a mammary cell line model, designed to undergo EMT, namely human mammary epithelial (HMLE) cells. In this study, pharmacological and genetic V-ATPase inhibition during EMT revealed a distinct implication on the generation of breast CSCs. In fact, Archazolid A decreased mammosphere formation of HMLE cells sustainably. Investigating the underlying mechanism showed that V-ATPase inhibition abrogates E-cadherin internalization and degradation by disturbed delivery from early endosomal to lysosomal compartments (Figure 1). Moreover, pharmacological V-ATPase inhibition overcame enhanced migration and breast CSC formation of mesenchymal HMLE cells, which have already undergone EMT.

In summary, this work outlines the pivotal role of targeting EMT by interfering with the endolysosomal recycling and degradation of E-cadherin and provides pioneer insights into V-ATPase inhibition-related repression of cancer stem-like characteristics.

In conclusion, this work suggests V-ATPase inhibition by Archazolid A as a potent new strategy for the treatment of premetastatic and metastatic breast cancer.

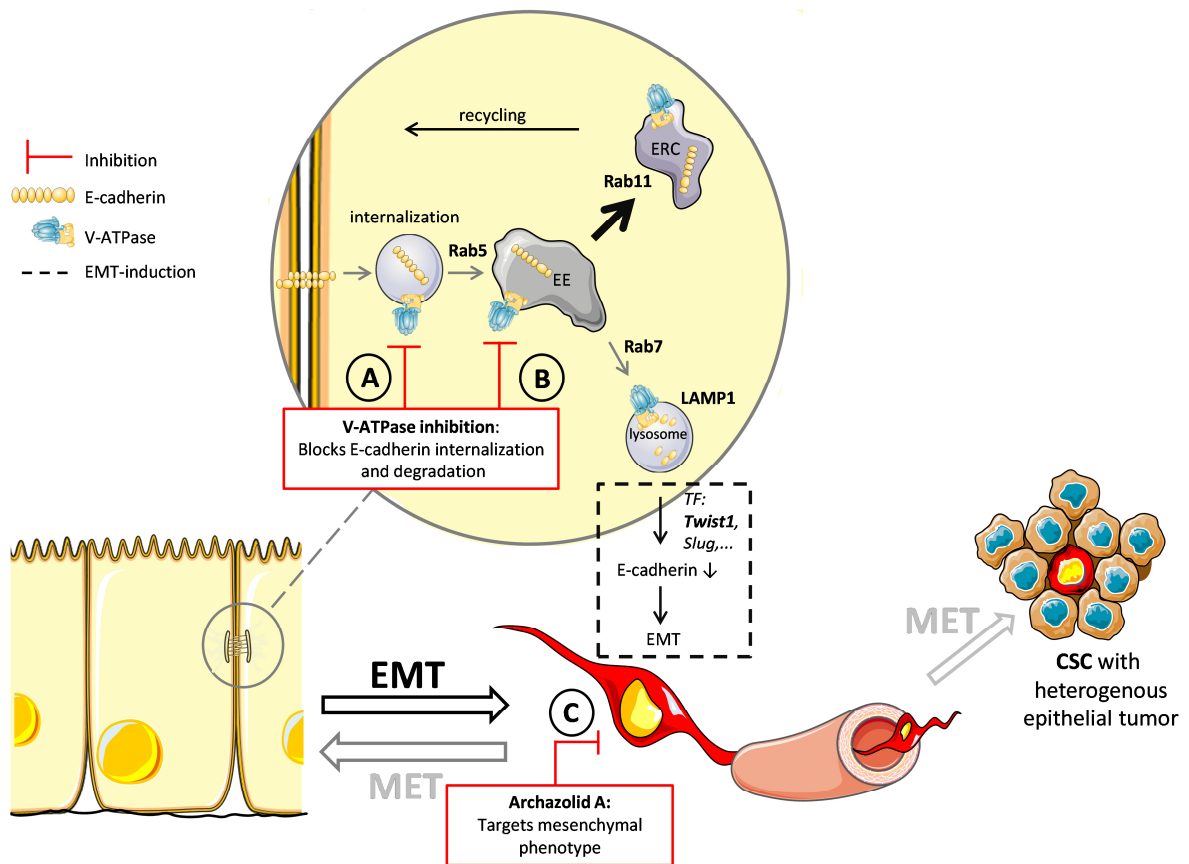


Figure 1: V-ATPase inhibition impedes EMT-induced migration and mammosphere formation by disrupting E-cadherin signaling. (A, B) V-ATPase inhibition blocks E-cadherin internalization (A) and degradation (B) in HMLE cells, by disabled translocation of E-cadherin from early endosomes to lysosomes. This leads to impaired EMT and thus to the inhibition of migration and mammosphere formation. (C) Archazolid A inhibits migration and mammosphere formation of mesenchymal HMLE cells. EE, early endosome; ERC, endocytic recycling compartment; LAMP1, lysosomal-associated membrane protein 1; EMT, epithelial-mesenchymal transition; MET, mesenchymal-epithelial transition; CSC, cancer stem cell.

INTRODUCTION

1 INTRODUCTION

1.1 Metastatic cancer

1.1.1 Metastatic breast cancer

Breast cancer accounts for 25 % of all cancer cases and is the leading cause for cancer-related deaths among females worldwide (5). Breast cancer originates from the malignant transition of breast epithelial cells, found either lining the milk ducts or in the milk-producing lobules of the breast. While it is highly treatable during primary stages, approximately 30 to 50 % of patients diagnosed with breast cancer will subsequently develop metastasis, which is accompanied with poor prognosis. Breast cancer tumors are heterogeneous in each individual patient and comprise subpopulations of cancer cells with extremely high tumorigenic potential, termed breast cancer stem cells (bCSCs) (1, 6). Besides enhanced resistance to chemo- and radiotherapy, bCSCs have also shown to induce metastasis (7, 8). These are major problems which limit therapeutic success of breast cancer treatment and result in reduced overall survival.

1.1.2 Cancer stem cells

In the vivid debate about the causes for drug resistance and tumor progression, two major theories are discussed. The clonal evolution model proposes that all tumor cells possess equal tumorigenic potential (9). However, the discovery of cancer stem cells (CSCs) in solid tumors assumes a hierarchical organization, by which only a small subpopulation of neoplastic cells within the tumor acquire stem cell-like properties. In this current model, only CSCs are supposed to drive tumorigenesis and cause relapse (10). In detail, CSCs are cancer cells possessing characteristics associated with multipotent stem cells (SC), including resistance to apoptosis and most importantly self-renewal. However, the development of the initial CSC, namely the tumor-initiating cell (TICs), is poorly characterized. During recent years several hypothesis have emerged. Amongst others, TICs are suggested to originate from adult stem or progenitor cells by malignant mutations (10, 11). Moreover, in 2008, Weinberg and colleagues revealed that CSC-like phenotype and properties can also evolve from mature, differentiated epithelial cells (Figure 2) (2). In line, recent reports showed that

self-renewal and invasiveness are closely associated with traits of cells undergoing epithelial-mesenchymal transition (EMT), a process which enables cancer cells to disseminate from primary tumors (12-14). Indeed, induction of EMT in immortalized human mammary epithelial (HMLE) cells exhibits increased expression of cancer stem-like markers and characteristics (2, 15).

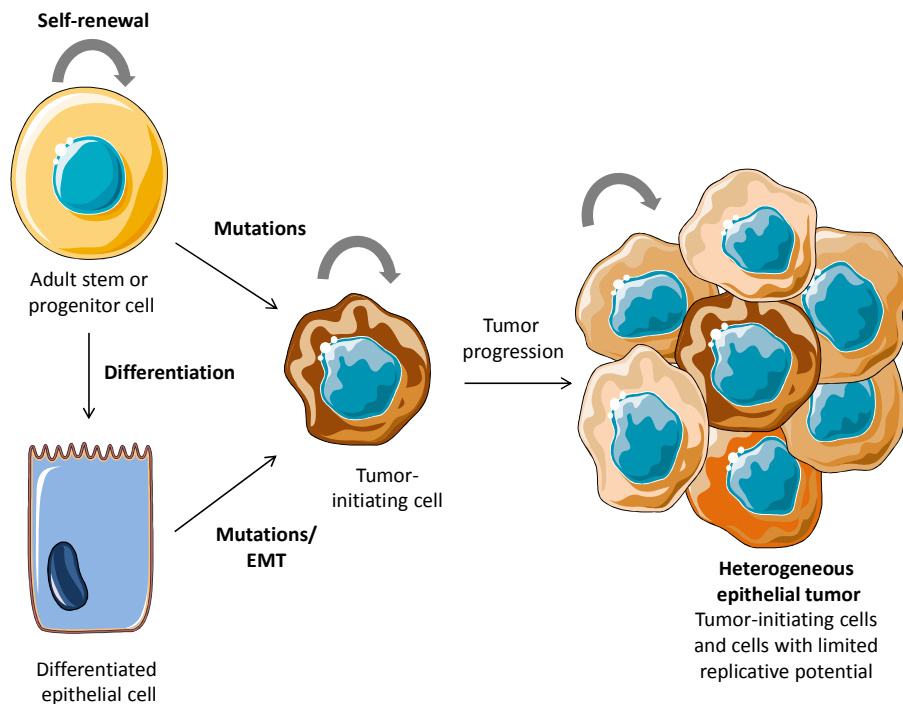


Figure 2: Theories about the origin of tumor-initiating stem cells (TIC). One theory assumes that TICs arise from malignant mutations of adult stem or progenitor cells. A further theory states that they develop from normal cells within epithelial tissues by mutations or spontaneous EMT, mediated by microenvironmental factors. Hereby, cells uncommonly acquire the feature of self-renewal. TICs form a heterogeneous epithelial tumor, comprising cells with limited replicative potential. Adapted from Martin-Belmonte *et al.* (16).

1.2 Epithelial-mesenchymal transition – A hallmark of cancer

1.2.1 Epithelial-mesenchymal transition

Epithelial-mesenchymal transition (EMT) describes a pivotal biological process by which epithelial cells lose their epithelial characteristics and gain mesenchymal properties. The loss of cell-cell adhesion and apical cell polarity results in complex changes in cell architecture and behavior. These are characterized by enhanced motility, elevated resistance to apoptosis and increased production of extra cellular matrix (ECM) components. Degradation of the basement membrane enables migration and invasion of cells into the vasculature. Multiple signaling molecules mediate EMT, including TGF- β , Wnt/ β -catenin, Notch and Hedgehog signaling by activation of EMT transcription factors like Twist1, Twist2, Snail2, Slug, ZEB1 and ZEB2. Some of the underlying signaling mechanisms are not fully revealed and still under investigation. Subsequent to EMT induction, expression of specific cell-surface proteins, reorganization and expression of cytoskeletal proteins, production of ECM-degrading enzymes and changes in the expression of specific microRNAs are induced. Several factors which are involved in the EMT process, including surface proteins (e.g. E- and N-cadherin), intermediate filament protein (e.g. vimentin) as well as transcription factors are often used as biomarkers to demonstrate the passage of a cell through EMT (Figure 3). One important transcription factor is Twist1. It is a highly conserved basic helix-loop-helix (bHLH) protein that plays an important role in embryogenesis and tumorigenesis. In terms of cancer, Twist1 is able to transform non-tumorigenic HMLE cells into stem-like cells via EMT (2). The reverse process of EMT is described by the mesenchymal-epithelial transition (MET), which involves the conversion of mesenchymal cells to epithelial cells (17, 18). EMT comprises a central role in the formation of many tissues and organs, in the development of the embryo as well as in pathological fibrosis. Importantly, as mentioned above, it also plays a pivotal role in CSC formation and therefore in cancer progression.

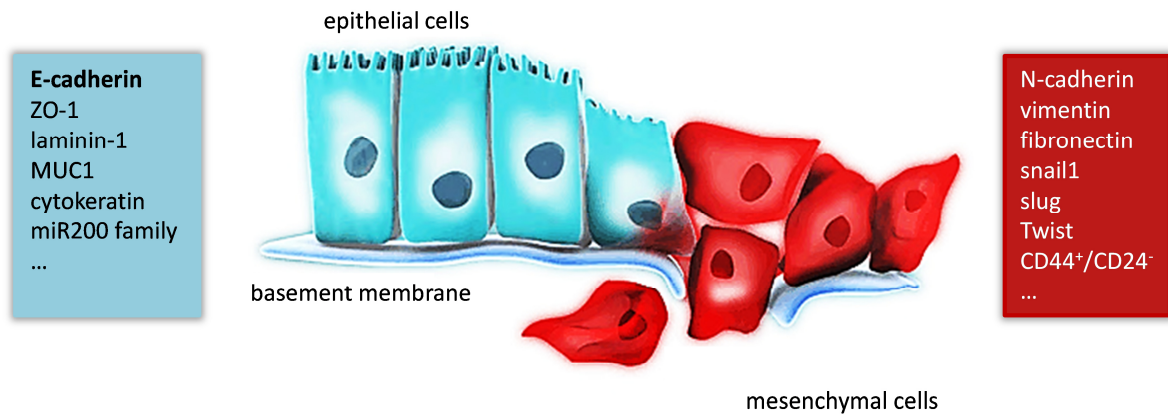


Figure 3: Epithelial-mesenchymal transition (EMT). EMT confers mesenchymal properties on epithelial cells. Hereby, epithelial cells lose their polarity, detach from the basement membrane and enter the circulation. The transition involves changes of several biomarkers. ZO-1, zona occludens-1; MUC1, mucin 1; miR200, microRNA 200. Adapted from *Qiagen*, 2012.

1.2.2 EMT in physiological and pathological events

1.2.2.1 EMT in embryogenesis and tissue organ development – type I

Developmental EMT is associated with implantation and genesis of the embryo as well as organ formation. Precursors of the cytotrophoblast cells, the trophoctoderm, undergo EMT, thereby facilitating the invasion of the endometrium and the subsequent proper placenta placement, thus enabling nutrient and gas exchange to the embryo. Organ formation requires the remodeling of a simple epithelium layer to a multilayer by delamination and invagination. EMT facilitates the conversion of epithelial into mesenchymal cells to form these layers by gastrulation (18).

1.2.2.2 EMT in fibrosis and tissue regeneration – type II

The repair-associated EMT is initiated following inflammation or trauma. Organ fibrosis is mediated by inflammatory cells and fibroblasts and occurs in a number of epithelial tissues, including kidney, liver, lung and intestine. However, once inflammation is attenuated, EMT ceases, as seen during tissue regeneration and wound healing. In the latter, keratinocytes at the border of the wound first undergo EMT and subsequently reepithelialization when the wound is closed (18).

1.2.2.3 EMT in cancer progression and metastasis – type III

In cancer biology, cells acquire the ability to migrate, invade and metastasize upon EMT induction. In detail, during the process of metastasis, cancer cells disseminate from a primary tumor, initiated by the loss of cell-cell contacts. Hereby, cells enter the bloodstream and reach distant sites, where they undergo MET and form secondary tumors (18). Malignant neoplasms at secondary sites are attributed to the ability of cancer cells to self-renew and thus gain CSC-like traits. Evidence shows, that epithelial cells, which have undergone EMT, display CSC-like characteristics, indicating a crosstalk between EMT and pathways involved in regulating stemness in cancer (2).

1.2.3 Regulation of EMT

1.2.3.1 EMT induction

The EMT program can be initiated by multiple extracellular inducers, including TGF- β , c-Met/HGF, hypoxia, Wnt and Notch signaling. Hereby, transcription factors are activated, which mediate EMT-inducing target gene expression.

One prominent EMT inducer is the cytokine TGF- β . It regulates cell proliferation, differentiation, apoptosis and development during embryogenesis (19). Postnatally, TGF- β facilitates EMT in wound healing, immune system and fibrosis. However, in terms of cancer, TGF- β comprises a dual role. It is released by blood platelets and stromal cells and prevents in most cases malignant transformation and tumor progression, by regulating cellular proliferation, differentiation, survival and adhesion. However, cancer cells may gain the ability to avoid suppressive influence of TGF- β . In turn, TGF- β alters its function and mediates tumor growth and immune surveillance (20). Moreover, TGF- β is also known to induce cancer cell invasion and dissemination by inducing EMT (21). Mechanistically, in mammary epithelial cells, TGF- β receptors are localized at tight junctions, which interact with two important regulators of cell polarity: Par6 and Occludin. Upon TGF- β stimulation, TGF- β -type II receptor phosphorylates these regulators. This leads to the loss of tight junctions and thereby to a morphological change of the cells from a cuboidal to an elongated spindle-like shape. However, TGF- β is also suggested to interact with Wnt, Notch and receptor tyrosine kinase

pathways, all of which lead to the loss of epithelial markers such as E-cadherin and gain of mesenchymal markers, including fibronectin and vimentin (22).

Furthermore, Notch1 signaling activation at least partly mediates EMT and is closely associated with the genesis of CSCs. Hereby, the Notch intracellular domain (NICD) is cleaved off the transmembrane Notch1 receptor by the γ -secretase. NICD translocates into the nucleus, inducing a mesenchymal phenotype and thus enhances tumorigenesis (23).

1.2.3.2 The major player in EMT: E-cadherin

A key hallmark of EMT is the change of cell surface proteins, most notably the replacement of the transmembrane calcium-dependent glycoprotein E-cadherin into neural-cadherin (N-cadherin). E-cadherin is a classical type I cadherin, consisting of five extracellular Ca^{2+} -binding domains (EC1-EC5) which establish homophilic interactions with adjacent E-cadherin molecules (Figure 4). These interactions are essential for the formation of adherens junctions in order to link epithelial cells to a functional monolayer (24-26). The cytoplasmic domain of E-cadherin interacts with three catenins: β -catenin, α -catenin and p120, which link E-cadherin to the actin cytoskeleton in order to facilitate cell integrity.

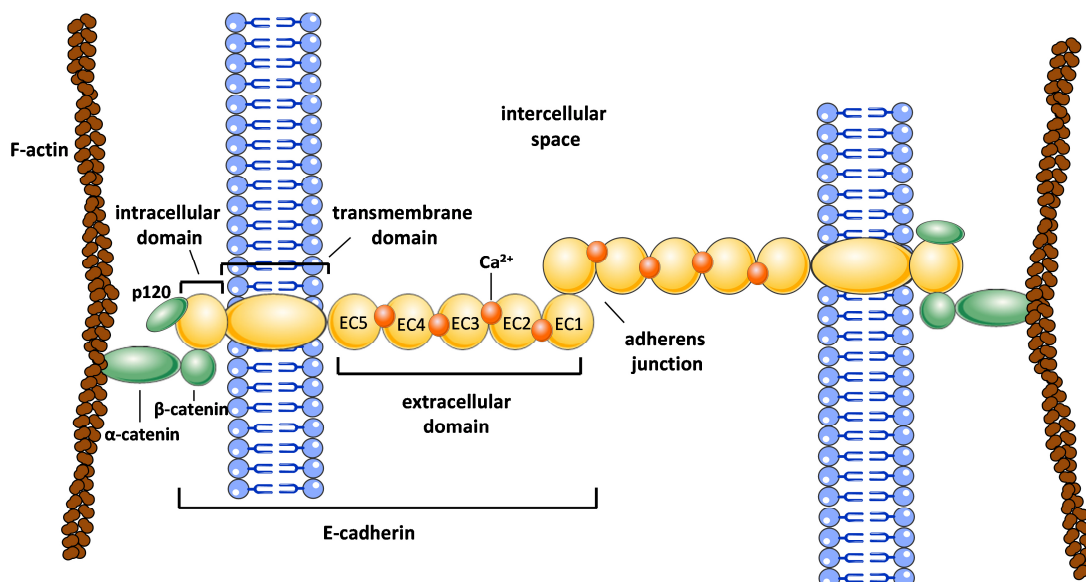


Figure 4: E-cadherin mediated adherens junction. E-cadherin is a transmembrane protein, comprising five Ca^{2+} -binding repeats (EC1-EC5) in the extracellular domain, one transmembrane domain and one intracellular domain which is associated with catenins (β -catenin, α -catenin and p120). This complex tethers E-cadherin to the F-actin cytoskeleton, forming stable adherens junctions between neighboring cells. EC, E-cadherin domains; F-actin, filamentous-actin.

The internalization of E-cadherin from cell surface into early endosomes, as well as recycling and trafficking to the lysosomes is a dynamic process and crucial to ensure the formation of adherens junctions and thus cell adhesion (27, 28).

Upon EMT induction, the loss of E-cadherin is regulated by multiple transcription factors: Either directly by binding of transcription factors such as Snail1/2, ZEB1/2, and Slug or indirectly by binding of Twist1 to the E-cadherin promoter containing an E-box element, which is responsible for its transcriptional repression (29-34). Thereby, multiple pathways are activated to induce the expression of mesenchymal proteins such as N-cadherin, vimentin and fibronectin. Thus, the interaction of cells with extracellular matrix proteins and cell migration is enabled.

Endosomal internalization and recycling or lysosomal degradation of receptors and surface proteins are crucial processes for the maintenance of cell homeostasis, as shown for example for the transferrin/transferrin-receptor recycling (35). As mentioned before, E-cadherin recycling and degradation is mediated by the endolysosomal machinery, which is in turn dependent on a functioning acidification of the endolysosomal system. This acidification is facilitated by proton pumping vacuolar H⁺-ATPases (V-ATPases) (3). Lysosomal degradation is enabled by the activated tyrosine kinases c-Met and Src. These kinases mediated phosphorylation of E-cadherin, which in turn promotes E-cadherin binding to Hakai E3-ligase. Upon Src expression, the GTPases Rab5 and Rab7 are activated, mediating the trafficking of E-cadherin/Hakai E3-ligase complex to the LAMP1-positive lysosomes where acidic pH-sensitive degrading enzymes mediate E-cadherin degradation (Figure 5) (36).

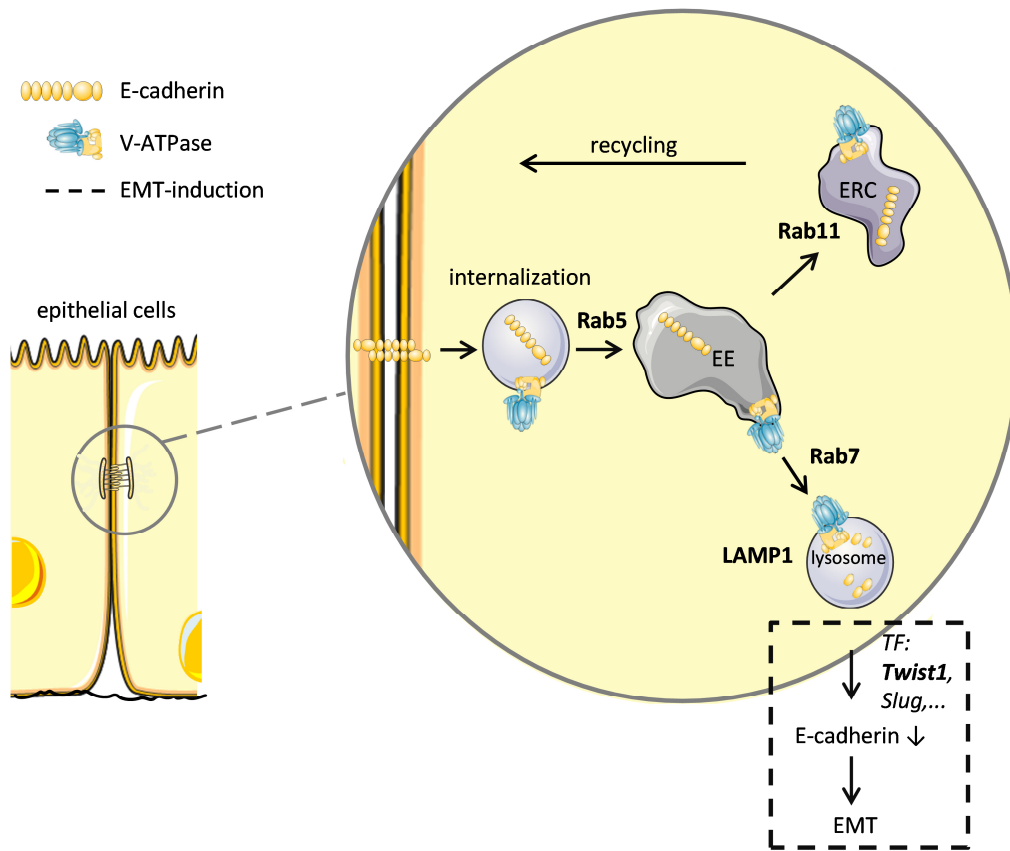


Figure 5: Endolysosomal trafficking of E-cadherin. E-cadherin is internalized from the cell surface and delivered to early endosomes. From here, it is either recycled back to the cell membrane or degraded by lysosomes. V-ATPase plays a crucial role throughout the trafficking. EE, early endosome; ERC, endocytic recycling compartment; TF, transcription factor; EMT, epithelial-mesenchymal transition.

1.3 V-ATPase - A potential target for EMT

1.3.1 Physiological function and structure

Vacuolar H⁺-ATPases (V-ATPases) are ubiquitous ATP-driven proton pumps, regulating the acidification of intracellular compartments, including endosomes, lysosomes, secretory vesicles and the Golgi-network (37). Additionally, V-ATPases in the plasma membrane of certain cells types, including osteoclasts, renal intercalated cells and epididymal clear cells function in processes such as bone resorption, renal acidification or sperm maturation (37, 38). Interestingly, in recent years, evidence is increasing that V-ATPase also plays a pivotal role in cancer cells by mediating an invasive cancer phenotype (39).

The V-ATPase is a large multi-subunit complex composed of 14 subunits organized into two major domains: the cytosolic ATP hydrolysis performing V₁ domain and the membrane-bound V₀ domain which transports protons (Figure 6). The V₁ domain is composed of eight different subunits: A, B, C, D, E, F, G and H. The central hexameric ring consists of three AB catalytic heterodimer building sites (A₃B₃) accomplishing the hydrolysis of ATP to ADP and a free phosphate (P_i). The V₀ domain consists of six different subunits: a, d, e, c, and c', whereas yeast additionally contain subunit c' and higher eukaryotes the accessory protein Ac45. The two domains V₀ and V₁ are connected by peripheral and central stalks (C-H). Protons enter subunit a of the V₀ domain through a cytoplasmic hemi-channel, thereby binding to one of the glutamic acid residues located on each subunit of the c-ring of V₀. Conformational change of subunit A upon ATP hydrolysis results in the rotation of the central stalk of the V-ATPase made up of subunits D and F of V₁ and d of V₀, consequently causing rotation of the c-ring. Thereby, each protonated glutamic acid residue of the c-ring of V₀ is in close proximity with a luminal hemi-channel in subunit a. Finally, the proton is released into the lumen by stabilizing the deprotonated glutamic acid through a subunit a located arginine residue (4).

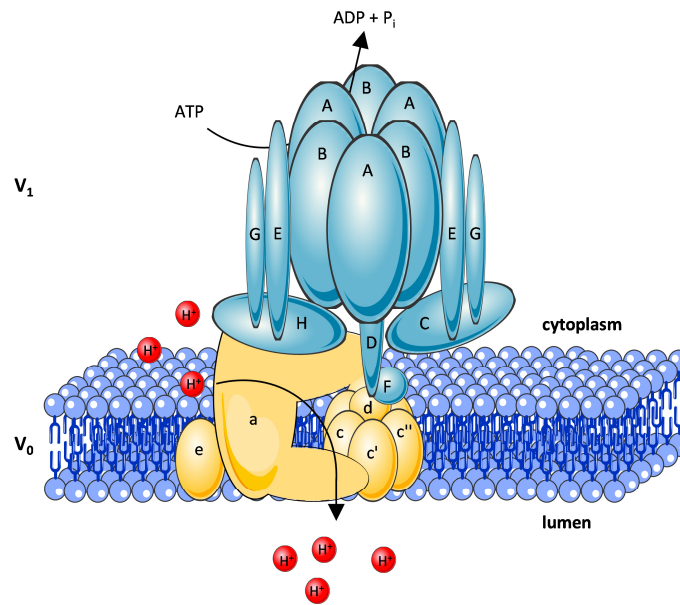


Figure 6: Structural model and function of the yeast vacuolar H^+ -ATPase (V-ATPase). The V-ATPase comprises two major complexes V_1 and V_0 : The cytosolic V_1 domain is made up of eight subunits (A-H) and is involved in ATP hydrolysis. The integral V_0 domain is located within the membrane and is made up of six subunits (a, d, e, c, c' and c'') conducting protons (H^+) across the membrane. Protons can enter the first of the two hemi-channels in the subunit a of V_0 and bind to a glutamate residue in one of the c-subunits of V_0 . Upon ATP hydrolysis in the A_3B_3 complex of V_1 the conformational change of subunit A causes a central stalk movement of subunits D and F of V_1 and d of V_0 . Upon rotation of the c-ring of V_0 , the proton translocates to the second hemi-channel, subsequently releasing it to the lumen. Illustrated according to the model of Forgac *et al.* (37).

1.3.2 Role of V-ATPase in cancer and metastasis

In recent years, many reports have supported the pivotal role of V-ATPase in cancer cells. Enhanced V-ATPase expression at the plasma membrane of cancer cells has been found to facilitate their invasion by acidifying the microenvironment (40, 41). Low extracellular pH accounts for invasiveness *in vitro* and *in vivo* in several cancer cells, including prostate, hepatocellular, pancreatic and breast cancer (42-47). Furthermore, loss of V-ATPase activity showed reduced cell growth and induced apoptosis in cancer cells (48). V-ATPase is also associated with drug resistance and its inhibition leads to restored drug sensitivity in cancers, such as in non-small-lung cancer (49). Markedly, recent evidence points to a potential role of V-ATPase-mediated lysosomal E-cadherin degradation during EMT (3). Nevertheless, a detailed study that characterizes the potential function of V-ATPase and the effects of its pharmacologic inhibition in CSCs is still missing.

1.3.3 The V-ATPase inhibitor: Archazolid A

Archazolid is a novel, highly specific V-ATPase inhibitor with an IC_{50} value in the low nanomolar range, exerting no effects on F-ATPases or Na^+/K^+ -ATPases (50, 51). It is a myxobacterial secondary metabolite, first isolated from myxobacteria *Archangium gephyra* and *Cystobacter violaceus* (52). Since 2009, Archazolid A and B are available by chemical total synthesis (53). Structurally, Archazolid is composed of a macrocyclic lactone ring with a thiazole side chain (Figure 7). It binds within the equatorial region of the V_0 rotor subunit c. In detail, Archazolid interacts with the essential glutamate within the highly conserved region of helix 4 of subunit c, thereby inhibiting the rotation of the c-ring and thus V-ATPase function (54).

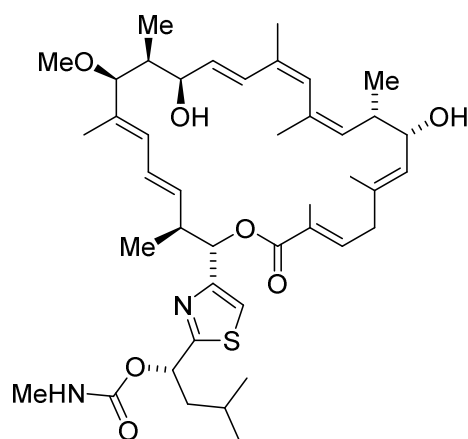


Figure 7: Chemical structure of Archazolid A. Chemical structure adapted from Huss *et al.* (50).

In previous years, the work of our group revealed that Archazolid A induces apoptotic cell death in cancer cells as well as affects migration in highly metastatic cancer cells (47, 48). Lately, anti-leukemic and anoikis resistance abrogating effects have been unveiled (55, 56). Moreover, Archazolid was shown to interfere with iron metabolism in breast cancer cells by disrupting transferrin receptor internalization, leading to iron deprivation and thus apoptosis (35). These promising anti-cancer effects need to be further exploited in order to develop potential applications in cancer therapy. So far, investigations on the pharmacological accessibility of V-ATPase in terms of CSCs do not exist.

1.4 Aim of the study

What we know so far:

1. Aggressive breast cancer is attributed to breast cancer stem cells (CSCs) (1, 6).
2. Breast CSC formation is associated with EMT (2).
3. V-ATPase plays an important role during EMT (3) and is a promising anti-cancer target (42, 47).

We investigated the intriguing question:

Is the pharmacologically accessible V-ATPase a new target to abrogate EMT and CSC formation?

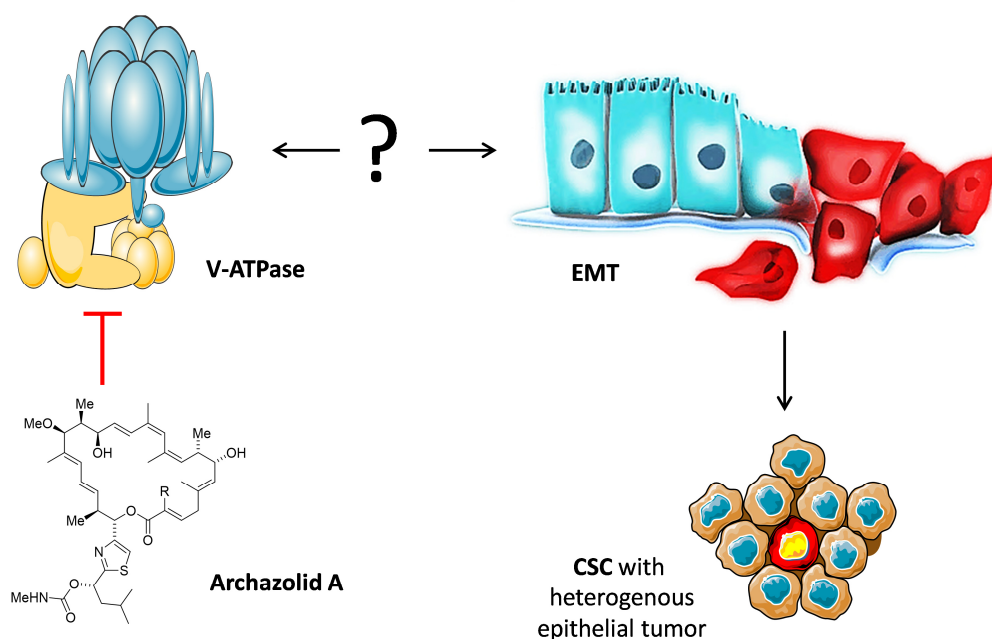


Figure 8: Investigation of the link between V-ATPase, EMT and CSC formation.

The aim of this study was to examine the effects of V-ATPase inhibition during EMT on bCSC formation, thereby investigating the major hallmarks of metastasis: tumor cell migration and cancer stem cell-induced mammosphere formation. In addition, the underlying cellular mechanism of V-ATPase inhibition during EMT was investigated.

MATERIALS AND METHODS

2 MATERIALS AND METHODS

2.1 Materials

2.1.1 Compound

Archazolid A was generously provided by Dr. Rolf Müller (Helmholtz Centre for Infection Research, Saarbrücken).

2.1.2 Reagents and technical equipment

Table 1: Biochemicals, kits, dyes and cell culture reagents

Reagent	Producer
4-hydroxytamoxifen	Sigma-Aldrich, Taufkirchen, Germany
B27 [®] Supplement (50x)	Gibco, Life Technologies, Carlsbad, USA
bFGF	Peprotech, Rocky Hill, USA
Blasticidin	Gibco, Germering, Germany
Bovine serum albumin	Sigma-Aldrich, Taufkirchen, Germany
Bradford Reagent [™]	Bio-Rad, Munich, Germany
Complete [®] EDTA free	Roche Diagnostics, Penzberg, Germany
Crystal violet	Carl Roth, Karlsruhe, Germany
DMSO	Sigma-Aldrich, Taufkirchen, Germany
EDTA	Carl Roth, Karlsruhe, Germany
EGTA	Sigma-Aldrich, Taufkirchen, Germany
EGF	Peprotech, Rocky Hill, USA
EMT Antibody Sampler Kit	Cell Signalling Technology, Cambridge, UK
FCS	Biochrom AG, Berlin, Germany
FluorSave [™] Reagent	Merck, Darmstadt, Germany
High-Capacity cDNA Reverse Transcription Kit	Applied Biosystems, Foster City, CA, USA
Hoechst 33342	Sigma-Aldrich, Taufkirchen, Germany
IPTG	Sigma-Aldrich, Taufkirchen, Germany
LysoTracker [®] dye	Moleculare Probes, Darmstadt, Germany

MECGM, ready-to-use	PromoCell GmbH, Heidelberg, Germany
MEGM™ Bullet Kit	Lonza, Basel, Switzerland
Methylcellulose	Sigma-Aldrich, Taufkirchen, Germany
Na ₃ VO ₄	ICN Biomedicals, Aurora, Ohio, USA
NaCl	Sigma-Aldrich, Taufkirchen, Germany
NaF	Merck, Darmstadt, Germany
Non-fat dry milk powder (Blotto)	Carl Roth, Karlsruhe, Germany
Page-Ruler™ Prestained Protein Ladder	Fermentas, St. Leon-Rot, Germany
Penicillin/Streptomycin	PAA Laboratories, Pasching, Austria
PFA	Sigma-Aldrich, Taufkirchen, Germany
PMSF	Sigma Aldrich, Munich, Germany
Polyacrylamid	Carl Roth, Karlsruhe, Germany
Poly-HEMA	Sigma-Aldrich, Taufkirchen, Germany
PowerUp™ SYBR Green Master Mix	Applied Biosystems, Foster City, CA, USA
Propidium iodide	Sigma-Aldrich, Taufkirchen, Germany
Puromycin Dihydrochloride	Sigma-Aldrich, Taufkirchen, Germany
Qiagen RNeasy Mini Kit	Qiagen, Hilden, Germany
RPMI 1640	PAN Biotech, Aidenbach, Gemrany
shRNA MISSION Lentiviral Transduction Particles	Sigma-Aldrich, Taufkirchen, Germany
Taqman Master Mix	Life Technologies Corporation, Carlsbad, USA
TCE	Sigma-Aldrich, Taufkirchen, Germany
TGF-β	Peprotech, Rocky Hill, USA
TNS	PromoCell GmbH, Heidelberg, Germany
Trisodium citrate dicydrate	Sigma-Aldrich, Taufkirchen, Germany
Triton X-100	Merck, Darmstadt, Germany
Trypsin	PAN Biotech, Aidenbach, Germany
Tween 20	Bio-Rad, Munich, Germany

Table 2: Commonly used solutions and media

PBS (pH 7.4)		PBS + Ca²⁺/Mg²⁺ (pH 7.4)	
NaCl	132.2 mM	NaCl	137 mM
Na ₂ HPO ₄	10.4 mM	KCl	2.68 mM
KH ₂ PO ₄	3.2 mM	Na ₂ HPO ₄	8.10 mM
in H ₂ O		KH ₂ PO ₄	1.47 mM
		MgCl ₂	0.25 mM
		in H ₂ O	
Mammary epithelial cell growth medium		RPMI	
MECGM	500 ml	RPMI 1640	500 ml
BPE	2 ml	FCS	10 %
EGF	5 µg	non-essential amino acid	1 %
Insulin	2.5 mg	Pyruvate	1 %
Hydrocortisone	250 µg	Insulin	10 µg/ml
P/S	1 %		
DMEM		Trypsin/EDTA (T/E)	
DMEM	500 ml	Trypsin	0.5 %
FCS	10 %	EDTA	0.20 %
P/S	1 %	in PBS	

Table 3: Technical equipment

Name	Producer
7300 Real Time-PCR System	Applied Biosystems, Foster City, CA, USA
Axiovert 25/200 microscope	Zeiss, Jena, Germany
Canon EOS 450D camera	Canon, Poing, Germany
ChemiDoc Touch Imaging System	Bio-Rad Laboratories GmbH, Munich, Germany
Consort Electrophoresis Power Supply E835	Sigma-Aldrich, Taufkirchen, Germany
Curix 60	Agfa, Cologne, Germany
FACS Calibur	Becton Dickinson, Heidelberg, Germany
ibiTreat μ -slide 8-well	ibidi GmbH, Munich, Germany
Leica-SP8 confocal microscope	Leica Microsystems, Wetzlar, Germany
NanoDrop [®] ND-1000 Spectrophotometer	Peqlab Biotechnology GmbH, Erlangen, Germany
Nitrocellulose membrane	Amersham Bioscience, Freiburg, Germany
PowerPac HC, Tank Blotting System	Bio-Rad, Munich, Germany
SpectraFluor Plus [™]	Tecan, Crailsheim, Germany
Transwell [®] permeable supports	Corning Incorporated, New York, NY, USA
Vi-Cell [™] XR	Beckman Coulter, Krefeld, Germany
X-ray film (Super RX)	Fuji, Düsseldorf, Germany
Zeiss LSM 510 Meta confocal laser	Zeiss, Jena, Germany

2.2 Methods

2.2.1 Cell culture

Immortalized human mammary epithelial (HMLE) cells, stably transduced with Twist1-ER were kindly provided by Dr. Christina Scheel (Helmholtz Centre Munich) and described by Casas *et al.* (32). HMLE cells were cultivated in Mammary Epithelial Cell Growth Medium (MECGM, Ready-to-use; PromoCell GmbH, Heidelberg, Germany), supplemented with penicillin/streptomycin (P/S; PAA Laboratories, Pasching, Austria) and 10 µg/ml blasticidin (Gibco, Germering, Germany). After reaching 80 % confluence, HMLE cells were sub-cultured (1:5-1:10) in 75 cm² culture flasks, or seeded either in multiwell-plates or ibidi µ-slides (ibidi GmbH, Munich, Germany) for respective experiments. Cells were washed once with prewarmed PBS and 1 ml Trypsin/EDTA (T/E) was added for 15-20 min at 37 °C. The detachment of the cells was stopped with Trypsin Neutralizing Solution (TNS; PromoCell GmbH, Heidelberg, Germany). Cells were plated after adjustment of the cell concentration with Vi-Cell™ XR (Beckman Coulter, Krefeld, Germany).

Highly invasive MDA-MB-231 cells were purchased from Cell Line Services (Eppelheim, Germany), cultivated in DMEM and passaged twice a week (1:10). The MCF-7 breast cancer cell line (ACC 115, DSMZ, Braunschweig, Germany) was cultured in RPMI and passaged twice a week (1:10). All cell lines were cultured under constant humidity at 37 °C and with 5 % CO₂.

2.2.2 Freezing and thawing

For freezing nitrogen stocks, HMLE cells with 80 % confluence were washed with PBS, trypsinized and centrifuged (1.000 rpm, 5 min at room temperature (RT)). 1 x 10⁶ cells were resuspended in 1 ml freezing medium and transferred to cryovials. Cells were first frozen at -20 °C and then transferred to either -80 °C or to liquid nitrogen (-196 °C) for long-term storage.

Table 4: Freezing medium HMLE cells

Freezing medium	
MECGM	70 %
FCS	20 %
DMSO	10 %

In order to thaw cells, one cryovial content was immediately dissolved in prewarmed MECGM. Subsequently, cells were centrifuged, resuspended in MECGM to remove DMSO and seeded in a 25 cm² culture flask. The next day, fresh MECGM was provided for the cells and after reaching 70-80 % confluence, cells were transferred to a 75 cm² culture flask.

2.2.3 Transduction of HMLE Twist1-ER cells with lentiviral V-ATPase shRNA

For the lentiviral transduction of HMLE Twist1-ER cells with V-ATPase shRNA MISSION[®] Lentiviral Transduction Particles (Vector: pLKO.1-puro-IPTG 3 x LacO; SHC332V-1EA; Clone ID: (1) TRCN0000029559, (2) TRCN0000029560 (3) TRCN0000029561, (4) TRCN0000029562, (5) TRCN0000029563; Sigma-Aldrich, Taufkirchen, Germany) and MISSION[®] 3 x LacO Inducible Non-Target shRNA Control Transduction Particles (SHC332V, Sigma-Aldrich, Taufkirchen, Germany) as a control were used according to the manufacturer's protocol. The pLKO vector contains a LacI (repressor) and a modified human U6 promoter with LacO (operator) sequence, binding to each other. Upon IPTG treatment, the allosteric LacI repressor changes confirmation, releasing itself from LacO modified human U6 promoter and subsequently permits expression of the shRNA. HMLE Twist1-ER cells were transduced with a multiplicity of infection (MOI) of one. Successfully transduced cells were selected by adding 0.5 µg/ml puromycin (Sigma-Aldrich, Taufkirchen, Germany) to the medium and puromycin was also added to the medium during cultivation. For sufficient shRNA expression, 1 mM IPTG was added for 96 h before experiments were performed. In order to ensure sustained V-ATPase downregulation, 1 mM IPTG was constantly added. V-ATPase knockdown was examined by PCR analysis. Most efficient knockdown was achieved with V-ATPase shRNA clones 1 and 3 which were used for further experiments.

2.2.4 V-ATPase inhibition and EMT induction in HMLE Twist1-ER cells and in HMLE Twist1-ER shRNA clones

2.2.4.1 Pharmacological V-ATPase inhibition with Archazolid A and EMT induction in HMLE Twist1-ER cells

Epithelial HMLE Twist1-ER cells were pretreated with 1 or 10 nM Archazolid A for 24 h before EMT induction. EMT induction was either mediated by 4-hydroxytamoxifen (4-OH-TX; Sigma-Aldrich, Taufkirchen, Germany) or by TGF- β (Peprotech, Rocky Hill, USA). For 4-OH-TX treatment, fresh MECGM was added with 20 nM for 10 days. 4-OH-TX is an active metabolite of tamoxifen and binds to the estrogen receptor (ER). Thereby, the transcription factor complex 4-OH-TX/Twist1-ER translocates into the nucleus where it binds to DNA and modulates EMT gene expression.

For TGF- β -mediated EMT induction, 5 ng/ml TGF- β was added to the medium for 12 days. In both cases, Archazolid A pretreated cells were stimulated with 0.1 nM Archazolid A for the respective EMT duration. Cells were split and supplied with fresh medium and respective stimulation reagents every three days.

Fully transitioned mesenchymal HMLE cells were treated with 1 or 10 nM Archazolid A for 24 h.

2.2.4.2 Genetic V-ATPase knockdown and EMT induction in HMLE Twist1-ER shRNA clones

V-ATPase shRNA clones were pretreated with 1 mM IPTG for 96 h in order to sufficiently induce V-ATPase knockdown. EMT induction was either mediated by 4-OH-TX or by TGF- β . For 4-OH-TX treatment, fresh MECGM was added with 20 nM 4-OH-TX for 10 days. For TGF- β treatment, 5 ng/ml TGF- β was added for 12 days. V-ATPase knockdown was ensured by concomitant 1 mM IPTG treatment for the respective EMT duration. Cells were split and supplied with fresh medium and respective stimulation reagents every three days.

2.2.4.3 Induction of Notch1 with EGTA

MDA-MB-231 and MCF-7 cells were stimulated with 1 or 10 nM Archazolid A for 24 h and subsequently treated with 500 nM EGTA for 2.5 h.

2.2.5 Immunoblotting

For protein detection, Western blot analysis was performed. For lysis of the cells, RIPA lysis buffer was added and cells were frozen at -80 °C. Protein concentrations of cell lysates were determined as described by Bradford (57) using Bradford Reagent™ (Bio-Rad, Munich, Germany) and measuring the absorbance with SpectraFluor Plus™ (Tecan, Crailsheim, Germany). Equal amounts of proteins were loaded onto sodium dodecyl sulfate (SDS)-gels, utilizing Page Ruler™ Prestained as a protein ladder indicator (Fermentas, St. Leon-Rot, Germany). Proteins were separated by SDS-polyacrylamide (Carl Roth, Karlsruhe, Germany) gel electrophoresis (SDS-PAGE; 20 min: 100 V, 45 min: 200 V) using the Consort Electrophoresis Power Supply E835 (Sigma-Aldrich, Taufkirchen, Germany) and transferred to nitrocellulose membranes (Amersham Bioscience, Freiburg, Germany) by tank blotting (1.5 h: 100 V, 4 °C; Bio-Rad, Munich, Germany). Membranes were blocked with 5 % non-fat dry milk powder (Carl Roth, Karlsruhe, Germany) in T-BST for 1 h. Primary antibodies were either incubated over night at 4 °C, or for 2 h at RT. Secondary antibodies were incubated for 2 h at RT. Antibodies were diluted in 5 % BSA (Sigma-Aldrich, Taufkirchen, Germany) in T-BST. HRP-coupled secondary antibodies were detected with ECL substrate and chemiluminescence was detected with ChemiDoc Touch Imaging System (Bio-Rad Laboratories GmbH, Munich, Germany). Quantification of bands was made with Image Lab™ Software (Bio-Rad Laboratories GmbH, Munich, Germany).

Table 5: Solutions and reagents for Western blot analysis

RIPA lysis buffer		5x SDS sample buffer	
Tris/HCl (pH 7.4)	50 mM	Tris/HCl (pH 6.8)	3.125 M
NaCl	150 mM	Glycerol	50 %
Nonidet NP-40	1 %	SDS	5 %
Sodium deoxycholate	0.25 %	DTT	2 %
SDS	0.10 %	Pyronin Y	0.025 %
activated Na ₃ VO ₄	0.3 mM	H ₂ O	
NaF	1 mM		
β-glycerophosphate	3 mM	Stacking gel	
pyrophosphate	10 mM	Rotiphorese™ Gel 30	17 %
H ₂ O		SDS	0.1 %
<i>added before usage:</i>		TEMED	0.2 %
Complete® EDTA free	4 mM	APS	0.1 %
PMSF	1 mM	H ₂ O	
H ₂ O ₂	0.5 mM	Separation gel 10%/12 %	
		Rotiphorese™ Gel 30	33%/40 %
		Tris (pH 8.8)	375 mM
		SDS	0.1 %
		TEMED	0.1 %
		APS	0.05 %
		TCE	0.05 %
		H ₂ O	

Table 6: Primary antibodies for Western blot analysis *

Antigen	Source	Dilution	Provider
Claudin-1	rabbit	1:200	Cell Signalling Technology
Ductin/c-subunit	rabbit	1:500	Merck
E-cadherin (24E10)	rabbit	1:200	Cell Signalling Technology
Fibronectin (C6F10)	mouse	1:500	Santa Cruz Biotechnology
N-cadherin	rabbit	1:200	Cell Signalling Technology
NICD	rabbit	1:1000	Cell Signalling Technology
Notch1	rabbit	1:500	Cell Signalling Technology
Vimentin (D21H3)	rabbit	1:200	Cell Signalling Technology
β -catenin (D10A8)	rabbit	1:200	Cell Signalling Technology

Table 7: Secondary antibodies for Western blot analysis *

Antibody	Dilution	Provider
HRP, Goat anti-rabbit IgG (H+L)	1:1000	Bio-Rad
HRP, Goat anti-mouse IgG	1:1000	Santa Cruz Biotechnology

* All antibodies were diluted in 5 % BSA and T-BST

Table 8: T-BST for antibody dilution

T-BST (pH 8)	
TRIS-Base	30 g
NaCl	111 g
Tween 20	20 ml
H ₂ O	ad 1000 ml

2.2.6 Quantitative real-time PCR analysis

Total mRNA was isolated from cell culture samples using Qiagen RNeasy Mini Kit (Qiagen, Hilden, Germany) according to the manufacturer's protocol. Messenger RNA (mRNA) concentrations were determined using the NanoDrop® ND-1000 spectrophotometer (NanoDrop Technologies, Erlangen, Germany). Reverse transcription of mRNA into complementary DNA (cDNA) was performed with the High-Capacity cDNA Reverse Transcription Kit (Applied Biosystems, Foster City, CA, USA) according to the manufacturer's instructions. cDNA was stored at 4 °C until quantitative Real-Time-Polymerase Chain Reaction (qRT-PCR) was performed with the ABI 7300 Real Time PCR System (Applied Biosystems, Fosterer City, CA, USA). Either TaqMan Universal PCR Mastermix (Life Technologies Corporation, Carlsbad, CA, USA) or SYBR Green Master Mix (ThermoFischer Scientific, Germering, Germany) were used, respective to the utilized primer. GAPDH (biomers.net, Ulm, Germany) or Actin (Applied Biosystems, Foster City, USA) were used as housekeeping genes.

Table 9: Primer for qRT-PCR

Primer	Forward	Reverse	Method	Provider
E-cadherin	5' CAG CAC GTA CAC AGC CCT AA 3'	5' AAG ATA CCG GGG GAC ACT CA 3'	SYBR Green	Metabion
Vimentin	5' CGG CGG GAC AGC AGG 3'	5' TCG TTG GTT AGC TGG TCC AC 3'	SYBR Green	Metabion
N-cadherin	5' ACA GTG GCC ACC TAC AAA GG 3'	5' CCG AGA TGG GGT TGA TAA TG 3'	SYBR Green	Metabion
Fibronectin	5' GCT GAC AGA GAA GAT TCC CGA 3'	5' CCA GGG TGA TGC TTG GAG AA 3'	SYBR Green	Metabion
V-ATPase	5' AAC GCT GCG GAG ATC CAG A 3'	5' GCG ACG ATG AGA CCG TAG AG 3'	TaqMan®	Applied Biosystems
GAPDH	5' ACC ACA GTC CAT GCC ATC AC 3'	5' TCC ACC ACC CTG TTG CTG TA 3'	TaqMan®	Biomers.net GmbH
Actin	5' TTC ACC TAC AGC AAG GAC GA 3'	5' GAA CTC GAA GAT GGG GTT GA 3'	SYBR Green	Applied Biosystems

Average CT values of target genes were normalized to control as ΔCT . Changes in mRNA expression levels were shown as fold expression ($2^{-\Delta\Delta CT}$) calculated by the $\Delta\Delta CT$ method (58).

2.2.7 Immunostaining

Cells were treated as indicated and seeded into ibidi 8-well μ -slides. For staining, cells were washed with PBS⁺ and fixed with 4 % paraformaldehyde (PFA; Sigma-Aldrich, Taufkirchen, Germany) for 10 min, washed again with PBS and permeabilized with 0.2 % Triton X-100 (Merck, Darmstadt, Germany). In order to avoid unspecific binding of the antibody, cells were blocked with 0.2 % BSA in PBS (30 min, RT). Primary antibodies were diluted in 0.2 % BSA in PBS, incubated overnight at 4 °C and concomitantly washed three times with PBS (3 x 5 min, RT). Secondary antibodies were also diluted in 0.2 % BSA in PBS and together with 5 μ g/ml Hoechst 33342 (Sigma-Aldrich, Taufkirchen, Germany), incubated for 45 min at RT. Subsequently, cells were mounted with FluorSaveTM Reagent (Merck, Darmstadt, Germany) and stored at 4 °C under exclusion of light. Images were obtained using Zeiss LSM 510 Meta confocal microscope (Zeiss, Jena, Germany) or Leica-SP8 confocal microscope (Leica Microsystems, Wetzlar, Germany).

Table 10: Primary antibodies for immunostaining

Antibody	Species	Dilution	Provider
E-cadherin (24E10)	rabbit	1:200	Cell Signalling
E-cadherin (HECD1)	mouse	1:1000	Invitrogen
LAMP-1	mouse	1:200	Developmental Studies Hybridoma Bank
N-cadherin (D4R1H) XP	rabbit	1:200	Cell Signalling
Notch1	rabbit	1:400	Cell Signalling
Rab5 (S-19)	rabbit	1:50	Santa Cruz Biotechnology
Rab7 (D95F2) XP	rabbit	1:100	Cell Signalling
Vimentin (D21H3) XP	rabbit	1:100	Cell Signalling
β -catenin (D10A8) XP	rabbit	1:100	Cell Signalling

Table 11: Secondary antibodies for immunostaining

Antibody	Dilution	Provider
Alexa Fluor 488 goat anti-rabbit	1:400	Invitrogen
Alexa Fluor 546 goat anti-mouse	1:400	Invitrogen

2.2.8 LysoTracker® staining

Cells were treated as described in figure legends and 25 000 cells/well seeded in 8-well μ -slides, stained for 60 min with 100 nM LysoTracker® dye (Molecular Probes, Darmstadt, Germany) and 5 μ g/ml Hoechst 33342 in PBS at 37 °C. Stained cells were imaged by confocal microscopy (LSM 510 Meta, Zeiss, Oberkochen, Germany) without fixation.

2.2.9 E-cadherin internalization assay

HMLE Twist1-ER cells were cultivated, as described, for 10 days. On day 10, cells were seeded in ibidi 8-well μ -slides. Cells were washed with ice-cold PBS and slides were kept at 4 °C for 10 min. In the following, samples were incubated with anti-E-cadherin antibody (HECD1, 2 μ g/ml; Invitrogen, Carlsbad, USA) for 45 min at 4 °C. After three washing steps with PBS, prewarmed MECGM medium was added and incubated for indicated time points (0, 5, 10 and 20 min) at 37 °C. Cells were fixed with 4 % PFA for 15 min at RT and washed with PBS. After incubation with the secondary antibody Alexa Fluor 488 goat anti-mouse IgG (H+L)(1:400) and 5 μ g/ml Hoechst 33342 for 30 min at RT, cells were washed three times with PBS and mounted with FluorSave™ Reagent and a coverslip. Slides were kept at 4 °C with exclusion of light until images were taken, using Leica-SP8 confocal microscope (Leica Microsystems, Wetzlar, Germany).

2.2.10 Mammosphere assay

Mammosphere formation assays were performed as described previously by Dontu *et al.* with modifications (59). In brief, cell viability was measured by Vi-CELL™ XR (Beckman Coulter, Krefeld, Germany) and 20 000 viable cells/well were resuspended in MEGM medium and seeded in ultra-low 12-well attachment plates, coated with poly-(2-hydroxyethyl methacrylate) (poly-HEMA). HMLE cells were incubated for 7 days (37 °C, 5 % CO₂), allowing mammosphere formation in the absence of additional stimulation.

For secondary mammosphere formation, primary mammospheres were dissociated by T/E into single cells and reseeded at 20 000 viable cells/well in poly-HEMA coated plates for 7 days (37 °C, 5 % CO₂). Each well was imaged by LSM 510 Meta confocal microscopy and quantity and size of mammospheres were analyzed by using ImageJ.

Table 12: MEGM mammosphere culture medium

Mammosphere medium	
MEGM™ Bullet Kit	500 ml
EGF	20 ng/ml
bFGF (human)	10 ng/ml
B-27® Supplements	50 ml
Methylcellulose	1 %

2.2.11 Boyden chamber assay

1×10^5 cells were suspended in MECGM without FCS and added on top of the Transwell® permeable supports (Corning Incorporated, New York, NY, USA). MECGM (negative control, NC) or MECGM with 10 % FCS (Biochrom AG, Berlin, Germany) was added on the bottom of the membrane. The Boyden chamber inserts were incubated at 37 °C and 5 % CO₂ for 6 h. Migrated cells were stained with crystal violet (Carl Roth, Karlsruhe, Germany). Cells on the upper side of the insert were removed with cotton swabs. Migrated cells were imaged using Zeiss Axiovert25 microscope (Zeiss, Jena, Germany) and Canon EOS 450D camera (Canon, Poing, Germany). Cells were counted using the ImageJ plugin cell counter and normalized to control.

2.2.12 Cell viability assay

2.2.12.1 Fluorescence activated cell sorting

Cell viability was measured according to Nicoletti *et al.* (60), by which the percentage of apoptotic nuclei after propidium iodide (PI; Sigma-Aldrich, Taufkirchen, Germany) staining is measured. Cells were treated as indicated, washed and harvested. Sub-diploid DNA content was determined by permeabilization and staining with hypotonic fluorochrome solution (HFS) buffer containing PI (0.1 % (v/v)) over night at 4 °C. Apoptotic cells were measured by fluorescence activated cell sorting (FACS) on BD FACS Calibur (Becton Dickinson, Heidelberg, Germany), analyzing the respective fluorescence intensity.

Table 13: HFS buffer with PI

HFS buffer	
Propidium iodide	75 µM
Trisodium citrate	0.1 %
Triton-X 100	0.1 %
PBS	

2.2.12.2 Cell viability in mammosphere assays

For mammosphere assays, cell viability was measured by Vi-CELL™ XR (Beckman Coulter, Krefeld, Germany) before seeding.

For visualizing dead cells among mammospheres 50 µg/ml PI (1 h) and for nuclei staining 5 µg/ml Hoechst 33342 (3 h) were added to the medium and subsequently imaged by LSM 510 Meta confocal microscopy.

2.2.13 Statistics

All experiments were performed at least three times unless otherwise indicated. Statistical analysis was accomplished using GraphPad Prism® software version 5.04 (GraphPad Software, Inc., La Jolla, CA, USA). Graph data represent means ± SEM. One-way ANOVA/Tukey's Multiple Comparison Test and individual student t-tests were conducted. *P* values less than 0.05 were considered significant.

RESULTS

3 RESULTS

3.1 Characterization of EMT in HMLE Twist1-ER cells

3.1.1 4-OH-TX induces EMT in HMLE Twist1-ER cells

In order to mimic EMT *in vitro* with a well-established model, immortalized HMLE cells transduced with Twist1-ER were utilized (2, 32). Upon 4-hydroxytamoxifen (4-OH-TX) stimulation, mesenchymal traits were conferred on epithelial cells, by activation and expression of the transcription factor Twist1 (Figure 9A). In line with recent reports, cuboidal epithelial cells transited into mesenchymal elongated, spindle shaped cells, building a dense monolayer (Figure 9B). Furthermore, the expression of the epithelial marker E-cadherin was completely reduced and the mesenchymal marker vimentin was increased significantly in cells which underwent EMT, as shown by qRT-PCR analysis (Figure 9C). These data indicate a gain of mesenchymal traits upon 4-OH-TX treatment.

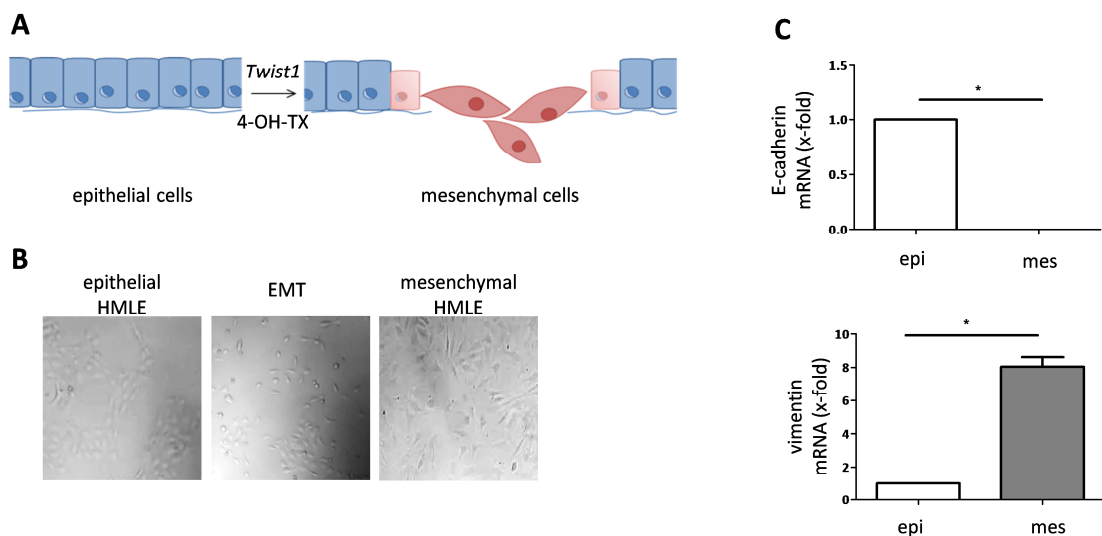


Figure 9: EMT in HMLE Twist1-ER cells upon 4-OH-TX stimulation. (A) Model for EMT induction in HMLE Twist1-ER cells. (B) Morphologic change of HMLE Twist1-ER cells treated with 20 nM 4-OH-TX for 10 days. (n=3). (C) mRNA expression of E-cadherin and vimentin in epithelial (epi) and mesenchymal (mes) HMLE Twist1-ER cells. (Student's *t*-test, **p*<0.05, n=3).

3.1.2 4-OH-TX induces translocation of Twist1-ER into the nucleus

Upon 4-OH-TX treatment, the fusion protein between Twist1 and the modified hormone-binding domain of estrogen receptor (Twist1-ER), is activated and translocates to the nucleus, where the transcription factor Twist1 induces EMT. In epithelial cells, Twist1 was distributed diffusely, whereas upon 4-OH-TX induction, Twist1 staining was enhanced in the nucleus (Figure 10A). This translocation was not modified by Archazolid A treatment. In line, mRNA expression of Twist1 after 10 days was upregulated in both, 4-OH-TX and Archazolid A treated cells, compared to epithelial cells (Figure 10B). These results show an effective Twist1 translocation to the nucleus upon 4-OH-TX treatment and exclude that V-ATPase inhibition impairs EMT by interfering with Twist1 translocation.

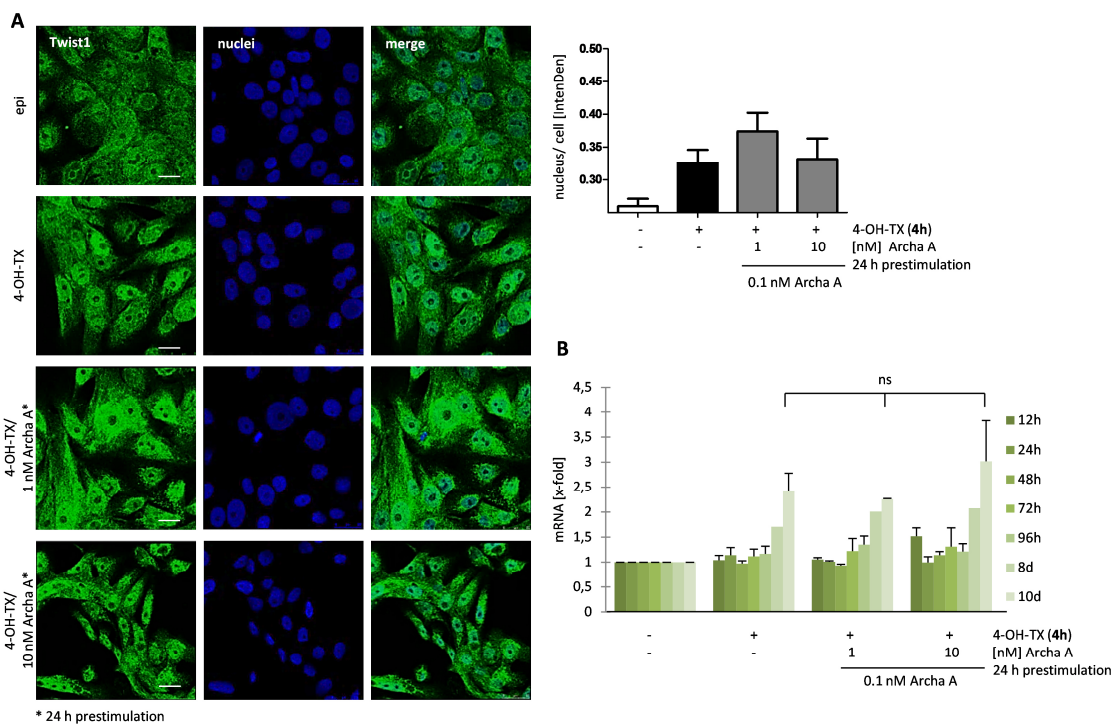


Figure 10: Twist1 translocation into the nucleus is induced by 4-OH-TX. (A) Twist1 staining (green) of HMLE cells without (epithelial, epi) and with 20 nM 4-OH-TX and with/without Archazolid A (Archa A) treatment in indicated concentrations is shown. Graph in the upper right panel depicts Twist1 fluorescence signal intensity of the nucleus (blue) relative to the entire cell signal (One-way ANOVA, Tukey's Multiple Comparison Test, n=3). (B) mRNA expression of Twist1 without and with EMT induction by 20 nM 4-OH-TX and with/without Archazolid A treatment in indicated concentrations and time points (12 h, 24 h, 48 h, 72 h, 96 h, 8 d, 10 d) is shown. (One-way ANOVA, Tukey's Multiple Comparison Test, SEM, ns= not significant, n=3).

Furthermore, expression of epithelial and mesenchymal markers was analyzed following Twist1 activation. Quantitative RT-PCR confirmed the data from Casas *et al.*, revealing significant E-cadherin downregulation after 8 days of 4-OH-TX treatment, whereas mesenchymal fibronectin and Snail1 were upregulated (Figure 11) (32). Interestingly, vimentin expression was enhanced after 48 h, while no difference on the expression regarding N-cadherin and Slug was observed over time. Taken together, these results confirm published data, suggesting suppression of E-cadherin and therefore EMT induction by Twist1 (32).

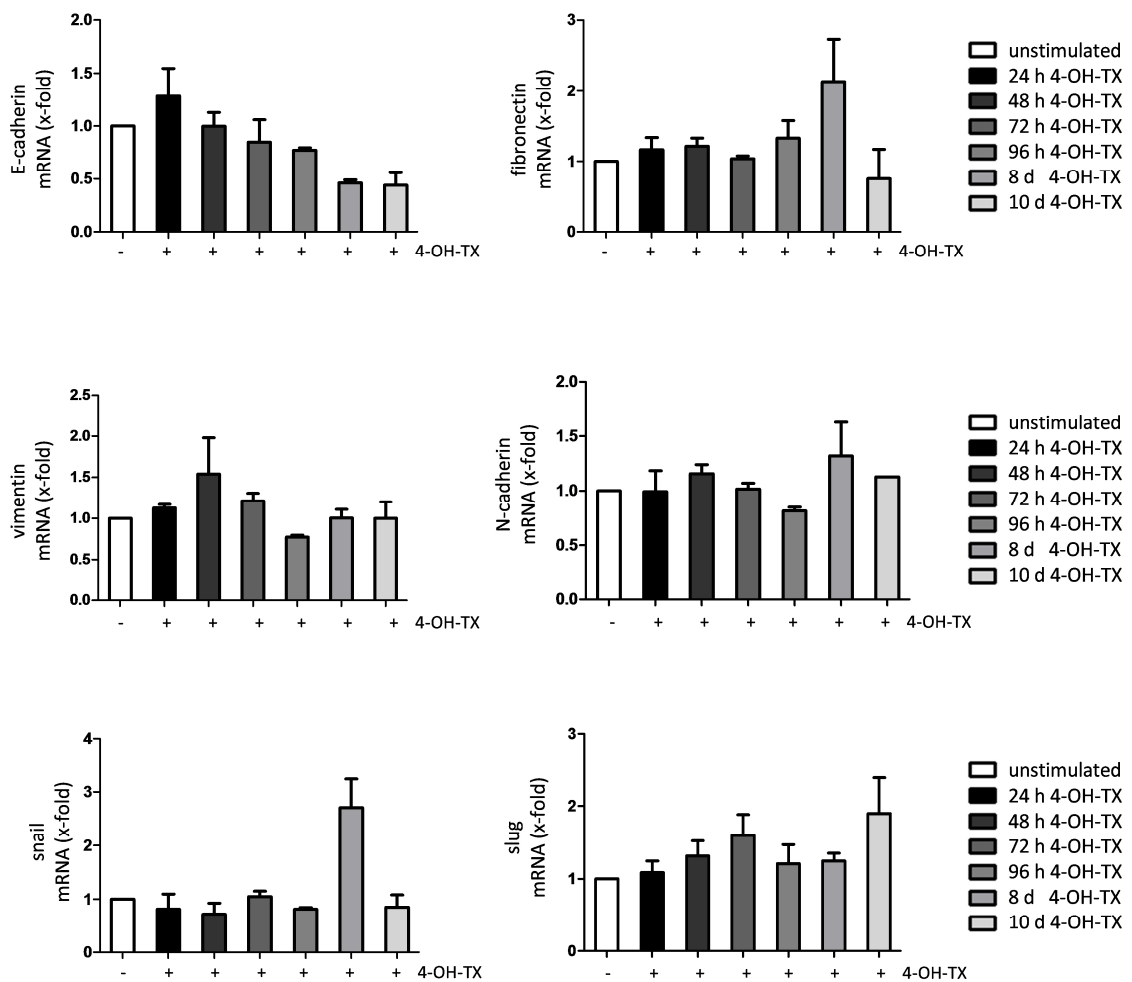


Figure 11: EMT marker expression over time. mRNA expression of E-cadherin, fibronectin, vimentin, N-cadherin, Snail1 and Slug in HMLE Twist1-ER cells for the indicated points: 24 h, 48 h, 72 h, 96 h, 8 d and 10 d, is shown. (One-way ANOVA, Tukey's Multiple Comparison Test, * $p < 0.05$, $n = 3$).

3.2 Role of V-ATPase in HMLE Twist1-ER cells during EMT

3.2.1 Archazolid A inhibits V-ATPase activity in HMLE Twist1-ER cells during EMT

Metastatic potential and thus malignancy of cancer cells often correlates with either enhanced expression of V-ATPase subunits or with increased V-ATPase activity (43). Endolysosomal pH monitoring by LysoTracker® dye was performed in HMLE Twist1-ER cells upon EMT induction for selective visualization of acidic organelles, in which the dye accumulates and stains them. Comparing control and 4-OH-TX-treated HMLE Twist1-ER cells a slight increase of cells with acidic compartments could be seen, suggesting increased V-ATPase activity. Acidification of lysosomes was markedly diminished upon V-ATPase inhibition by Archazolid A (Figure 12).

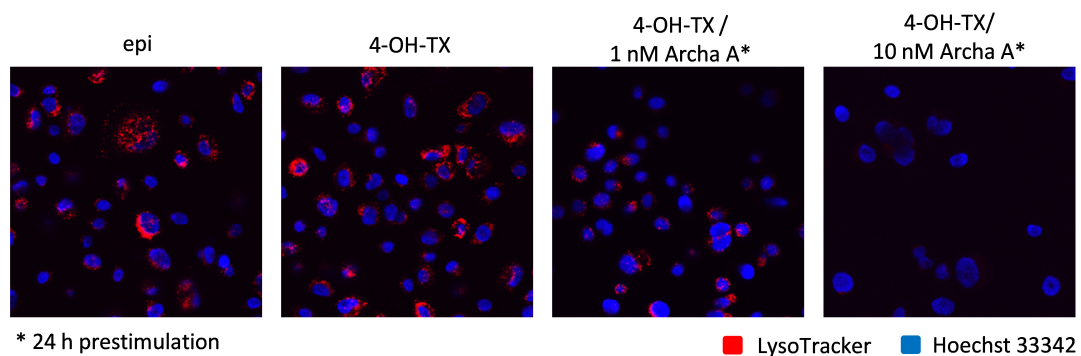


Figure 12: Archazolid A inhibits V-ATPase activity of HMLE Twist1-ER cells after EMT. LysoTracker® staining of acidic endolysosomal compartments (red) of HMLE Twist1-ER cells without (epithelial, epi) and with EMT induction by 20 nM 4-OH-TX and with/without Archazolid A (Archa A) treatment in indicated concentrations is shown. Nuclei (blue) were stained with 5 µg/ml Hoechst 33342. Scale bars 20 µm (n=2).

No difference between the protein and mRNA expression of V-ATPase subunit c between epithelial and mesenchymal HMLE Twist1-ER cells were seen, as shown by Western blot and qRT-PCR analysis (Figure 13A, B).

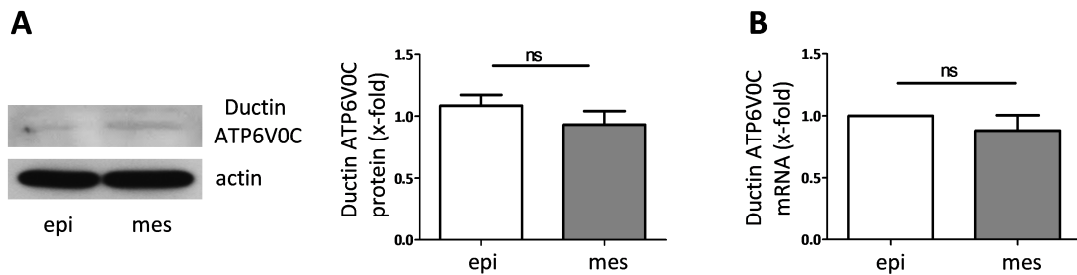


Figure 13: V-ATPase expression is comparable in epithelial and mesenchymal HMLE Twist1-ER cells. (A) Protein expression of V-ATPase in epithelial (epi) and mesenchymal (mes) HMLE Twist1-ER cells with anti-V-ATPase (Ductin ATP6V0C) and anti-actin antibodies is shown (Student's *t*-test, SEM, ns=not significant, n=3) (B) mRNA expression of V-ATPase (Ductin ATP6V0C) in epithelial and mesenchymal HMLE cells is shown. (Student's *t*-test, SEM, ns= not significant, n=3).

3.2.2 Archazolid A treatment during EMT impedes migration and mammosphere formation of HMLE cells

3.2.2.1 Archazolid A treatment during EMT inhibits migration

Impaired motility of invasive breast cancer cells upon V-ATPase inhibition has been shown in recent years (43, 46, 47). However, the role of V-ATPase on migration during EMT is unknown to date. To investigate whether Archazolid A inhibits EMT-induced migration, HMLE cells were pretreated with Archazolid A for 24 h before EMT induction. The transwell migration assay revealed that the induced migratory ability of mesenchymal HMLE Twist1-ER cells was successfully inhibited with Archazolid A treatment (Figure 14). This result indicates an important function for V-ATPase during EMT on migration.

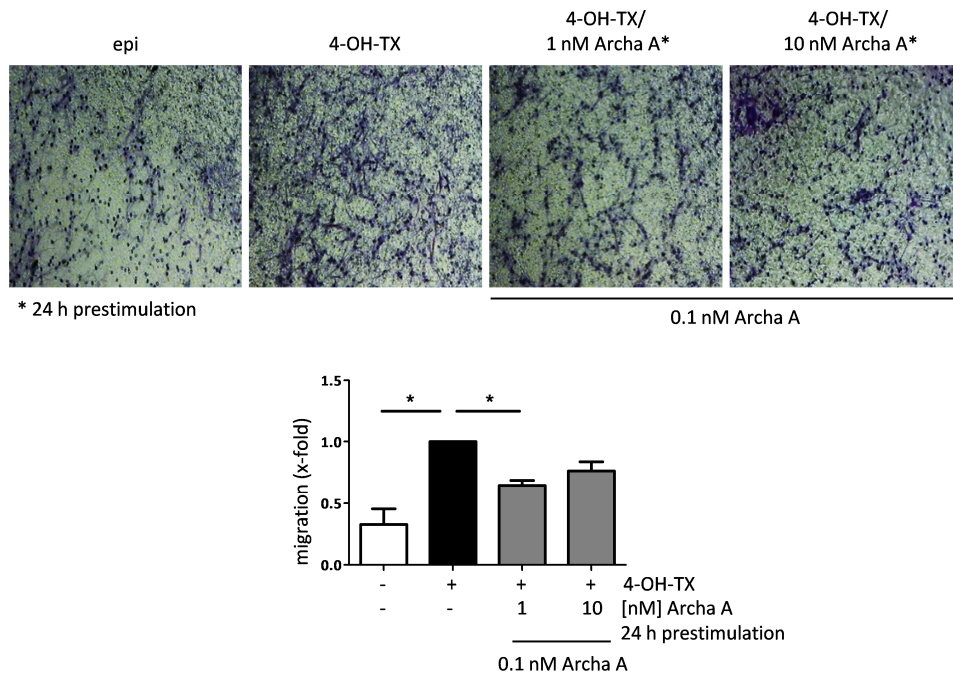


Figure 14: Archazolid A hampers migration after induction of EMT in epithelial HMLE Twist1-ER cells. Transwell migration of HMLE Twist1-ER cells without (epithelial, epi) and with EMT induction by 20 nM 4-OH-TX and with/without Archazolid A (Archa A) treatment in indicated concentrations is shown. Migrated HMLE Twist1-ER cells were stained with crystal violet (purple) and quantified using ImageJ cell counter. The graph shows the number of migrated cells after 6 h, normalized to 4-OH-TX treated cells. (One-way ANOVA, Tukey's Multiple Comparison Test, SEM, * $p < 0.05$, $n = 4$).

3.2.2.2 Archazolid A inhibits mammosphere formation

To analyze the role of V-ATPase on bCSC formation, mammosphere assays were performed. Dontu *et al.* developed this assay in order to evaluate the mammosphere-forming and therefore tumor-initiating potential of cells *in vitro* in an ultra-low attachment environment (59). Mesenchymal HMLE cells that had undergone EMT showed increased mammosphere-forming ability and mammosphere size. The induced mammosphere formation was diminished significantly by Archazolid A (Figure 15A). This effect was not mediated by increased apoptosis upon Archazolid A treatment (Figure 15B). Cells which were unable to form mammospheres on the ultra-low attachment poly-HEMA coated plates died as shown by PI staining, whereas maintained viability of cells which were able to proliferate and to form mammospheres was seen (Figure 15C). Taken together, these results indicate a pivotal role for Archazolid A on mammosphere formation.

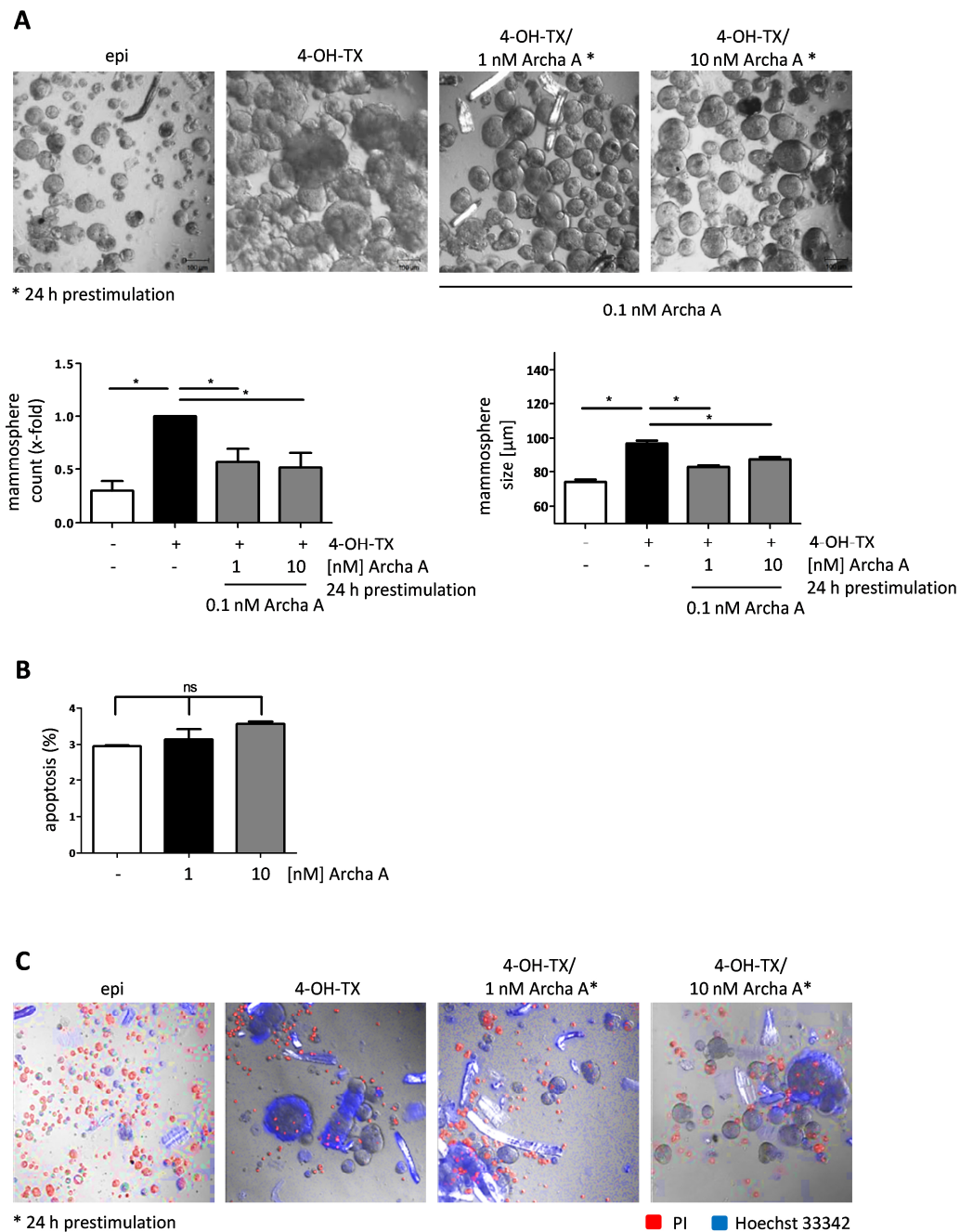


Figure 15: Archazolid A inhibits mammosphere formation after induction of EMT in epithelial HMLE Twist1-ER cells. (A) Mammosphere formation of HMLE Twist1-ER cells without (epithelial, epi) and with EMT induction by 20 nM 4-OH-TX for 10 days and with/without Archazolid A (Archa A) treatment in indicated concentrations is shown. Graphs depict mammosphere count ($> 50 \mu\text{m}$; left graph) normalized to 4-OH-TX treated mesenchymal controls and size (right graph). (One-way ANOVA, Tukey's Multiple Comparison Test, SEM, $*p < 0.05$, $n=5$). (B) Nicoletti assay of cells treated with Archazolid A (1 and 10 nM) for 24 h is shown. (One-way ANOVA, Tukey's Multiple Comparison Test, SEM, ns=not significant, $n=3$). (C) $50 \mu\text{g/ml}$ PI (red) staining of dead cells and $5 \mu\text{g/ml}$ Hoechst 33342 staining of nuclei (blue) are shown ($n=2$).

3.2.2.3 Archazolid A sustainably prevents mammosphere formation

For the sustainability of reduced malignancy, the maintenance of diminished mammosphere formation is of major importance and can be analyzed by repeated mammosphere assay. In second round mammosphere assays, the mammosphere-forming ability of 4-OH-TX-treated HMLE Twist1-ER cells was preserved and also the inhibitory effect of Archazolid A was still given (Figure 16).

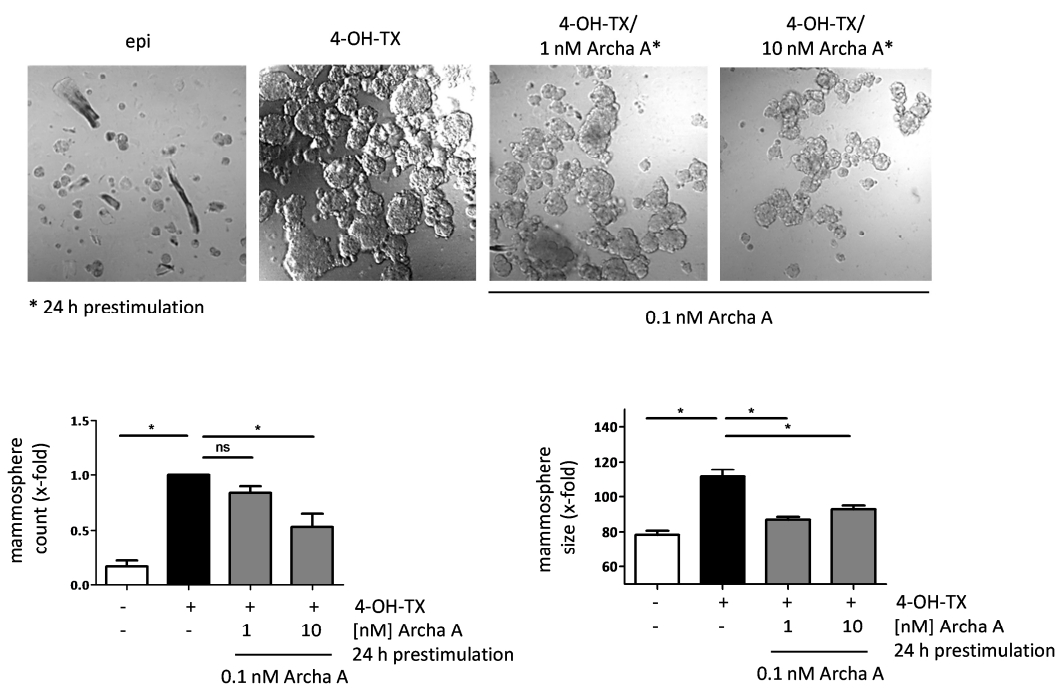
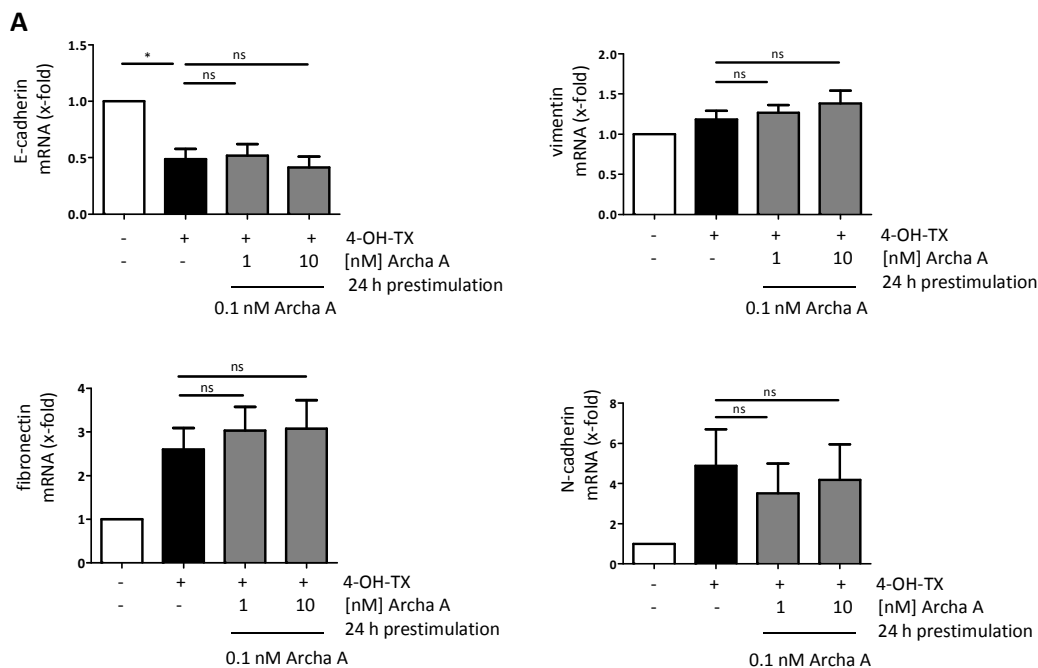


Figure 16: Archazolid A inhibits 2nd round mammosphere formation. 1st round mammospheres were disrupted, 20 000 viable single cells/well were reseeded in poly-HEMA coated 12-well plates and incubated for 7 days without further stimulation. The graphs depict mammosphere count (> 50 μ m) normalized to 4-OH-TX treated cells (left graph) and size (right graph). (One-way ANOVA, Tukey's Multiple Comparison Test, * p <0.05, ns=not significant, n =3).

Taken together, this set of data demonstrates that Archazolid A inhibits two crucial functional characteristics of cancer stem cells: migration and self-renewal.

3.2.3 Archazolid A preserves an epithelial phenotype during EMT

So far, the presented data point to a noticeable effect of Archazolid A treatment during EMT on migration and mammosphere formation. In a next step, the underlying signaling mechanism of EMT regulation was investigated. Quantitative RT-PCR analysis revealed significant decrease of epithelial E-cadherin expression upon 4-OH-TX treatment, but no influence of Archazolid A. The mesenchymal markers vimentin, fibronectin and N-cadherin showed increased expression after 4-OH-TX treatment but were also not influenced by Archazolid A treatment (Figure 17A). Interestingly, on protein level, epithelial E-cadherin, β -catenin and claudin-1 were reduced in 4-OH-TX treated cells but strongly increased by Archazolid A (Figure 17B). In line, the increased expression of the mesenchymal markers, fibronectin and vimentin was strikingly reduced upon Archazolid A stimulation. These results were confirmed by staining of EMT markers: epithelial E-cadherin and β -catenin were visible at the cell membrane and clearly diminished upon 4-OH-TX treatment. Both epithelial markers were enhanced upon Archazolid A treatment. Mesenchymal vimentin and N-cadherin were visible in the 4-OH-TX-induced HMLE Twist1-ER cells and signals were decreased by Archazolid A stimulation (Figure 17C). These results suggest a post-translational regulation of EMT markers upon V-ATPase inhibition.



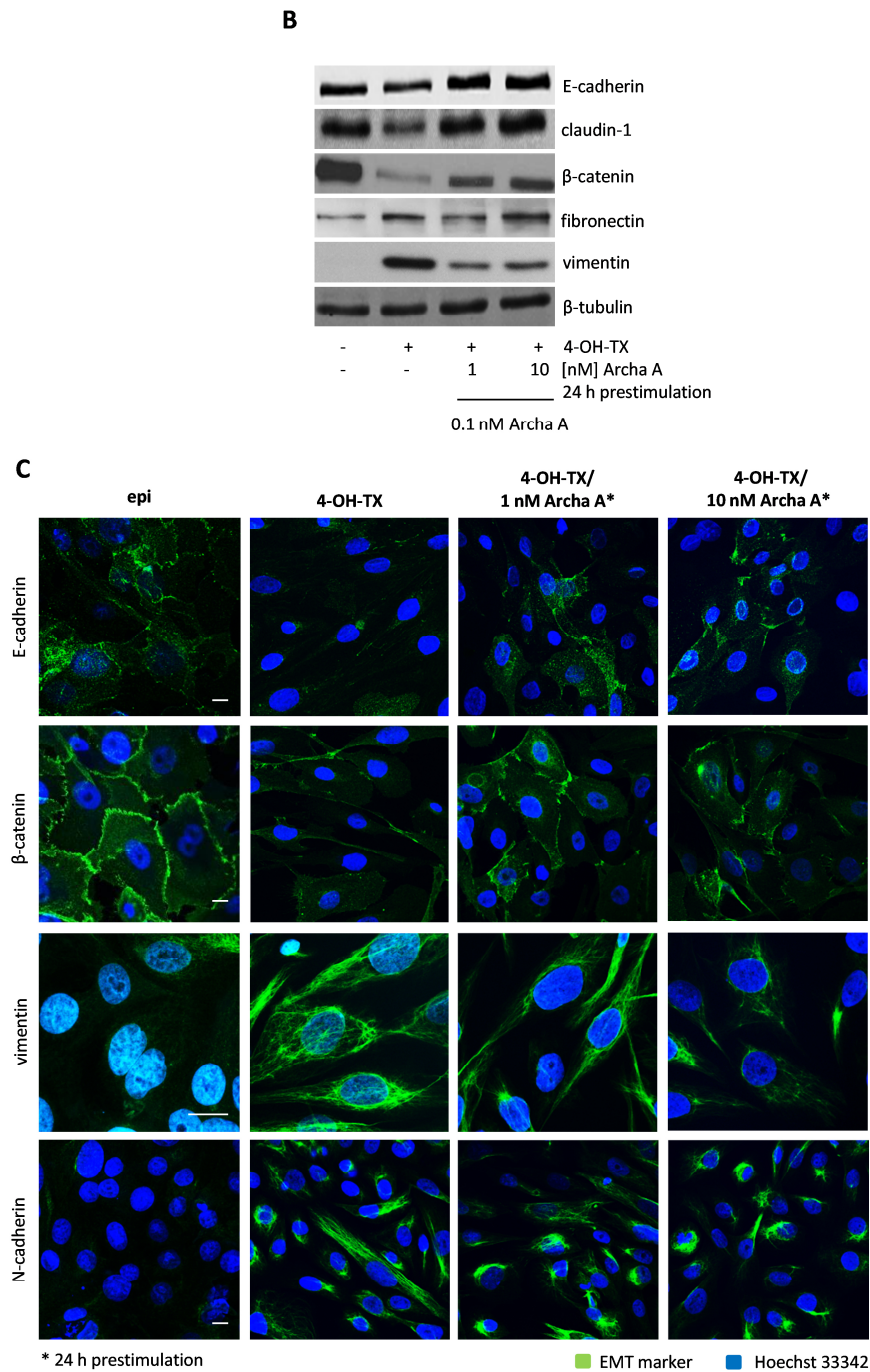
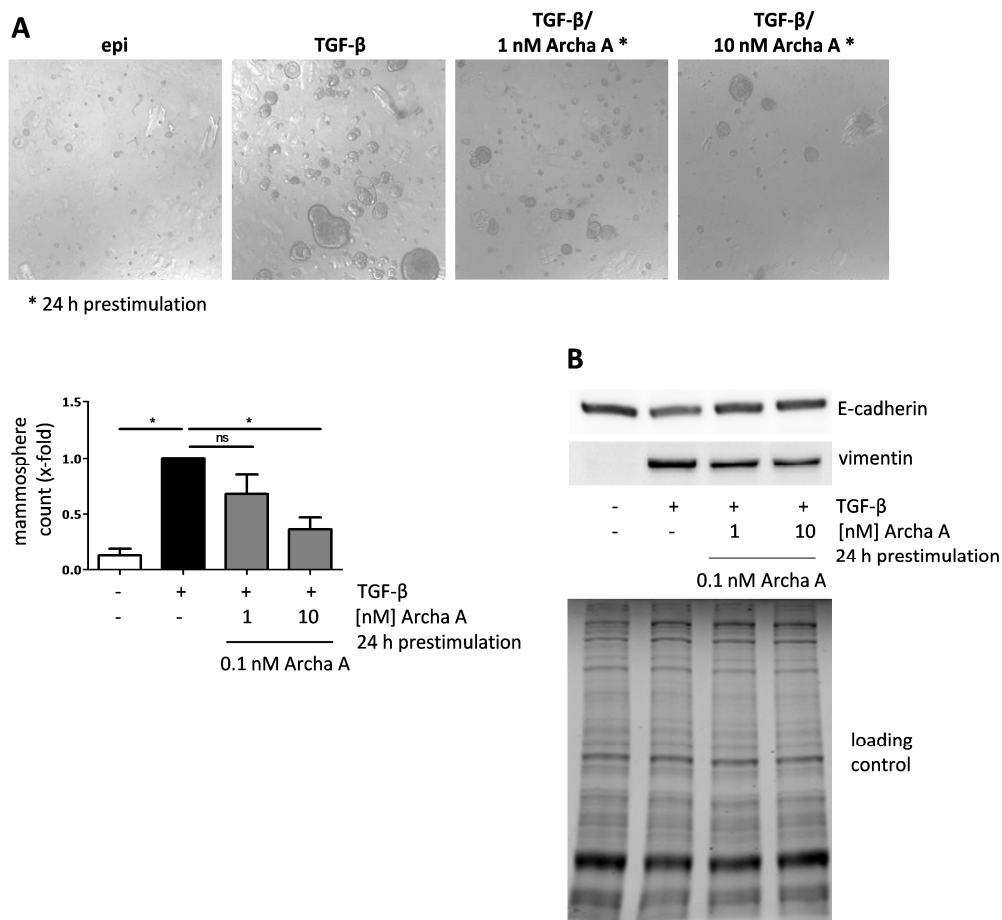


Figure 17: Effects of Archazolid A on EMT marker. (A) mRNA expression of E-cadherin, vimentin, fibronectin and N-cadherin without (epithelial, epi) and with EMT induction by 20 nM 4-OH-TX and with/without Archazolid A (Archa A) treatment in indicated concentrations is shown. (One-way ANOVA, Tukey's Multiple Comparison Test, SEM, * $p < 0.05$, ns=not significant, $n=3$). (B) Immunoblots of HMLE Twist1-ER cells without and with EMT induction by 20 nM 4-OH-TX and with/without Archazolid A in indicated concentrations probed with anti-E-cadherin, anti-claudin, anti- β -catenin, anti-fibronectin, anti-vimentin and anti- β -tubulin antibodies are shown ($n=3$). (C) Immunostainings with anti-E-cadherin, anti- β -catenin, anti-vimentin and anti-N-cadherin antibodies (green) and 5 $\mu\text{g}/\text{ml}$ Hoechst 33342 (blue) are shown. Scale bars 10 μm ($n=3$).

3.2.4 TGF- β -induced EMT is inhibited by Archazolid A

TGF- β plays an important role in EMT and possesses a crucial part in tumor progression, thus it was used as an alternative inducer for EMT (22). Confirming previous results, Archazolid A significantly inhibited the TGF- β -induced mammosphere formation (Figure 18A). In line, Archazolid A treatment was able to abrogate TGF- β -mediated decrease of E-cadherin protein expression and could also diminish enhanced vimentin expression (Figure 18B). Additionally, the EMT marker staining confirmed these results (Figure 18C). Especially for β -catenin, the TGF- β -treated HMLE Twist1-ER cells showed accumulation of β -catenin in cellular vesicles. Interestingly, Archazolid A-treated cells showed enlarged intracellular β -catenin bodies. N-cadherin signal was strongly decreased, particularly in the 10 nM Archazolid A-treated cells. These findings indicate that Archazolid A is able to successfully inhibit TGF- β -induced EMT, suggesting a general influence of V-ATPase on EMT.



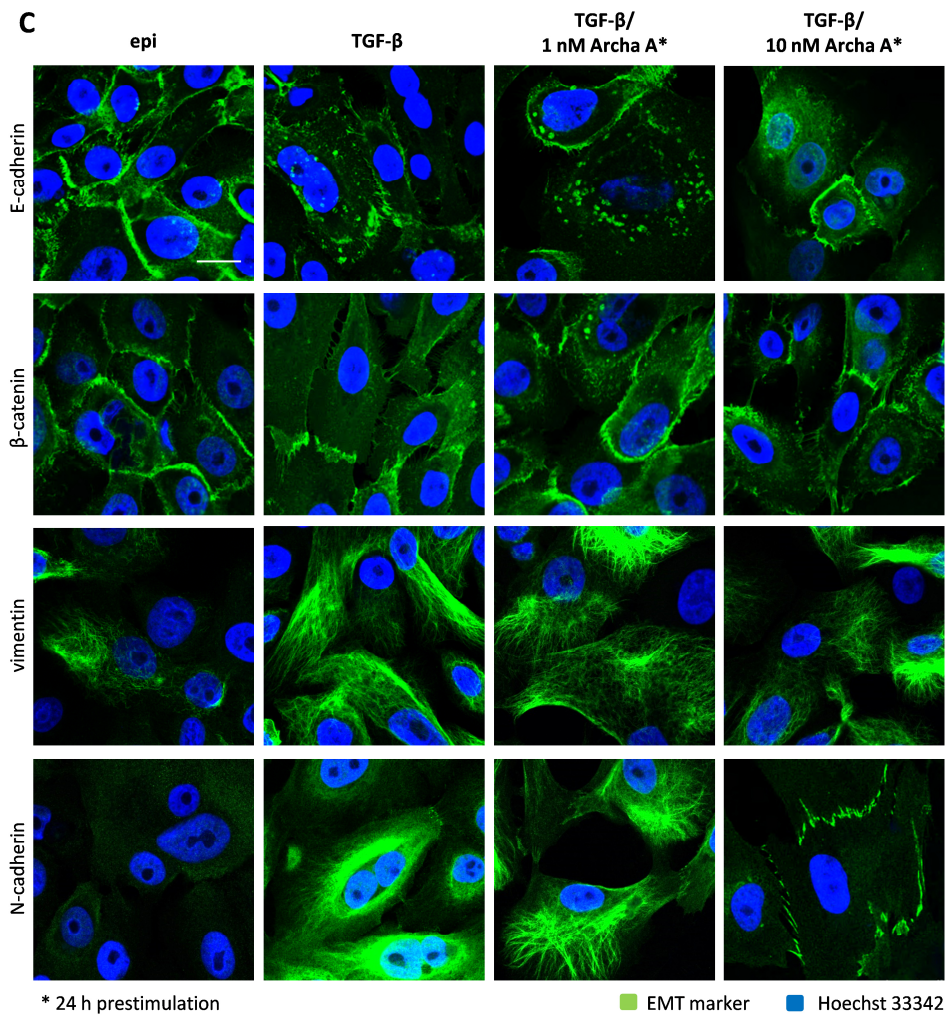


Figure 18: Archazolid A inhibits TGF- β -induced EMT. (A) Mammosphere formation without (epithelial, epi) and with EMT induction by 5 ng/ml TGF- β for 12 days and with/without Archazolid A (Archa A) treatment in indicated concentrations is shown. Graph depicts mammosphere count (> 50 μ m) normalized to TGF- β -treated cells. (One-way ANOVA, Tukey's Multiple Comparison Test, SEM, * p <0.05, ns=not significant, n =3). (B) Immunoblots of HMLE Twist1-ER cells without and with EMT induction by TGF- β and with/without Archazolid A treatment in indicated concentrations probed with anti-E-cadherin, anti-vimentin antibodies and a prestained gel as loading control are shown (n =3). (C) Immunostaining with anti-E-cadherin, anti- β -catenin, anti-vimentin and anti-N-cadherin antibodies (green) and 5 μ g/ml Hoechst 33342 (blue) are shown. Scale bars 25 μ m (n =3).

3.2.5 Archazolid A impedes Notch1-induced signaling

Notch1 signaling is also known to be regulated by endolysosomal pathways (61) and to induce EMT(62). Deregulated Notch1 signaling is implicated in CSC promotion of primary and metastatic tumors and known to regulate both: the acquisition of a mesenchymal phenotype and the formation of CSC (62, 63). In preliminary studies, we showed that basal Notch1 levels are enhanced upon Archazolid A treatment in MCF-7 and MDA-MB-231 cells (Figure 19A). EGTA-induced Notch1 signaling was abrogated upon Archazolid A treatment as shown by markedly diminished NICD (Figure 19B). In line, Notch1 staining revealed an enhanced accumulation of Notch1 in intracellular compartments by Archazolid A treatment (Figure 19C). Together, with the results from TGF- β -induced EMT, this set of data strengthens the assumption that Archazolid A in general regulates endolysosomal pathways, which are associated with EMT.

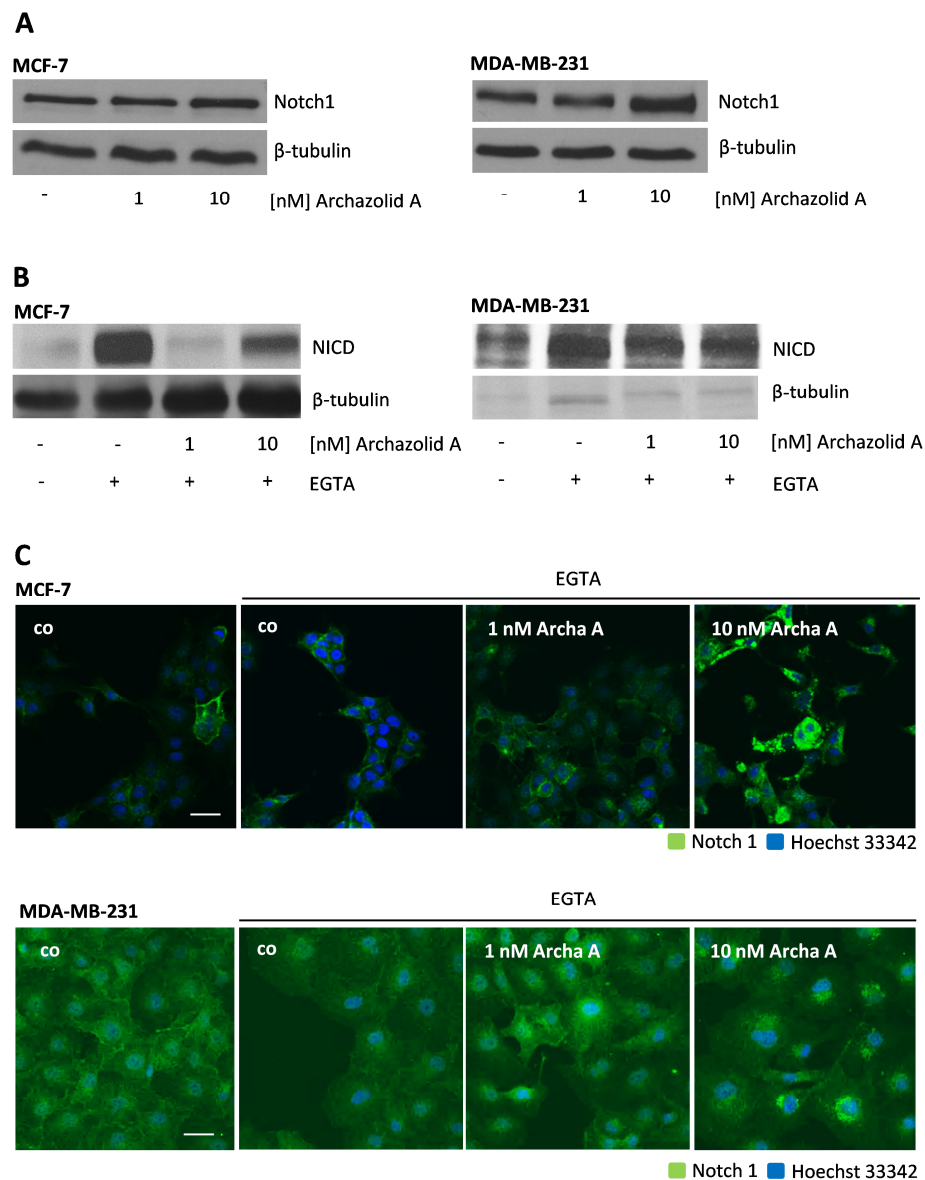


Figure 19: Notch1 signaling is diminished upon Archazolid A stimulation. (A) Immunoblots of MCF-7 and MDA-MB-231 without (co) and with Archazolid A (Archa A) treatment in indicated concentrations probed with anti-Notch1 and anti- β -tubulin antibodies control are shown (n=2). (B) Immunoblots of MCF-7 and MDA-MB-231 without (co) and with 24 h Archazolid A (1 or 10 nM) treatment and with/without subsequent 500 nM EGTA stimulation for 2.5 h is shown. Samples were probed with anti-NICD and anti- β -tubulin antibodies (n=2). (C) Immunostaining with anti-Notch1 antibody (green) and 5 μ g/ml Hoechst 33342 (blue) is shown. Scale bars 25 μ m (n=2).

3.2.6 V-ATPase knockdown inhibits EMT

In order to analyze whether the seen functional and signaling effects of Archazolid A are attributed to the V-ATPase, the V_0 subunit c of the V-ATPase, which is the binding site for Archazolid A, was knocked down. HMLE Twist1-ER cells were stably transduced with an IPTG-inducible V-ATPase shRNA vector. Out of the five V-ATPase shRNA transductions, most effective knockdown of V-ATPase shRNA was achieved in clone 1 (to 30 %) and clone 3 (to 10 %) upon IPTG treatment (Figure 20A). Downregulation of V-ATPase was confirmed by LysoTracker® staining, which showed decreased acidification of lysosomes upon IPTG treatment (Figure 20B). Notably, the mammosphere-forming potential was strongly inhibited in the V-ATPase shRNA knockdown clones (Figure 20C). Similar to Archazolid A treatment the protein expression of the EMT marker shifted to rather epithelial than mesenchymal properties, as confirmed by β -catenin and vimentin staining (Figure 20D). These findings support the assumption that V-ATPase plays a crucial role during EMT.

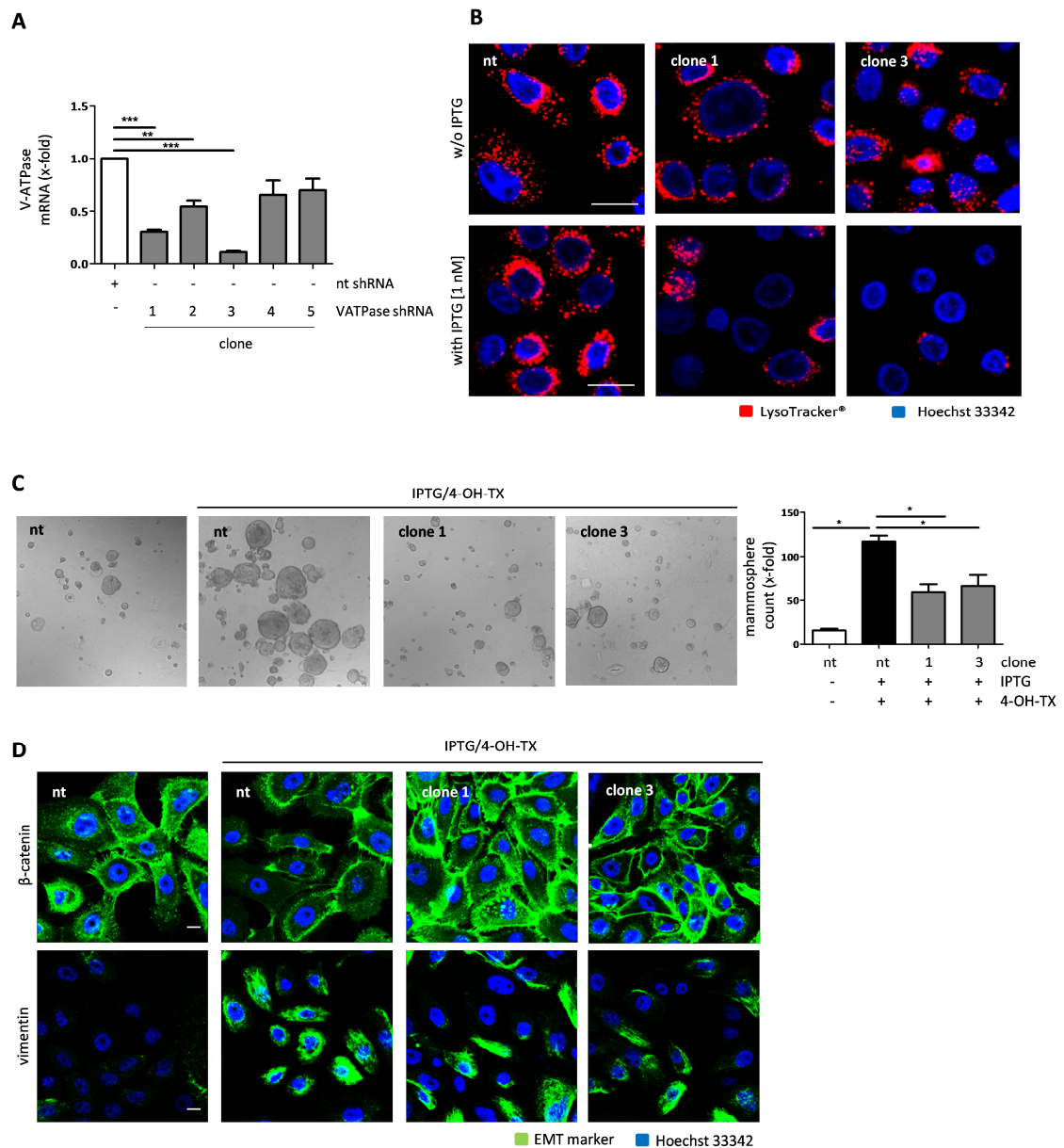


Figure 20: V-ATPase knockdown reduces mammosphere formation and promotes epithelial characteristics. (A) Expression of V-ATPase subunit c in non-targeting (nt) and V-ATPase shRNA HMLE Twist1-ER clones (1 and 3) after 1 mM IPTG treatment for 96 h is shown. (One-way ANOVA, Tukey's Multiple Comparison Test, SEM, $*p < 0.05$, $n=3$). (B) Acidic endolysosomal compartments are shown by LysoTracker[®] staining (red) in HMLE Twist1-ER cells with/without 1 mM IPTG treatment. Nuclei were stained with 5 $\mu\text{g}/\text{ml}$ Hoechst 33342 (blue). Scale bars 25 μm ($n=3$). (C) Mammosphere assay with nt shRNA cells without EMT induction and nt and V-ATPase shRNA cells with EMT induction by 4-OH-TX is shown. Graph depicts number of mammospheres counted ($> 50 \mu\text{m}$). (One-way ANOVA, Tukey's Multiple Comparison Test, SEM, $*p < 0.05$, $n=3$). (D) Immunostaining with nt shRNA cells without EMT induction and nt and V-ATPase shRNA cells with EMT induction, probed with anti- β -catenin, anti-vimentin (green) antibodies and 5 $\mu\text{g}/\text{ml}$ Hoechst 33342 (blue) is shown. Scale bars 10 μm ($n=3$).

3.2.7 E-cadherin internalization is repressed by Archazolid A

Our data convincingly demonstrated a crucial role for V-ATPase on EMT. A main event in this occurrence is the enhanced internalization and degradation of E-cadherin (64). In order to elucidate the mechanism underlying impaired EMT upon V-ATPase inhibition, surface E-cadherin internalization was analyzed. As this is a dynamic process, not only cell surface E-cadherin was detected in epithelial HMLE cells, but also a distinct part was internalized after 20 min, which was recycled back to the cell membrane (Figure 21). Expectedly, 4-OH-TX treatment diminished surface and cytosolic E-cadherin, indicating the already initiated transition. Archazolid A treatment strongly increased initial membranous E-cadherin compared to solely 4-OH-TX-treated cells. In the course of 20 min, E-cadherin was accumulated intracellularly, while it also remained at the cell surface by low dose treatment. Of note, in the 10 nM Archazolid A-treated cells, E-cadherin surface and intracellular localization was strongly diminished. Taken together, disturbed internalization as well as increased intracellular accumulation of E-cadherin upon Archazolid A treatment promotes E-cadherin patterns which resemble epithelial cells.

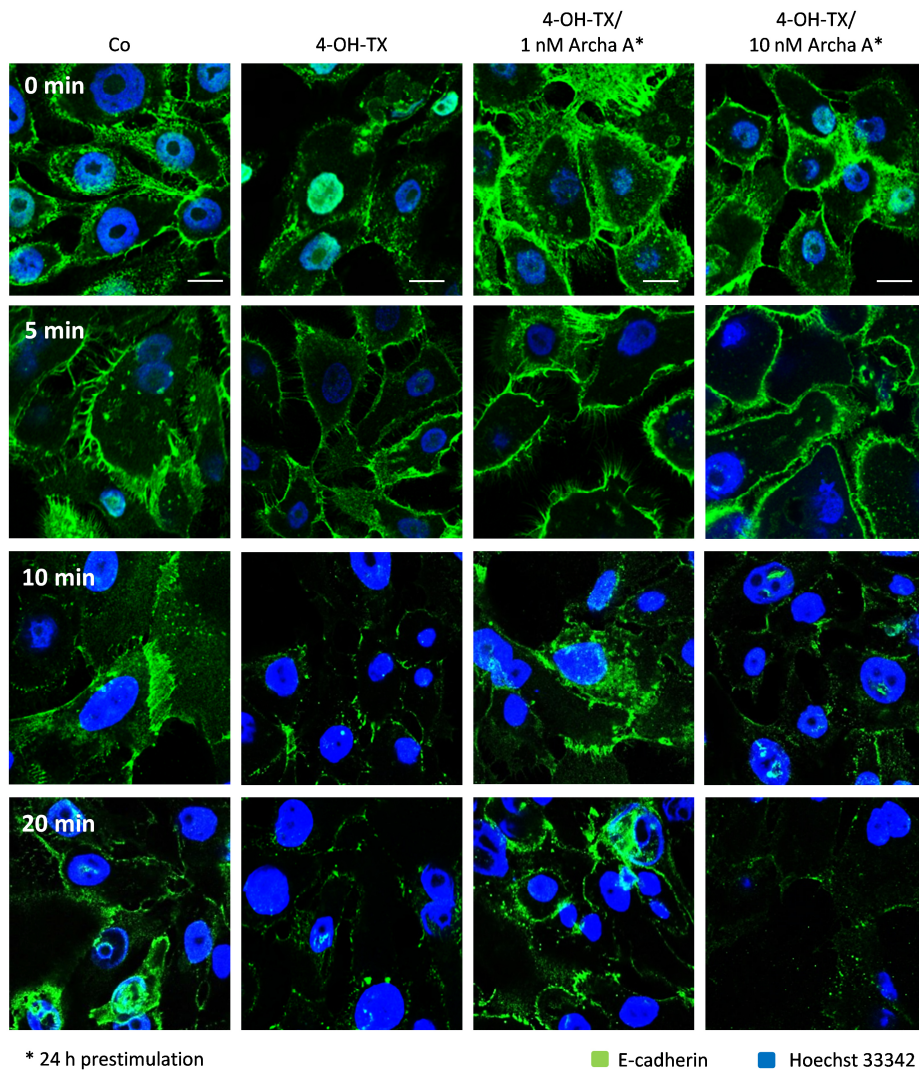


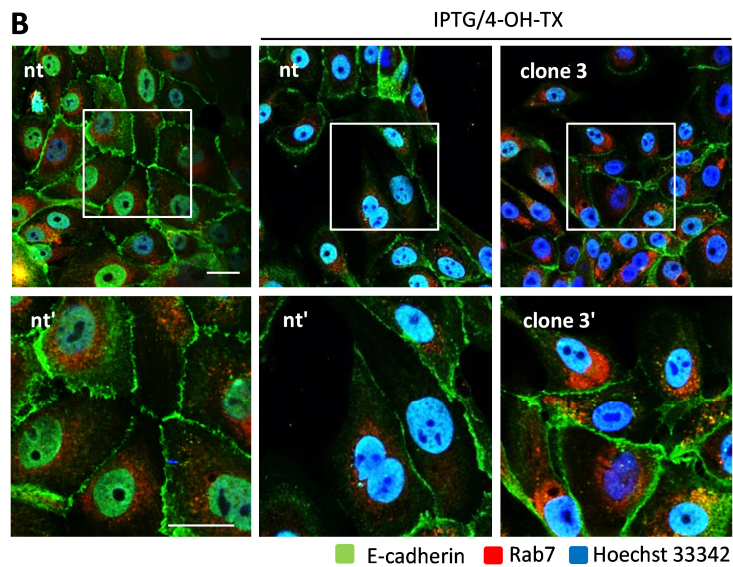
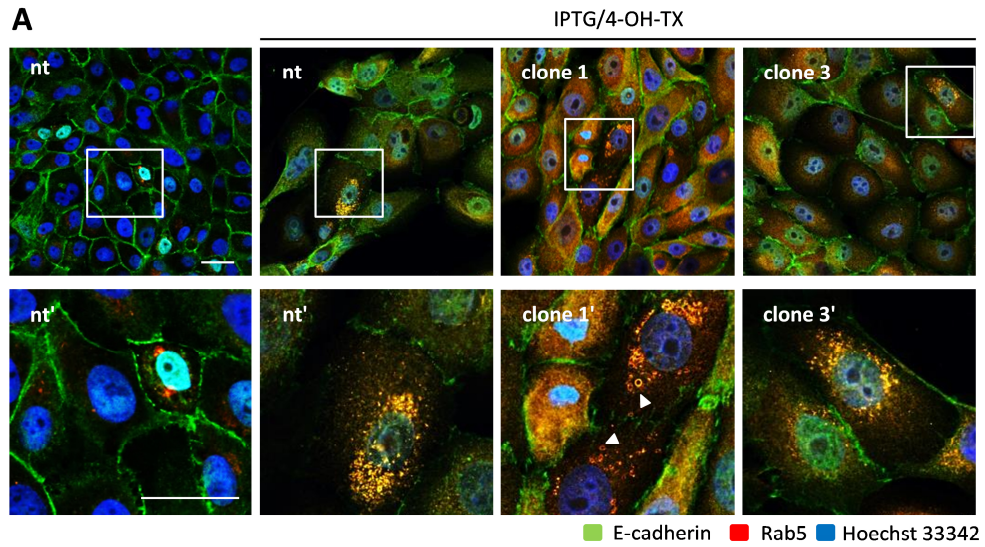
Figure 21: EMT-induced internalization of E-cadherin is diminished by Archazolid A. Surface E-cadherin (HECD1, green) recycling of HMLE Twist1-ER cells without (epithelial, epi) and with EMT induction by 4-OH-TX and with/without Archazolid A (Archa A) treatment in indicated concentrations is shown. Subsequent to surface E-cadherin staining, cells were fixed after 0, 5, 10, and 20 min of recycling at 37 °C and 5 % CO₂. Nuclei were stained with 5 µg/ml Hoechst 33342 (blue). Images were taken using Leica-SP8 confocal microscope. Scale bars 10 µm (n=3).

3.2.8 E-cadherin recycling is inhibited upon V-ATPase inhibition

In search for the cause of enhanced surface as well as intracellular E-cadherin upon V-ATPase inhibition during EMT, a more detailed analysis of the endolysosomal compartments was performed. The early endosomal marker Rab5 endorses the fusion of early endosomes, containing endocytosed molecules as E-cadherin, and thus serves to enhance their transport either back to the cell membrane or to lysosomes for degradation. In control cells, E-cadherin was localized mainly on the membrane and was also intracellularly distributed (Figure 22A). Rab5 also showed a diffuse distribution in the cell. To the contrary, in mesenchymal HMLE Twist1-ER cells, E-cadherin was strongly diminished at cell-cell contacts and localized mainly in the nuclei. Here, Rab5 was predominantly localized in perinuclear clusters congruent with E-cadherin. V-ATPase shRNA clones treated with 4-OH-TX exhibited enlarged Rab5-positive endosomes, which contained E-cadherin.

Rab7 labels late endosomes as it promotes the carriage of endosomal E-cadherin from early endosomes towards the lysosome instead of its recycling back to the cell membrane (65). In control HMLE Twist1-ER cells E-cadherin was present at cell-cell junctions, whereas Rab7 was located in the perinuclear area (Figure 22B). In mesenchymal cells, E-cadherin was distributed within the cell and located strongly in the nucleus of the cells. Also, colocalization of E-cadherin and Rab7 could be seen. Interestingly, in V-ATPase shRNA clone 3, enlarged E-cadherin- and Rab7-positive compartments were visible. Furthermore, E-cadherin was clearly increased at cell-cell contacts, while it was not colocalized with Rab7. This result was confirmed by EMT induction with TGF- β (Figure 22C). Immunostaining for the lysosomal-associated membrane glycoprotein 1 (LAMP-1) and E-cadherin were made in order to investigate lysosomal-localized E-cadherin (Figure 22D). In control cells, LAMP-1 was accumulated and localized intracellularly upon 4-OH-TX stimulation and E-cadherin was colocalized in LAMP1-positive compartments. Remarkably, the amount of E-cadherin protein on the cell surface was increased upon Archazolid A treatment. Additionally, in the Archazolid A-treated HMLE Twist1-ER cells, E-cadherin was increased not only on the cell surface but is also trapped in lysosomes, especially perinuclearly. This set of data point to the fact that the carriage of E-cadherin from

endosomal to lysosomal compartments is inhibited by V-ATPase inhibition, suggesting impeded EMT by diminished E-cadherin degradation.



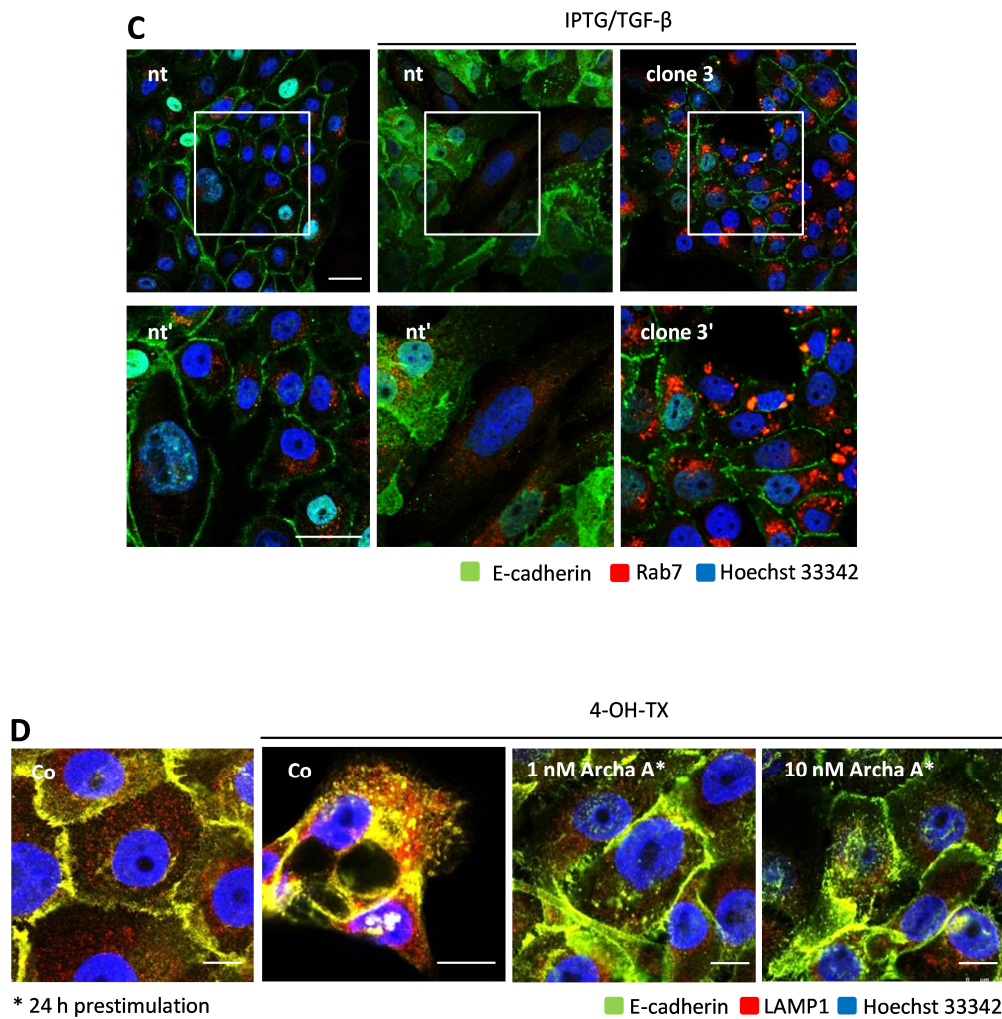


Figure 22: E-cadherin is trapped in early endosomes but is not processed to late lysosomes during EMT. (A) Immunostaining of E-cadherin (HECD1; green) and Rab5 (red) of nt shRNA cells without EMT induction and of nt and V-ATPase shRNA cells with EMT induction is shown. Colocalization (orange, arrowheads) was revealed by double immunofluorescence. Nuclei were stained with Hoechst 33342 (blue). Scale bars 25 μ m (n=2). (B, C) Immunostaining of E-cadherin (HECD1; green) and Rab7 (red) of nt shRNA cells and of nt and V-ATPase shRNA cells with EMT induction by 4-OH-TX (B) or TGF- β (C) is shown. Colocalization (orange) was revealed by double immunofluorescence. Nuclei were stained with Hoechst 33342 (blue). Scale bars 25 μ m (n=3). (D) Immunostaining of HMLE Twist1-ER cells without (co) and with EMT induction by 4-OH-TX and with/without Archazolid A (Archa A) treatment in indicated concentrations is shown for the proteins: E-cadherin (green), LAMP1 (red). Nuclei were stained with 5 μ g/ml Hoechst 33342 (blue). Merged signals are depicted in orange. Scale bars 10 μ m (n=3).

3.3 Archazolid A reduces migration and mammosphere formation of mesenchymal HMLE cells

So far, our data convincingly show that EMT and bCSC formation were successfully inhibited by V-ATPase inhibition. Yet, it is also of clinical utmost importance to target already existing, poorly accessible CSC. In order to investigate if V-ATPase inhibition exhibits a debilitating effect on preexisting CSC, fully transitioned mesenchymal HMLE cells were used. These cells comprise stem cell-like characteristics, such as enhanced motility and mammosphere-forming ability.

3.3.1 Archazolid A reduces migration of mesenchymal HMLE cells

Initially, the role of V-ATPase on the migration of mesenchymal HMLE cells was examined. Treatment with Archazolid A (1 nM and 10 nM) significantly inhibited migration as shown by Boyden chamber experiments (Figure 23A). An apoptotic effect of Archazolid A on the cells during treatment and migration could be excluded, as shown by Nicoletti assay (Figure 23B).

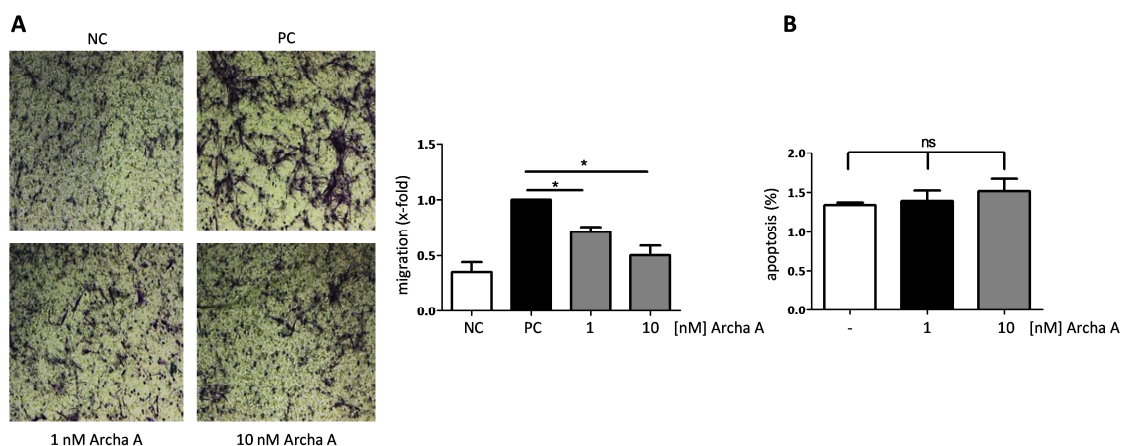


Figure 23: Archazolid A inhibits migration of mesenchymal HMLE cells. (A) Transwell migration of HMLE cells prestimulated with/without Archazolid A (1 or 10 nM) for 24 h determined by Boyden chamber experiments is shown. Graph displays the number of migrated cells after 6 h normalized to positive control (PC). For negative control (NC), medium without FCS was added. (One-way ANOVA, Tukey's Multiple Comparison Test, SEM, * $p < 0.05$, $n = 3$). (B) Apoptosis rate of HMLE cells after 24 h Archazolid A (1 nM and 10 nM) treatment is shown. (One-way ANOVA, Tukey's Multiple Comparison Test, SEM, ns=not significant, $n = 3$).

3.3.2 Archazolid A reduces mammosphere formation in mesenchymal HMLE cells

The ability of mesenchymal HMLE cells to form mammosphere formation was significantly inhibited by Archazolid A treatment (Figure 24). These results indicate an important role of V-ATPase on cancer stem cell-like traits.

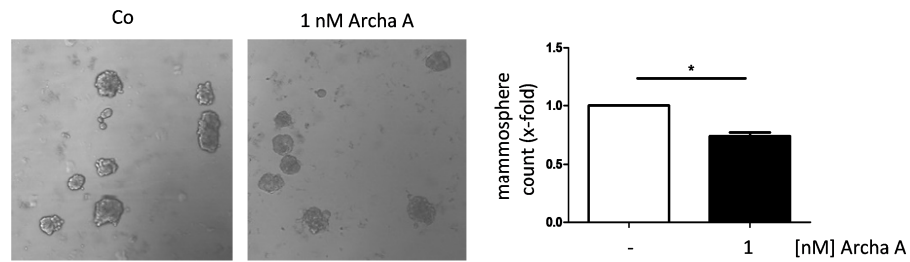


Figure 24: Archazolid A inhibits mammosphere formation of mesenchymal HMLE cells. Mammosphere formation of mesenchymal HMLE cells with/without 1 nM Archazolid A treatment for 24 h is shown. Images were taken with Zeiss LSM 510 Meta confocal microscope and mammospheres > 50 μm were counted. The graph displays the mammosphere count related to untreated control (Student's *t*-test, SEM, * $p < 0.05$, $n=3$).

DISCUSSION

4 DISCUSSION

Inhibiting the genesis of cancer stem-like cells in order to diminish progression of cancer is a very new and promising approach. In recent years, a pivotal role for EMT in cancer metastasis has been postulated. So far, only TGF- β -induced EMT inhibition was successful in clinical trials (66, 67), hence further strategies are urgently needed to overcome EMT-induced metastasis. This work introduces V-ATPase inhibition as a promising new strategy to diminish bCSC formation by impeding EMT.

4.1 EMT, CSCs and the relevance of V-ATPase in this context

EMT programs emerged as important regulators for cancer cells, for example by mediating their transition into stem-like cells. Evidence indicates that the EMT program is used by both, normal epithelial as well as neoplastic carcinoma cell populations, to gain stem cell-like traits (2, 68). In fact, pleiotropically acting transcription factors, such as Twist1, are known to induce EMT when expressed in epithelial cells and have also been linked to self-renewal programs in cancer cells. Indeed, Twist1 overexpression in epithelial HMLE Twist1-ER cells is associated with poor clinical outcome in cancers such as bladder cancer, oral squamous cell carcinoma, ovarian cancer, cervical cancer as well as breast cancer (69-73). Hence, the investigation of the Twist1-mediated EMT induction in this work is highly important in order to develop new treatment options.

Much is still to be learned about the machinery of EMT regulation. In fact, elevated V-ATPase expression and activity are well described for cells which have undergone EMT and are highly invasive (74, 75). Although, enhanced V-ATPase expression in fully transitioned mesenchymal HMLE cells could not be confirmed in this work, our results indicate increased V-ATPase activity upon EMT induction. Of note, the abrogated V-ATPase activity by Archazolid A treatment was clearly visible. To this end, our study intended to establish a new strategy to address the clinical relevant issue of targeting EMT and therefore CSCs by the inhibition of the V-ATPase.

Although, an increasing number of CSC-targeting therapies emerged in recent years, only very few showed promising results in clinic. In detail, several Notch pathway inhibitors were

clinically tested, but revealed cytotoxic effects. Yet, novel γ -secretase inhibitors in combination with chemotherapy reduced bCSCs in patients (76). Indeed, in our study we could show that Archazolid A inhibition in malignant breast cancer cells also affected the Notch1 activation, suggesting this drug to be a further potent inhibitor of CSCs. Moreover, the monoclonal antibody catumaxomab, which consists of anti-EpCAM and anti-CD3, showed improved quality of life in clinical phase II and III studies (77). A further clinically important inducer of EMT and metastasis is the cytokine TGF- β . Indeed, compounds which are able to block TGF- β -induced EMT, such as galunisertib and fresolimumab revealed successful anti-tumor activity in clinical trials (66, 67). This prompted us to investigate the role of V-ATPase in TGF- β -mediated signaling, which indeed revealed promising anti-tumor effects *in vitro*.

The encouraging, yet very few clinical reports pave the way for further therapeutic investigations on CSC therapy. In this work we show that V-ATPase inhibition interferes with diverse EMT-mediating pathways, such as Twist1, TGF- β and Notch 1. Hereby, we introduce the V-ATPase as a new druggable target for EMT inhibition and thus CSC formation and by this perform pioneer work.

4.2 V-ATPase inhibition diminishes cancer stem cell-like traits and promotes epithelial characteristics

During recent years, V-ATPase has proven to be a very promising target for cancer therapy. Yet, major part of the previous work focused on the implication of V-ATPase in cancer cell metastasis, invasion, tumor cell death and anoikis resistance (35, 43, 46, 47, 56). In fact, metastasis is the main cause for cancer-induced mortality (78). Of note, EMT is increasingly accepted to preserve a crucial role in tumor metastasis. Thus, pharmacological targeting may represent an effective strategy to inhibit metastasis. Up to now, only very few reports investigate the crosstalk between V-ATPase and EMT in cancer cells (3).

Mani *et al.* revealed that EMT induction by Twist1 or Snail1 transcription factors in human, non-tumorigenic mammary epithelial cells promotes a mesenchymal phenotype and exhibits bCSC like characteristics (2). This knowledge enables fundamental investigations during the course of EMT. Utilizing this model, research on the significance of V-ATPase during the course of EMT was successfully performed in this work.

We for the first time showed that targeting V-ATPase through specific gene knockdown or pharmacological inhibition abrogates sustainably EMT-induced bCSC formation, migration and expression of stem cell markers. In detail, this work disclosed that enhanced mammosphere formation upon EMT was abolished by Archazolid A and stable V-ATPase subunit c shRNA knockdown. Most notably, the demonstrated sustainability of this effect may improve long term survival in breast cancer patients. These findings indicate that V-ATPase is involved in the acquisition and most notably in the maintenance of bCSC. Moreover, we could show that EMT-induced downregulation of the epithelial E-cadherin, β -catenin and claudin-1 proteins was successfully abrogated by Archazolid A. Notably, mesenchymal vimentin, fibronectin and N-cadherin overexpression in cancer is correlated with metastasis and thus poor prognosis (79-84). Indeed, we could show that enhanced protein expression of these markers was strongly reduced upon V-ATPase inhibition, whereas transcriptional regulation was not influenced by V-ATPase during EMT. Therefore, V-ATPase is suggested to regulate EMT on a post-transcriptional level.

Consistent with these findings, TGF- β -mediated EMT-induction and therefore the accompanied gain of mesenchymal traits, were successfully diminished by V-ATPase inhibition. The effective decrease of mammosphere-forming ability by Archazolid A treatment suggests a promising new strategy to target metastasis. Taken together, rising evidence points to the fact that V-ATPase inhibition overall preserves epithelial characteristics in HMLE cells.

4.3 E-cadherin: the major player in V-ATPase-related EMT

A hallmark in the advent of EMT is the post-translational loss of E-cadherin, which can be used as a direct predictor of negative clinical outcome (85). Indeed, several studies showed evidence that it is of major importance for metastasis *in vitro* and *in vivo* (86-88). Onder *et al.* revealed that E-cadherin loss, and with that cell-cell dissemination, is pivotal for EMT induction in mammary epithelial breast cells (89). Notably, E-cadherin trafficking is balanced by endolysosomal pathways, which in turn are dependent on the ability of V-ATPase to acidify the respective compartments (4, 28). According to recent reports, a general influence of V-ATPase inhibition on internalization, degradation as well as recycling processes back to

the cell membrane is evident. For example, V-ATPase inhibition by Archazolid was shown to alter EGFR localization and to reduce its internalization after long time treatment (47). Moreover, it has also shown to inhibit transferrin/transferrin-R uptake in breast cancer cells (35). In order to investigate the role of V-ATPase on E-cadherin signaling during EMT, we utilized an *in vitro* EMT-mimicking model by using Twist1-inducible HMLE cells. Substantial E-cadherin repression upon EMT induction occurred not until 8 days after initial Twist1 translocation into the nucleus. This delayed response, can be explained by the fact that Twist1 binds to the E-box on the Snail2 promoter to activate its transcription. Only after Snail2 expression, E-cadherin expression is suppressed (32). Interestingly, Twist1-mediated EMT induction reduced cell surface E-cadherin compared to epithelial control, whereas treatment with Archazolid A during EMT increased surface E-cadherin as well as enhanced intracellular E-cadherin.

Rab5 is known to be the major regulator of endocytosis by controlling the biogenesis and fate of early endosomes. From here, E-cadherin is either recycled back to the plasma membrane or degraded by the lysosomal pathway, which in turn is mediated by Rab7 (90). In fact, our presented results indicate a pivotal role for V-ATPase-mediated endolysosomal shuttling of E-cadherin. In detail, upon V-ATPase inhibition, E-cadherin remained in Rab5-positive early endosomes and was not translocated to lysosomal compartments via the Rab5-Rab7-LAMP1 axis. Hence, intracellular accumulation of E-cadherin presumably impeded further internalization from cell surface. It remains to be elucidated, if endosomal E-cadherin is shuttled back to the cell membrane, possibly by a delayed recycling or permanently remains in the endosomes (Figure 25). Therefore, the velocity and directions of E-cadherin trafficking may be investigated by live cell E-cadherin imaging. In line with Onder *et al.*, we confirm that deprivation of E-cadherin is necessary to induce EMT and a sole disruption of surface E-cadherin while protein levels remain high, is not sufficient (89).

Remarkably, we revealed in this work the underlying mechanism of how V-ATPase regulates E-cadherin dynamics. We were able to show, that pharmacological V-ATPase inhibition results in preserved E-cadherin protein and therefore supports the epithelial-like phenotype. By this, the diminished functional effects on mammosphere formation and migration can be explained.

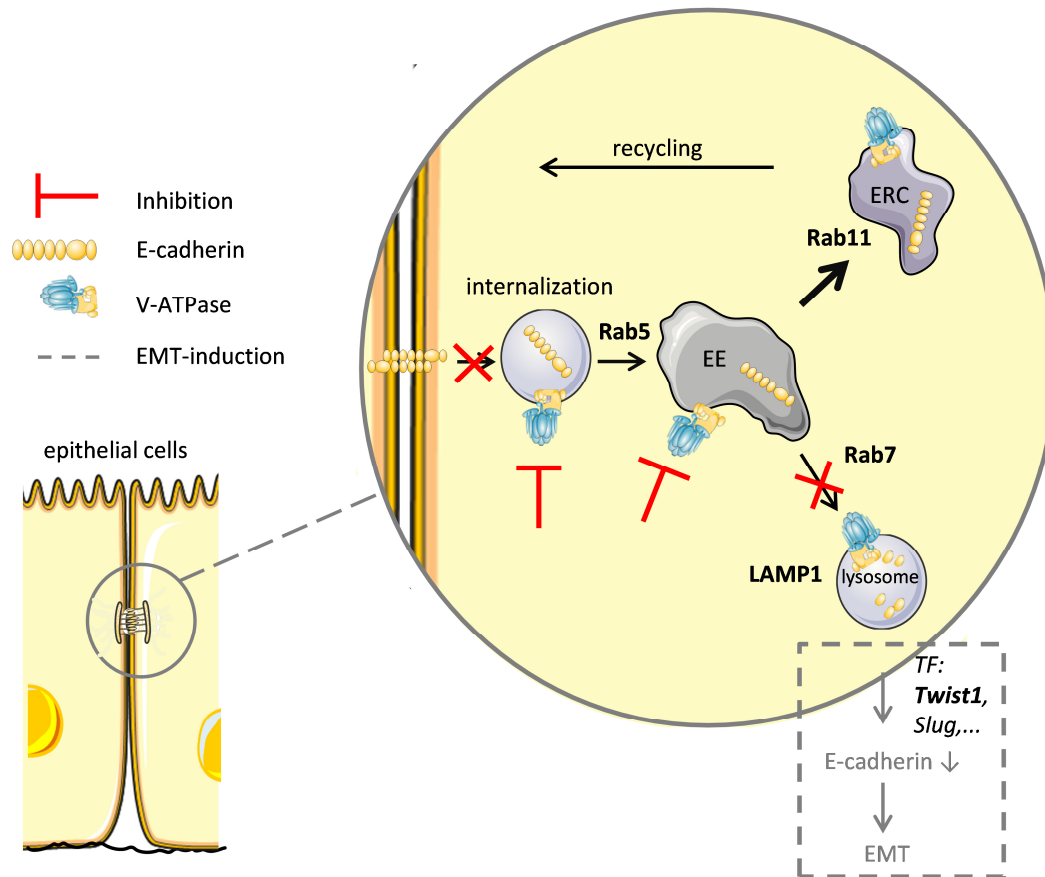


Figure 25: Proposed influence of V-ATPase inhibition on E-cadherin recycling. After E-cadherin internalization, endocytic vesicles fuse with the early endosome (EE), where proteins destined for degradation are sorted and transported either to the lysosome or are recycled back to the cell membrane. Our results suggest that V-ATPase inhibition prevents the internalization of E-cadherin. Furthermore, we postulate that in the rapid dynamic process of E-cadherin recycling, already internalized surface protein at the time of V-ATPase inhibition is trapped in Rab5-positive EE and is not delivered to lysosomes. From here, E-cadherin may move back to the cell surface by either taking a fast recycling route directly from the EE or a slower route via the ERC. However, this needs to be elucidated in future studies. EE, early endosome; ERC, endocytic recycling compartment; LAMP1, lysosomal associated membrane protein 1; EMT, epithelial-mesenchymal transition; TF, transcription factor.

4.4 Archazolid A inhibits preexisting mesenchymal traits

Besides inhibiting EMT and therefore CSC formation, targeting of already existing CSCs represents an important goal regarding the improvement of cancer therapy. So far, the genesis of EMT-induced CSCs has been discussed. However, recent reports point to the fact, that V-ATPase inhibition is also a promising approach to target preexisting CSCs (74, 75). Indeed, inhibiting V-ATPase in embryonic rhabdomyosarcoma disease has shown to eradicate CSCs (75). Furthermore, pharmacological V-ATPase inhibition by bafilomycin A1, a first generation V-ATPase inhibitor, and its genetic knockdown diminished glioblastoma neurosphere forming ability and suppressed expression of stem cell markers (74). In this work, we introduce the inhibition of V-ATPase not only as a novel strategy to abrogate EMT-mediated CSC formation, but also as a pharmacologically accessible target to diminish preexisting malignant CSCs. In detail, we successfully showed that Archazolid A impedes migration and mammosphere formation in mesenchymal CSC-like HMLE cells, suggesting a requirement for proton pump activity in mesenchymal breast epithelia cells.

4.5 Targeting of EMT in clinic: advantages and limitations

In recent years, a growing body of evidence revealed a clinical relevance for EMT-induced cancer cell intravasation and metastatic dissemination in the progression of breast cancer (91-93). Thus, the inhibition of EMT induction is suggested as a potent new treatment strategy for patients with high risk of developing metastasis. Yet, these approaches have advantages but also possible limitations in the context of developing effective clinical agents. In detail, targeting EMT induction is severely limited for patients with preexisting metastasis at the time of diagnosis. Yet, agents like Archazolid A might still be of benefit, as they also affect malignant traits of preexisting stem-like cells. Hence, Archazolid A may be highly effective as adjuvant therapy to prevent early metastasis.

Furthermore, the success of the therapy might also be limited as other EMT-inducing pathways arise upon suppression of another. This work focused mainly on the repercussions of Twist1 and TGF- β signaling inhibition. One potential alternative EMT-inducing pathway

may be Notch1 signaling. In fact, first hints indicate that Notch1 signaling induction can be diminished upon pharmacological inhibition of the V-ATPase.

A further implication of impeding EMT is associated with resistance to chemotherapy and radiation. For example, non-small cell lung carcinoma cells appear to be less sensitive to cisplatin and paclitaxel treatment upon EMT induction with either EGF or TGF- β (94, 95). The approach of EMT inhibition as early adjuvant therapy may increase the sensitivity of cancer cells to chemotherapeutics, thereby shortening the duration of therapy and reducing the possibility of relapse.

By discussing the benefits for EMT targeting, it has to be taken into account that by this, epithelial traits are promoted and mesenchymal characteristics are impeded, thereby encouraging MET. MET is a process, which enables circulating tumor cells to exit the bloodstream and to form metastatic tumors (96). At the same time, targeting MET may promote the mesenchymal phenotype and thus drive therapy resistance in premetastatic cancers. These issues necessitate a personalized cancer treatment, depending on the cancer type and stage of cancer progression.

Furthermore, targeting existing or the development of cancer stem cells is a highly sensitive approach. Obtaining specificity is urgently required in order to spare normal stem cells. One successful attempt to acquire specificity in therapy was the linkage between a specific monoclonal antibody which recognizes known bCSC markers and an anti-metastatic prodrug (97, 98).

Conclusively, EMT appears to have a pivotal role in cancer metastasis. Nevertheless, in future it will be of outmost importance to have a better understanding of cancers in which EMT is essential. The identification of appropriate cancer stage-dependent biomarkers may be a key step towards the clinical use of pharmacological agents, leading to personalized cancer treatment.

4.6 Conclusion and further perspectives

This study for the first time presents a novel and pivotal function of V-ATPase in EMT-induced motility and bCSC formation. V-ATPase was shown to be a major determinant of E-cadherin recycling processes. Pharmacological and genetic targeting of V-ATPase during EMT remarkably abrogated malignant stem-like traits. Furthermore, Archazolid A successfully inhibited migration and mammosphere formation in cancer stem-like cells.

This study shows highly promising results in targeting EMT-associated stemness by V-ATPase inhibition. Therefore it enables promising new options for further research on the *in vivo* efficacy. Additionally, combinatorial treatment of clinically approved chemotherapeutics with Archazolid A as adjuvant therapy in regards of diminished resistance remains a highly worthwhile approach for future studies.

Concluding, this work provides first evidence for targeting EMT by V-ATPase inhibition as a promising approach to inhibit malignant cancer stem-like traits in mammary breast epithelial cells *in vitro*. Hence, this may evolve as highly beneficial in therapeutic targeting of breast cancer in patients with a high potential to develop lethal metastasis.

REFERENCES

5 REFERENCES

1. Al-Hajj M, Wicha MS, Benito-Hernandez A, Morrison SJ, & Clarke MF (2003) Prospective identification of tumorigenic breast cancer cells. *Proc Natl Acad Sci U S A* 100(7):3983-3988.
2. Mani SA, *et al.* (2008) The epithelial-mesenchymal transition generates cells with properties of stem cells. *Cell* 133(4):704-715.
3. Cao X, *et al.* (2012) V-ATPase promotes transforming growth factor-beta-induced epithelial-mesenchymal transition of rat proximal tubular epithelial cells. *Am J Physiol Renal Physiol* 302(9):F1121-1132.
4. Cotter K, Stransky L, McGuire C, & Forgac M (2015) Recent Insights into the Structure, Regulation, and Function of the V-ATPases. *Trends Biochem Sci* 40(10):611-622.
5. Torre LA, *et al.* (2015) Global cancer statistics, 2012. *CA: a cancer journal for clinicians* 65(2):87-108.
6. Sims AH, Howell A, Howell SJ, & Clarke RB (2007) Origins of breast cancer subtypes and therapeutic implications. *Nature clinical practice. Oncology* 4(9):516-525.
7. Shekhar MP (2011) Drug resistance: challenges to effective therapy. *Curr Cancer Drug Targets* 11(5):613-623.
8. Jordan CT, Guzman ML, & Noble M (2006) Cancer stem cells. *The New England journal of medicine* 355(12):1253-1261.
9. Polyak K & Weinberg RA (2009) Transitions between epithelial and mesenchymal states: acquisition of malignant and stem cell traits. *Nature reviews. Cancer* 9(4):265-273.
10. Reya T, Morrison SJ, Clarke MF, & Weissman IL (2001) Stem cells, cancer, and cancer stem cells. *Nature* 414(6859):105-111.
11. Scheel C & Weinberg RA (2011) Phenotypic plasticity and epithelial-mesenchymal transitions in cancer and normal stem cells? *International journal of cancer. Journal international du cancer* 129(10):2310-2314.
12. Martin A & Cano A (2010) Tumorigenesis: Twist1 links EMT to self-renewal. *Nature cell biology* 12(10):924-925.
13. Ansieau S, *et al.* (2008) Induction of EMT by twist proteins as a collateral effect of tumor-promoting inactivation of premature senescence. *Cancer cell* 14(1):79-89.
14. Yang J, *et al.* (2004) Twist, a master regulator of morphogenesis, plays an essential role in tumor metastasis. *Cell* 117(7):927-939.
15. Morel AP, *et al.* (2008) Generation of breast cancer stem cells through epithelial-mesenchymal transition. *PloS one* 3(8):e2888.
16. Martin-Belmonte F & Perez-Moreno M (2012) Epithelial cell polarity, stem cells and cancer. *Nature reviews. Cancer* 12(1):23-38.
17. Thiery JP, Acloque H, Huang RY, & Nieto MA (2009) Epithelial-mesenchymal transitions in development and disease. *Cell* 139(5):871-890.
18. Kalluri R & Weinberg RA (2009) The basics of epithelial-mesenchymal transition. *The Journal of clinical investigation* 119(6):1420-1428.
19. Shi Y & Massague J (2003) Mechanisms of TGF-beta signaling from cell membrane to the nucleus. *Cell* 113(6):685-700.
20. Massague J (2008) TGFbeta in Cancer. *Cell* 134(2):215-230.

21. Katsuno Y, Lamouille S, & Derynck R (2013) TGF-beta signaling and epithelial-mesenchymal transition in cancer progression. *Current opinion in oncology* 25(1):76-84.
22. Xu J, Lamouille S, & Derynck R (2009) TGF-beta-induced epithelial to mesenchymal transition. *Cell Res* 19(2):156-172.
23. Espinoza I, Pochampally R, Xing F, Watabe K, & Miele L (2013) Notch signaling: targeting cancer stem cells and epithelial-to-mesenchymal transition. *OncoTargets and therapy* 6:1249-1259.
24. Gumbiner BM (1996) Cell adhesion: the molecular basis of tissue architecture and morphogenesis. *Cell* 84(3):345-357.
25. Nagafuchi A, Shirayoshi Y, Okazaki K, Yasuda K, & Takeichi M (1987) Transformation of cell adhesion properties by exogenously introduced E-cadherin cDNA. *Nature* 329(6137):341-343.
26. van Roy F & Berx G (2008) The cell-cell adhesion molecule E-cadherin. *Cellular and molecular life sciences : CMLS* 65(23):3756-3788.
27. Bryant DM & Stow JL (2004) The ins and outs of E-cadherin trafficking. *Trends Cell Biol* 14(8):427-434.
28. Le TL, Yap AS, & Stow JL (1999) Recycling of E-cadherin: a potential mechanism for regulating cadherin dynamics. *The Journal of cell biology* 146(1):219-232.
29. Batlle E, *et al.* (2000) The transcription factor snail is a repressor of E-cadherin gene expression in epithelial tumour cells. *Nat Cell Biol* 2(2):84-89.
30. Hajra KM, Chen DY, & Fearon ER (2002) The SLUG zinc-finger protein represses E-cadherin in breast cancer. *Cancer research* 62(6):1613-1618.
31. Eger A, *et al.* (2005) DeltaEF1 is a transcriptional repressor of E-cadherin and regulates epithelial plasticity in breast cancer cells. *Oncogene* 24(14):2375-2385.
32. Casas E, *et al.* (2011) Snail2 is an essential mediator of Twist1-induced epithelial mesenchymal transition and metastasis. *Cancer research* 71(1):245-254.
33. Bolos V, *et al.* (2003) The transcription factor Slug represses E-cadherin expression and induces epithelial to mesenchymal transitions: a comparison with Snail and E47 repressors. *Journal of cell science* 116(Pt 3):499-511.
34. Cheng CW, *et al.* (2001) Mechanisms of inactivation of E-cadherin in breast carcinoma: modification of the two-hit hypothesis of tumor suppressor gene. *Oncogene* 20(29):3814-3823.
35. Schneider LS, *et al.* (2015) Vacuolar-ATPase Inhibition Blocks Iron Metabolism to Mediate Therapeutic Effects in Breast Cancer. *Cancer research* 75(14):2863-2874.
36. Palacios F, Tushir JS, Fujita Y, & D'Souza-Schorey C (2005) Lysosomal targeting of E-cadherin: a unique mechanism for the down-regulation of cell-cell adhesion during epithelial to mesenchymal transitions. *Mol Cell Biol* 25(1):389-402.
37. Forgac M (2007) Vacuolar ATPases: rotary proton pumps in physiology and pathophysiology. *Nature reviews. Molecular cell biology* 8(11):917-929.
38. Breton S & Brown D (2013) Regulation of luminal acidification by the V-ATPase. *Physiology* 28(5):318-329.
39. Sennoune SR, *et al.* (2004) Vacuolar H⁺-ATPase in human breast cancer cells with distinct metastatic potential: distribution and functional activity. *American journal of physiology. Cell physiology* 286(6):C1443-1452.

40. Martinez-Zaguilan R, Lynch RM, Martinez GM, & Gillies RJ (1993) Vacuolar-type H(+)-ATPases are functionally expressed in plasma membranes of human tumor cells. *The American journal of physiology* 265(4 Pt 1):C1015-1029.
41. Sennoune SR, Luo D, & Martinez-Zaguilan R (2004) Plasmalemmal vacuolar-type H+-ATPase in cancer biology. *Cell biochemistry and biophysics* 40(2):185-206.
42. Michel V, Licon-Munoz Y, Trujillo K, Bisoffi M, & Parra KJ (2013) Inhibitors of vacuolar ATPase proton pumps inhibit human prostate cancer cell invasion and prostate-specific antigen expression and secretion. *International journal of cancer. Journal international du cancer* 132(2):E1-10.
43. Hinton A, et al. (2009) Function of a subunit isoforms of the V-ATPase in pH homeostasis and in vitro invasion of MDA-MB231 human breast cancer cells. *The Journal of biological chemistry* 284(24):16400-16408.
44. Xu J, et al. (2012) Expression and functional role of vacuolar H(+)-ATPase in human hepatocellular carcinoma. *Carcinogenesis* 33(12):2432-2440.
45. Chung C, et al. (2011) The vacuolar-ATPase modulates matrix metalloproteinase isoforms in human pancreatic cancer. *Laboratory investigation; a journal of technical methods and pathology* 91(5):732-743.
46. Cotter K, et al. (2015) Activity of plasma membrane V-ATPases is critical for the invasion of MDA-MB231 breast cancer cells. *J Biol Chem* 290(6):3680-3692.
47. Wiedmann RM, et al. (2012) The V-ATPase-inhibitor archazolid abrogates tumor metastasis via inhibition of endocytic activation of the Rho-GTPase Rac1. *Cancer research* 72(22):5976-5987.
48. von Schwarzenberg K, et al. (2013) Mode of cell death induction by pharmacological vacuolar H+-ATPase (V-ATPase) inhibition. *The Journal of biological chemistry* 288(2):1385-1396.
49. Lu Q, et al. (2013) The expression of V-ATPase is associated with drug resistance and pathology of non-small-cell lung cancer. *Diagnostic pathology* 8:145.
50. Huss M, et al. (2005) Archazolid and apicularen: novel specific V-ATPase inhibitors. *BMC biochemistry* 6:13.
51. Huss M & Wieczorek H (2009) Inhibitors of V-ATPases: old and new players. *The Journal of experimental biology* 212(Pt 3):341-346.
52. Sasse F, Steinmetz H, Hofle G, & Reichenbach H (2003) Archazolids, new cytotoxic macrolactones from *Archangium gephyra* (Myxobacteria). Production, isolation, physico-chemical and biological properties. *The Journal of antibiotics* 56(6):520-525.
53. Menche D, Hassfeld J, Li J, Mayer K, & Rudolph S (2009) Modular total synthesis of archazolid A and B. *The Journal of organic chemistry* 74(19):7220-7229.
54. Bockelmann S, et al. (2010) Archazolid A binds to the equatorial region of the c-ring of the vacuolar H+-ATPase. *The Journal of biological chemistry* 285(49):38304-38314.
55. Zhang S, et al. (2015) Anti-leukemic effects of the V-ATPase inhibitor Archazolid A. *Oncotarget* 6(41):43508-43528.
56. Schempp CM, et al. (2014) V-ATPase inhibition regulates anoikis resistance and metastasis of cancer cells. *Molecular cancer therapeutics* 13(4):926-937.
57. Bradford MM (1976) A rapid and sensitive method for the quantitation of microgram quantities of protein utilizing the principle of protein-dye binding. *Anal Biochem* 72:248-254.

58. Fleige S, *et al.* (2006) Comparison of relative mRNA quantification models and the impact of RNA integrity in quantitative real-time RT-PCR. *Biotechnol Lett* 28(19):1601-1613.
59. Dontu G, *et al.* (2003) In vitro propagation and transcriptional profiling of human mammary stem/progenitor cells. *Genes Dev* 17(10):1253-1270.
60. Nicoletti I, Migliorati G, Pagliacci MC, Grignani F, & Riccardi C (1991) A rapid and simple method for measuring thymocyte apoptosis by propidium iodide staining and flow cytometry. *J Immunol Methods* 139(2):271-279.
61. Fortini ME & Bilder D (2009) Endocytic regulation of Notch signaling. *Current opinion in genetics & development* 19(4):323-328.
62. Wang Z, Li Y, Kong D, & Sarkar FH (2010) The role of Notch signaling pathway in epithelial-mesenchymal transition (EMT) during development and tumor aggressiveness. *Current drug targets* 11(6):745-751.
63. Wang Z, Li Y, Banerjee S, & Sarkar FH (2009) Emerging role of Notch in stem cells and cancer. *Cancer letters* 279(1):8-12.
64. Manuel Iglesias J, *et al.* (2013) Mammosphere formation in breast carcinoma cell lines depends upon expression of E-cadherin. *PLoS one* 8(10):e77281.
65. Pfeffer SR (2001) Rab GTPases: specifying and deciphering organelle identity and function. *Trends Cell Biol* 11(12):487-491.
66. Morris JC, *et al.* (2014) Phase I study of GC1008 (fresolimumab): a human anti-transforming growth factor-beta (TGFbeta) monoclonal antibody in patients with advanced malignant melanoma or renal cell carcinoma. *PLoS one* 9(3):e90353.
67. Herbertz S, *et al.* (2015) Clinical development of galunisertib (LY2157299 monohydrate), a small molecule inhibitor of transforming growth factor-beta signaling pathway. *Drug design, development and therapy* 9:4479-4499.
68. Shimono Y, *et al.* (2009) Downregulation of miRNA-200c links breast cancer stem cells with normal stem cells. *Cell* 138(3):592-603.
69. Wallerand H, *et al.* (2010) The epithelial-mesenchymal transition-inducing factor TWIST is an attractive target in advanced and/or metastatic bladder and prostate cancers. *Urologic oncology* 28(5):473-479.
70. da Silva SD, *et al.* (2014) TWIST1 is a molecular marker for a poor prognosis in oral cancer and represents a potential therapeutic target. *Cancer* 120(3):352-362.
71. Hosono S, *et al.* (2007) Expression of Twist increases the risk for recurrence and for poor survival in epithelial ovarian carcinoma patients. *British journal of cancer* 96(2):314-320.
72. Shibata K, *et al.* (2008) Twist expression in patients with cervical cancer is associated with poor disease outcome. *Annals of oncology : official journal of the European Society for Medical Oncology / ESMO* 19(1):81-85.
73. Martin TA, Goyal A, Watkins G, & Jiang WG (2005) Expression of the transcription factors snail, slug, and twist and their clinical significance in human breast cancer. *Annals of surgical oncology* 12(6):488-496.
74. Di Cristofori A, *et al.* (2015) The vacuolar H⁺ ATPase is a novel therapeutic target for glioblastoma. *Oncotarget* 6(19):17514-17531.

75. Salerno M, *et al.* (2014) Impairment of lysosomal activity as a therapeutic modality targeting cancer stem cells of embryonal rhabdomyosarcoma cell line RD. *PloS one* 9(10):e110340.
76. Schott AF, *et al.* (2013) Preclinical and clinical studies of gamma secretase inhibitors with docetaxel on human breast tumors. *Clinical cancer research : an official journal of the American Association for Cancer Research* 19(6):1512-1524.
77. Wimberger P, *et al.* (2012) Deterioration in quality of life (QoL) in patients with malignant ascites: results from a phase II/III study comparing paracentesis plus catumaxomab with paracentesis alone. *Annals of oncology : official journal of the European Society for Medical Oncology / ESMO* 23(8):1979-1985.
78. Chaffer CL & Weinberg RA (2011) A perspective on cancer cell metastasis. *Science* 331(6024):1559-1564.
79. Fernandez-Garcia B, *et al.* (2014) Expression and prognostic significance of fibronectin and matrix metalloproteases in breast cancer metastasis. *Histopathology* 64(4):512-522.
80. Liu CY, Lin HH, Tang MJ, & Wang YK (2015) Vimentin contributes to epithelial-mesenchymal transition cancer cell mechanics by mediating cytoskeletal organization and focal adhesion maturation. *Oncotarget* 6(18):15966-15983.
81. Satelli A & Li S (2011) Vimentin in cancer and its potential as a molecular target for cancer therapy. *Cellular and molecular life sciences : CMLS* 68(18):3033-3046.
82. Otsuki S, *et al.* (2011) Vimentin expression is associated with decreased survival in gastric cancer. *Oncology reports* 25(5):1235-1242.
83. Wang M, *et al.* (2016) N-cadherin promotes epithelial-mesenchymal transition and cancer stem cell-like traits via ErbB signaling in prostate cancer cells. *International journal of oncology* 48(2):595-606.
84. Yan X, *et al.* (2015) N-cadherin, a novel prognostic biomarker, drives malignant progression of colorectal cancer. *Molecular medicine reports* 12(2):2999-3006.
85. Zhai X, *et al.* (2014) Abnormal expression of EMT-related proteins, S100A4, vimentin and E-cadherin, is correlated with clinicopathological features and prognosis in HCC. *Med Oncol* 31(6):970.
86. Schipper JH, *et al.* (1991) E-cadherin expression in squamous cell carcinomas of head and neck: inverse correlation with tumor dedifferentiation and lymph node metastasis. *Cancer research* 51(23 Pt 1):6328-6337.
87. Umbas R, *et al.* (1994) Decreased E-cadherin expression is associated with poor prognosis in patients with prostate cancer. *Cancer research* 54(14):3929-3933.
88. Yonemura Y, *et al.* (1995) Decreased E-cadherin expression correlates with poor survival in patients with gastric cancer. *Anal Cell Pathol* 8(2):177-190.
89. Onder TT, *et al.* (2008) Loss of E-cadherin promotes metastasis via multiple downstream transcriptional pathways. *Cancer research* 68(10):3645-3654.
90. Feng Y, Press B, & Wandinger-Ness A (1995) Rab 7: an important regulator of late endocytic membrane traffic. *The Journal of cell biology* 131(6 Pt 1):1435-1452.
91. Bonnomet A, *et al.* (2012) A dynamic in vivo model of epithelial-to-mesenchymal transitions in circulating tumor cells and metastases of breast cancer. *Oncogene* 31(33):3741-3753.

92. Trimboli AJ, *et al.* (2008) Direct evidence for epithelial-mesenchymal transitions in breast cancer. *Cancer research* 68(3):937-945.
93. Sarrio D, *et al.* (2008) Epithelial-mesenchymal transition in breast cancer relates to the basal-like phenotype. *Cancer research* 68(4):989-997.
94. Thomson S, Petti F, Sujka-Kwok I, Epstein D, & Haley JD (2008) Kinase switching in mesenchymal-like non-small cell lung cancer lines contributes to EGFR inhibitor resistance through pathway redundancy. *Clinical & experimental metastasis* 25(8):843-854.
95. Shintani Y, *et al.* (2011) Epithelial to mesenchymal transition is a determinant of sensitivity to chemoradiotherapy in non-small cell lung cancer. *The Annals of thoracic surgery* 92(5):1794-1804; discussion 1804.
96. Yao D, Dai C, & Peng S (2011) Mechanism of the mesenchymal-epithelial transition and its relationship with metastatic tumor formation. *Molecular cancer research : MCR* 9(12):1608-1620.
97. Riechelmann H, *et al.* (2008) Phase I trial with the CD44v6-targeting immunoconjugate bivatuzumab mertansine in head and neck squamous cell carcinoma. *Oral oncology* 44(9):823-829.
98. Mau-Sorensen M, *et al.* (2015) A phase I trial of intravenous catumaxomab: a bispecific monoclonal antibody targeting EpCAM and the T cell coreceptor CD3. *Cancer chemotherapy and pharmacology* 75(5):1065-1073.

APPENDIX

6 APPENDIX

6.1 Abbreviations

4-OH-TX	4-hydroxytamoxifen
ANOVA	Analysis Of Variance
APS	Ammoniumpersulfat
bCSC	Breast cancer stem cell
bFGF	Basic Fibroblast Growth Factor
BPE	Bovine Pituitary Extract
BSA	Bovine Serum Albumin
DMSO	Dimethylsulfoxide
DNA	Deoxyribonucleic acid
DTT	Dithiothreitol
ECL	Enhanced Chemiluminescence
ECM	Extracellular matrix
EDTA	Ethylenediaminetetraacetic acid
EGF	Epidermal Growth Factor
EGTA	Ethylene glycol tetraacetic acid
EMT	Epithelial mesenchymal transition
FCS	Fetal calf serum
h	hour(s)
HCl	Hydrogen chloride
HFS	Hypotonic fluorochrome solution
HGF	Hepatocyte growth factor
HMLE	Human Mammary Large T Epithelial cell
HRP	Horseradish peroxidase
IPTG	Isopropyl β -D-1-thiogalactopyranoside
KH ₂ PO ₄	Monopotassium phosphate
LAMP-1	Lysosomal Associated Membrane Protein-1
ME(C)GM	Mammary Epithelial (Cell) Growth Medium

MET	Mesenchymal epithelial transition
MgCl ₂	Magnesium chloride
min	minutes
MOI	Multiplicity of Infection
Na ₂ HPO ₄	Disodium phosphate
Na ₃ VO ₄	Sodium orthovanadate
NaCl	Sodium chloride
NaF	Sodium fluoride
N-cadherin	Neural-cadherin
PBS	Phosphate buffered saline
PFA	Paraformaldehyde
PI	Propidium iodide
PMSF	Phenylmethanesulfonyl fluoride
Poly-HEMA	Poly-(hydroxyethyl)-methacrylate
RIPA	Radioimmunoprecipitation assay buffer
RT	Room temperature
SDS-PAGE	Sodium Dodecyl Sulphate-Polyacrylamide Gel Electrophoresis
SEM	Standard Error of the Mean
shRNA	small hairpin ribonucleic acid
T-BST	Tris-Buffered Saline and Tween 20
TCE	2, 2, 2-Trichlorethanol
TEMED	Tetramethylethylenediamine
TGF-β	Transforming growth factor-β
TNS	Trypsin Neutralizing Solution
TRIS	Tris-(hydroxymethyl)-aminomethane
Twist1-ER	Twist1-estrogen receptor
V-ATPase	Vacuolar-type H ⁺ -ATPase

6.2 Publications

6.2.1 Articles

Henriette Merk, Siwei Zhang, Thorsten Lehr, Christoph Müller, Melanie Ulrich, James A. Bibb, Ralf H. Adams, Franz Bracher, Stefan Zahler, Angelika M. Vollmar, Johanna Liebl; *Inhibition of endothelial Cdk5 reduces tumor growth by promoting non-productive angiogenesis*; 2015, **Oncotarget**, Vol. 7, No. 5

Henriette Merk, Melanie Ulrich, Christina Scheel, Angelika M Vollmar, Johanna Liebl; *Inhibition of the V-ATPase – a new strategy to inhibit EMT and CSC formation*; 2016, in preparation

6.2.2 Oral presentations

Henriette Merk, R. Müller, AM Vollmar, J Liebl; *V-ATPase regulates epithelial-mesenchymal transition in breast cancer cells*; 7th FOR 1406 Meeting, July 16-18, 2013, Saarbrücken, Germany

Henriette Merk, R. Müller, AM Vollmar, J Liebl; *V-ATPase regulates epithelial-mesenchymal transition (EMT) in breast cancer cells*; 6th FOR 1406 Meeting, January 8-9, 2014, Munich, Germany

Henriette Merk, R. Müller, AM Vollmar, J Liebl; *V-ATPase regulates epithelial-mesenchymal transition (EMT) in breast cancer cells*; 5th FOR 1406 Meeting, July 30-July 1, 2015, Saarbrücken, Germany

6.2.3 Poster presentations

Henriette Merk, R. Müller, AM Vollmar, J Liebl; *V-ATPase regulates epithelial-mesenchymal transition in breast cancer cells*; 2nd European Conference on Natural Products: Research and Applications, September 7-9, 2015, Frankfurt, Germany

Henriette Merk, R. Müller, AM Vollmar, J Liebl; *V-ATPase regulates epithelial-mesenchymal transition in breast cancer cells*; 5th International HIPS-Symposium, July 2, 2015, Saarbrücken, Germany

Henriette Merk, R. Müller, AM Vollmar, J Liebl; *V-ATPase regulates epithelial-mesenchymal transition in breast cancer cells*; V-ATPase Symposium, May 13-15, 2015, Milan, Italy

Henriette Merk, R. Müller, AM Vollmar, J Liebl; *V-ATPase regulates epithelial-mesenchymal transition in breast cancer cells*; Deutsche Pharmazeutische Gesellschaft (DPhG) Jahrestagung 2014, September 24-26, 2014, Frankfurt, Germany

6.3 Original article

During my PhD, I was fortunate enough to get the opportunity to contribute to a second highly interesting project, which we successfully published. Please find attached the original article:

Inhibition of endothelial Cdk5 reduces tumor growth by promoting non-productive angiogenesis

Henriette Merk, Siwei Zhang, Thorsten Lehr, Christoph Müller, Melanie Ulrich, James A. Bibb, Ralf H. Adams, Franz Bracher, Stefan Zahler, Angelika M. Vollmar, Johanna Liebl; 2015, **Oncotarget**

Inhibition of endothelial Cdk5 reduces tumor growth by promoting non-productive angiogenesis

Henriette Merk¹, Siwei Zhang¹, Thorsten Lehr², Christoph Müller³, Melanie Ulrich¹, James A. Bibb⁴, Ralf H. Adams^{5,6}, Franz Bracher³, Stefan Zahler¹, Angelika M. Vollmar¹, Johanna Liebl¹

¹Department of Pharmacy, Pharmaceutical Biology, Ludwig-Maximilians-University, 81377 Munich, Germany

²Clinical Pharmacy, Saarland University, 66123 Saarbrücken, Germany

³Department of Pharmacy, Pharmaceutical Chemistry, Ludwig-Maximilians-University, 81377 Munich, Germany

⁴Department of Psychiatry and Neurology and Neurotherapeutics, The University of Texas Southwestern Medical Center, Dallas, Texas 75390-9070, USA

⁵Department of Tissue Morphogenesis, Max Planck Institute for Molecular Biomedicine, 48149 Münster, Germany

⁶University of Münster, Faculty of Medicine, 48149 Münster, Germany

Correspondence to: Johanna Liebl, **e-mail:** johanna.liebl@cup.uni-muenchen.de

Keywords: *Cdk5*, *angiogenesis*, *cancer*, *Notch*

Received: June 24, 2015

Accepted: December 29, 2015

Published: January 08, 2016

ABSTRACT

Therapeutic success of VEGF-based anti-angiogenic tumor therapy is limited due to resistance. Thus, new strategies for anti-angiogenic cancer therapy based on novel targets are urgently required. Our previous *in vitro* work suggested that small molecule Cdk5 inhibitors affect angiogenic processes such as endothelial migration and proliferation. Moreover, we recently uncovered a substantial role of Cdk5 in the development of lymphatic vessels. Here we pin down the *in vivo* impact of endothelial Cdk5 inhibition in angiogenesis and elucidate the underlying mechanism in order to judge the potential of Cdk5 as a novel anti-angiogenic and anti-cancer target. By the use of endothelial-specific Cdk5 knockout mouse models and various endothelial and tumor cell based assays including human tumor xenograft models, we show that endothelial-specific knockdown of Cdk5 results in excessive but non-productive angiogenesis during development but also in tumors, which subsequently leads to inhibition of tumor growth. As Cdk5 inhibition disrupted Notch function by reducing the generation of the active Notch intracellular domain (NICD) and Cdk5 modulates Notch-dependent endothelial cell proliferation and sprouting, we propose that the Dll4/Notch driven angiogenic signaling hub is an important and promising mechanistic target of Cdk5. In fact, Cdk5 inhibition can sensitize tumors to conventional anti-angiogenic treatment as shown in tumor xenograft models. In summary our data set the stage for Cdk5 as a drugable target to inhibit Notch-driven angiogenesis condensing the view that Cdk5 is a promising target for cancer therapy.

INTRODUCTION

Inhibition of angiogenesis has shown clinical efficacy and represents a valid approach in cancer therapy. Patients benefit from the combination of chemotherapeutics or radiation with angiogenesis inhibitors. The VEGF pathway is currently the predominant target for anti-angiogenic therapy and

anti-VEGF biologics (Bevacizumab) or small molecule inhibitors (Sorafenib, Sunitinib) are given clinically [1]. Unfortunately, non-responsiveness or resistance to anti-angiogenic treatment and subsequent tumor recurrence and metastasis limit therapeutic success [2]. Thus, finding new strategies for anti-angiogenic therapy represents an important and challenging objective in cancer research.

In this context, the Dll4/Notch pathway has emerged as an interesting target. In physiological angiogenesis, Dll4/Notch signaling regulates VEGF-induced vessel sprouting and branching and defines tip and stalk cell specification [3]. In tumors, activation of the Notch pathway promotes tumor growth [4] and mediates resistance to chemotherapy [5]. Of note, the disruption of Dll4/Notch signaling results in inhibition of tumor growth [4–8] and was associated with excessive but non-productive angiogenesis and impaired tumor vessel perfusion [6, 7]. Consequently, the blockade of the Dll4/Notch pathway is considered as a promising option for anti-angiogenic treatment. In fact, γ -secretase inhibitors or anti-Dll4/anti-Notch biologics are currently being evaluated in open clinical trials for cancer therapy [9, 10]. Furthermore, preclinical models indicated that the combination of targeting the Dll4/Notch pathway and anti-VEGF treatment leads to synergistic tumor growth inhibitory effects [5, 8]. However, little is known about the regulation of Dll4/Notch in tumor angiogenesis [9]. Moreover, the chemosensitization by combination therapies to overcome resistance to anti-angiogenic treatment demands more attention in order to develop new treatment strategies.

In this respect the protein kinase cyclin dependent kinase 5 (Cdk5) represents a particular interesting potential target to explore. Cdk5 is a serine/threonine kinase that is highly expressed in the central nervous system (CNS) and is essential for neuronal development and function [11–13], but its role in the periphery and in cancer is not well explored. During the recent years, the awareness about roles of Cdk5 besides the CNS has grown. Cdk5 is expressed in various non-neuronal tissues [14–16] and has been implicated in various types of cancer including pancreatic [17–19], prostate [20, 21], thyroid [22, 23], glioma [24], pituitary [25], breast [26], lung [27], ovarian [28], and hepatocellular [29] cancers affecting various targets such as retinoblastoma protein and downstream cell cycle regulators [22, 23], the PIKE-A-Akt pathway [24], Ras-Ral signaling [17], or DNA damage response [29]. Further, by applying cell-based assays, our former studies demonstrated that small molecule Cdk5 inhibitors exert anti-angiogenic properties [30, 31] and that Cdk5 regulates endothelial cell migration [32] which was restricted to *in vitro* assays. However, to nail down the *in vivo* significance of Cdk5 in the endothelium, we have recently generated constitutive and inducible endothelial-specific Cdk5 knockout mouse models, elucidating an indispensable requirement of Cdk5 for lymphatic vessel development and function [33].

Here, by using the endothelial-specific Cdk5 knockout mouse models, endothelial and tumor cells, and human tumor xenografts, we investigate the heretofore unknown *in vivo* function of Cdk5 in the blood vessel endothelium. Moreover, the contribution of endothelial Cdk5 to tumor angiogenesis and the underlying mechanism

such as the Dll4/Notch driven angiogenic signaling are important subjects of this work.

RESULTS

Inhibition of Cdk5 in the endothelium induces hypervascularization

As also shown in our former study [33], Cdk5 is ubiquitously expressed in the endothelium (Figure 1A). Specific disruption of Cdk5 in the mouse endothelium using the Cre/loxP system [33] changed blood vessel patterning during development, whereas, as we could show previously, blood vessel morphology was not affected [33]. In detail, constitutive knockdown of endothelial Cdk5 with the Tie2Cre promoter [33] induced hypervascularization of yolk sacs and skin of Cdk5^{fl/fl}Tie2Cre embryos (Figure 1B, 1C). Consistent with these effects, postnatal knockdown of endothelial Cdk5 with a tamoxifen-inducible VE-Cadherin Cre promoter (Cdh5(PAC)-CreERT2, *i.e.* VECCre [33, 34]) (Supplementary Figure 1A) resulted in hypervascularization of the developing retina (Figure 1D). Moreover, hypervascularization of retinæ of pups treated with the small molecule Cdk5 inhibitor roscovitine demonstrated pharmacological accessibility of Cdk5 (Figure 1E). In sum, phenotyping of endothelial specific knockout mouse models revealed an important role of Cdk5 in blood vessel development.

Endothelial knockdown of Cdk5 reduces tumor growth by promoting non-productive angiogenesis

To examine the influence of endothelial Cdk5 on tumor growth, a syngeneic tumor model was applied. Tumor growth of subcutaneously implanted B16F1 melanoma cells was reduced in Cdk5^{fl/fl}VECCre mice (Figure 2A and Supplementary Figure 1B). Analysis of tumor angiogenesis revealed that the number of vessels was increased in tumors of Cdk5^{fl/fl}VECCre mice (Figure 2B). Interestingly, tumor vessels from Cdk5^{fl/fl}VECCre mice were smaller in comparison to tumor vessels from control littermates (Figure 2B). Moreover, reduced smooth muscle cell (SMC) coverage of vessels from Cdk5 knockdown tumors demonstrated an increased incidence of immature vessels (Figure 2C). Finally, the functionality of tumor vessels was assessed by visualizing the ability of tumor vessels to perfuse FITC-lectin. Whereas control mice tumors displayed predominant overlap of FITC-lectin and CD31 staining, tumor vessels from Cdk5^{fl/fl}VECCre mice were much less perfused (Figure 2D). This set of data indicates that the deletion of endothelial Cdk5 promotes non-productive angiogenesis, which resulted in reduced tumor growth.

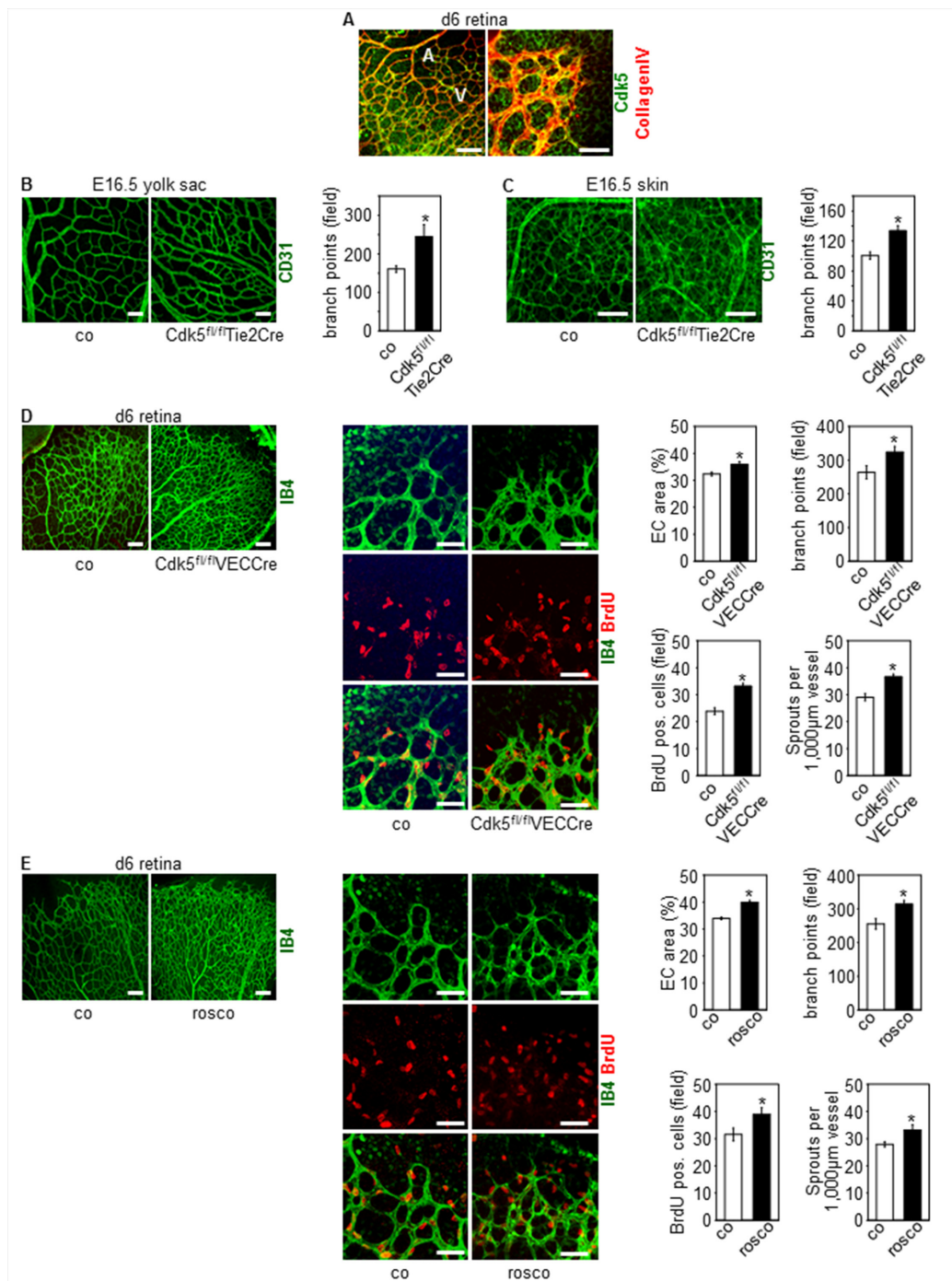


Figure 1: Knockdown and pharmacological inhibition of Cdk5 in the endothelium induces hypervascularization. (A) Expression of Cdk5 in the mouse endothelium is shown by immunostainings of the developing retina (d6) for Cdk5 (green) and collagen IV (red). Arteries (A) and veins (V) (left panel) are indicated. $n = 3$. Scale bar (left panel) 100 μm . Scale bar (right panel) 50 μm . (B) CD31 stainings (green) of yolk sacs of E16.5 embryos with control and Cdk5^{fl/fl}Tie2Cre genotype are shown. Scale bar 100 μm . Quantification of branching points is displayed. *t*-test, SEM, $*p = 0.023$, control: $n = 13$; Cdk5^{fl/fl}Tie2Cre: $n = 5$. (C) CD31 stainings (green) of skin of E16.5 embryos with control and Cdk5^{fl/fl}Tie2Cre genotype are shown. Scale bar 100 μm . Quantification of branching points is displayed. *t*-test, SEM, $*p = 0.004$, control: $n = 9$; Cdk5^{fl/fl}Tie2Cre: $n = 5$. (D) Isolectin B4 staining (IB4, green) and BrdU labeling (red) of retinae from control ($n = 8$) and Cdk5^{fl/fl}VECCre ($n = 10$) pups (d6) is shown. Scale bars (upper panels) 100 μm . Scale bars (lower panels) 50 μm . Quantifications of the area covered by ECs (*t*-test, SEM, $*p = 0.015$), the numbers of branch points per field (*t*-test, SEM, $*p = 0.034$), of BrdU positive cells per field (*t*-test, SEM, $*p \leq 0.001$), and of sprouts per 1,000 μm vessel length (*t*-test, SEM, $*p \leq 0.001$) is shown. (E) Isolectin B4 staining (IB4, green) and BrdU labeling (red) of retinae from pups (d6) treated with solvent (co, $n = 8$) or roscovitine (rosco, $n = 7$) is shown. Scale bars (upper panels) 100 μm . Scale bars (lower panels) 50 μm . Quantifications of the area covered by ECs (*t*-test, $*p \leq 0.001$), the numbers of branch points per field (*t*-test, SEM, $*p = 0.005$), of BrdU positive cells per field (*t*-test, SEM, $*p = 0.049$), and of sprouts per 1,000 μm vessel length (*t*-test, SEM, $*p \leq 0.02$) is shown.

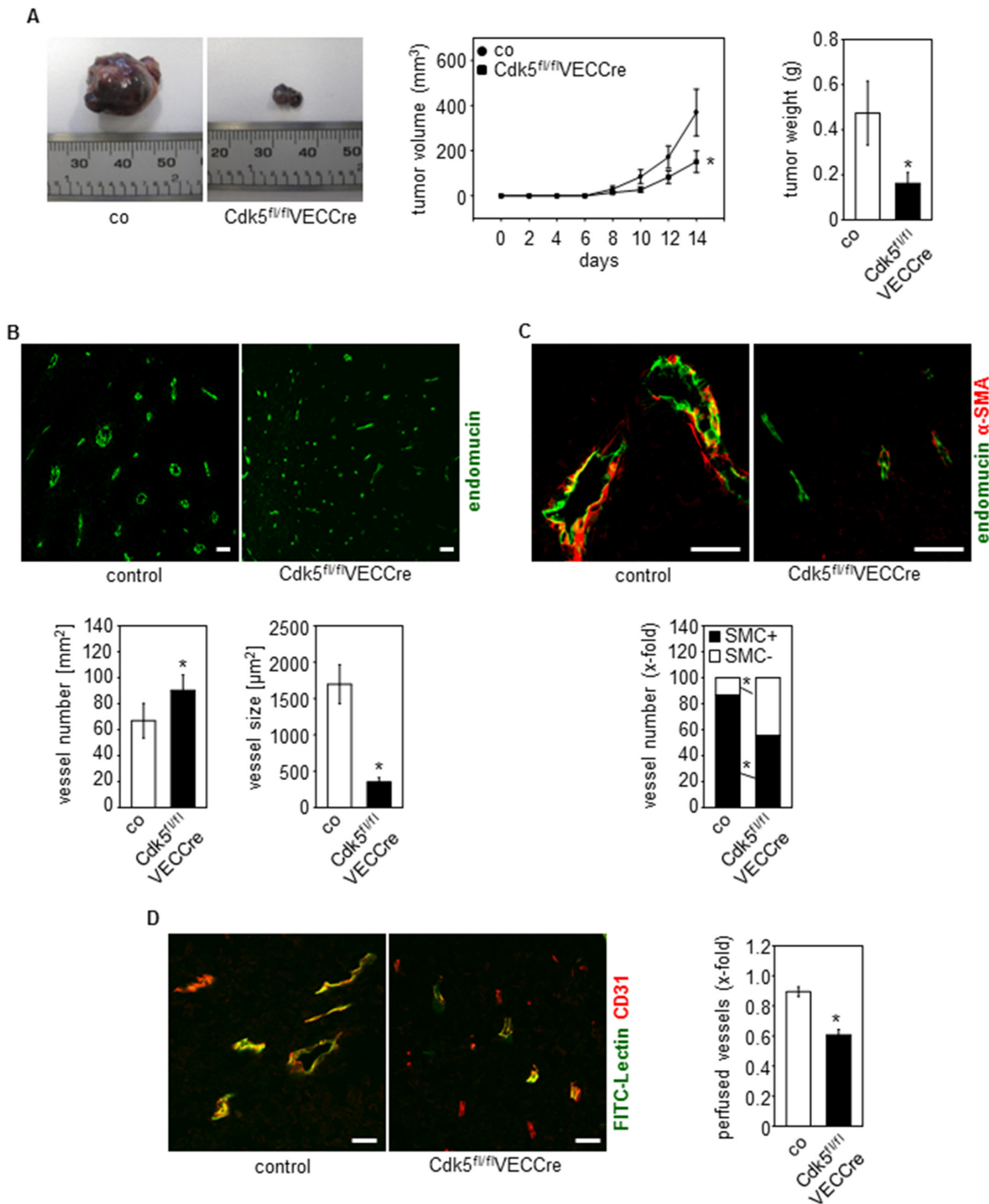


Figure 2: Endothelial Cdk5 knockdown reduces tumor growth with hypervascularization of tumors with non-functional vessels. (A) Tumor growth is reduced in EC-specific Cdk5 knockout mice. B16F1 tumors from control (co, $n = 12$) and Cdk5^{fl/fl}VECCre ($n = 11$) mice are shown. Time course of tumor growth (Rank Sum test, SEM, $*p = 0.029$) and quantification of tumor weight (Rank Sum test, SEM, $*p = 0.036$) is displayed. (B) Tumors from EC-specific Cdk5 knockout mice show hypervascularization with small blood vessels. Staining of tumors from control littermates (co, $n = 12$) and Cdk5^{fl/fl}VECCre mice ($n = 11$) for endomucin (green) is shown. Scale bar 50 μ m. Quantification of vessel number (Rank sum test, SEM, $*p = 0.01$) and vessel size (Rank sum test, SEM, $*p = 0.01$) is shown. (C) Immature tumor blood vessels in EC-specific Cdk5 knockout mice. Staining of tumors from control littermates (co, $n = 12$) and Cdk5^{fl/fl}VECCre mice ($n = 11$) for endomucin (green) and α -SMA (red) is shown. Scale bar 50 μ m. Quantification of the number of tumor vessels covered with SMCs (t -test, SEM, $*p \leq 0.002$) is shown. (D) Tumor vessel perfusion is impaired in EC-specific Cdk5 knockout mice. FITC-lectin (green) labels perfused vessels, CD31 (red) marks blood vessels. Colocalization of FITC-Lectin green and CD31 indicates perfused vessels. Control mice (co, $n = 5$) and Cdk5^{fl/fl}VECCre mice ($n = 4$). Scale bar 100 μ m. Quantification of perfused tumor vessels is displayed (t -test, SEM, $*p \leq 0.001$).

Cdk5 regulates the Notch pathway in the endothelium

Although various targets of Cdk5 have been described in cancer and endothelial cells, as one mechanism by which Cdk5 might regulate tumor angiogenesis, the Notch pathway particularly attracted our attention since the phenotype of endothelial Cdk5 knockout mice resembles that of mice with defective Dll4/Notch signaling [3]. In fact, genetic or pharmacologic inhibition of Cdk5 in endothelial cells (HUVECs) impaired Dll4-induced Notch downstream target expression (Figure 3A, 3B) as well as Notch reporter activity (Figure 3C). Consistent with these effects, blood vessel endothelial cells (BECs) from Cdk5^{fl/fl}Tie2Cre embryos displayed reduced expression of Notch target genes after Notch activation by Dll4 (Figure 3D). Furthermore, the expression of the Notch downstream target genes Hey1 and Hey2 was decreased in tumors from endothelial Cdk5 knockout mice (Figure 3E). All these findings point to a Cdk5-Notch pathway for the regulation of angiogenesis. However, genetic or pharmacological inhibition of Cdk5 did not abrogate the Jagged1-induced Notch target expression (Figure 4A, 4B), suggesting a specific regulation of Dll4-driven Notch signaling by Cdk5.

Cdk5 regulates NICD generation

To understand the link between Cdk5 and the Dll4-Notch pathway, further experiments focused on the regulation of the Notch intracellular domain (NICD), the key mediator of Notch signaling [35]. After ligand-induced proteolytic cleavage of the Notch receptor, NICD is released and translocates to the nucleus to drive target gene transcription before the signal is terminated by proteasomal degradation of NICD [35]. Inhibition of Cdk5 by either knockdown or pharmacologic approaches decreased Dll4-induced NICD generation (Figure 5A, 5B). This was not based on changed Notch receptor expression as Cdk5 silencing neither influenced Notch receptor mRNA (Figure 5C) nor protein (Figure 5D). Furthermore, the inhibition of the proteasomal degradation by MG132 did not abrogate the Cdk5 siRNA mediated decrease of NICD (Figure 5E). To prove the functionality of MG132, β -catenin was used as a positive control as it is degraded by the proteasome [36]. Increased β -catenin in the presence of MG132 proved that MG132 inhibited the proteasomal degradation (Figure 5F). In line, exogenously expressed NICD that is not dependent on Notch receptor cleavage, was not affected by Cdk5 inhibition (Figure 5G). Both results suggest that Cdk5 preferentially contributes to NICD generation rather than its degradation. Cdk5 knockdown by siRNA as well as Cdk5 inhibition by roscovitine decreased levels of phosphorylated and total presenilin, the catalytic subunit of the γ -secretase multiprotein complex capable of mediating NICD generation. (Figure 5H, 5I). This set of data suggests

that Cdk5 provides negative tonus on Notch-dependent signaling.

Cdk5 regulates Notch dependent endothelial functions

We next asked if Cdk5 could contribute to Notch dependent endothelial functions like proliferation and sprouting of endothelial cells [37, 38]. In fact, inhibition of endothelial Cdk5 abrogated the Dll4-mediated decrease of endothelial cell proliferation (Figure 6A). In line, Cdk5 inhibition increased sprouting of spheroids embedded into Dll4-containing gels (Figure 6B). Moreover, in line with the immunoblots in Figure 5 that showed reduced NICD levels by Cdk5 inhibition, immunostainings suggest reduced NICD levels in spheroids generated from Cdk5 siRNA treated cells (Figure 6C). Thus, inhibition of Cdk5 impaired endothelial cell functions which are dependent on Dll4-driven Notch activation.

Cdk5 inhibition reduces tumor growth and improves sensitivity to anti-angiogenic treatment

As described above, knockout of endothelial Cdk5 reduced tumor growth of wildtype B16F1 melanoma cells (Figure 2A), demonstrating that endothelial Cdk5 regulates tumor growth. To investigate the influence of Cdk5 inhibition on tumor growth in a more therapeutic context, we used systemic treatment with the small molecule Cdk5 inhibitor roscovitine. Although, like most kinase inhibitors, roscovitine is not selective for the inhibition of Cdk5 but also addresses other Cdks like Cdk1, Cdk2, Cdk7, and Cdk9, it represents the best-established inhibitor for Cdk5 and therefore was used as a model substance for our studies [39–41]. We used a subcutaneous human U87 glioblastoma cell xenograft model as glioblastoma represent highly vascularized and aggressive tumors [42]. Roscovitine was given after tumors had established and reduced glioblastoma growth as shown by a significantly reduced growth rate of tumors from roscovitine treated mice (Figure 7A). In endothelial-specific Cdk5 knockout mice, systemic treatment with roscovitine slightly but not significantly reduced tumor growth and decreased tumor cell proliferation as shown by Ki67 staining (Figure 7B). Moreover, roscovitine had no effect on vessel number in tumors grown in endothelial Cdk5 knockout mice (Figure 7B). This set of data suggests that Cdk5 indeed is the primary target of roscovitine, but that roscovitine also acts on tumor cells as well and inhibits other Cdks besides Cdk5. Pharmacokinetic studies showed plasma concentrations of roscovitine comparable to doses used in our cell-based assays (Figure 7C).

Together with the reduced growth of wildtype tumors in endothelial Cdk5 knockout mice (Figure 2A), this set of data provides evidence for Cdk5 as a drugable target for anti-angiogenic therapy. Finally, we assessed the

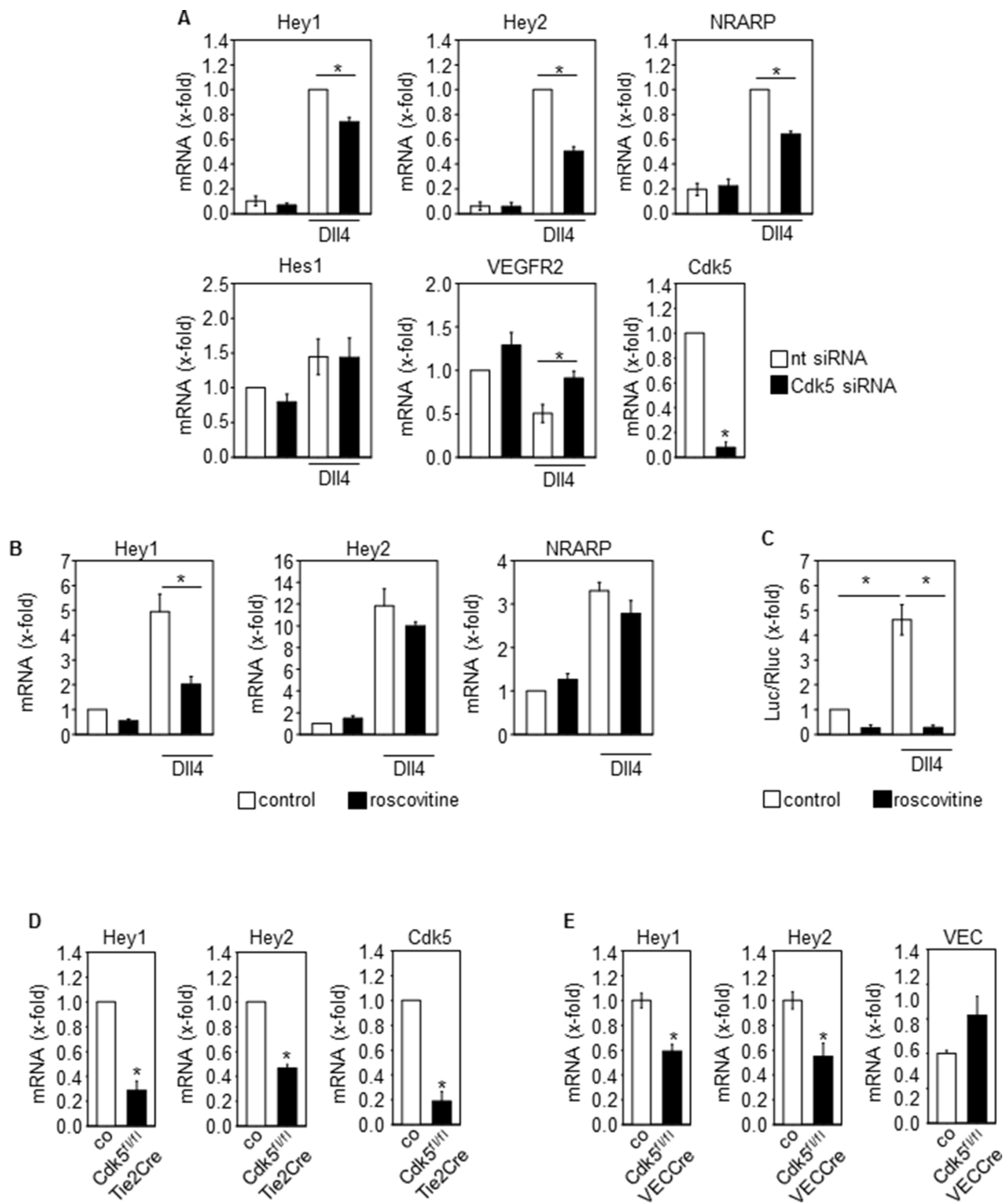


Figure 3: Cdk5 regulates the Notch pathway in the endothelium. (A) Effect of Cdk5 siRNA on DII4-induced expression of Notch downstream target genes Hey1, Hey2 and NRARP, Hes1, and VEGFR2 in HUVECs is shown (One-Way ANOVA, Holm-Sidak, SEM, $*p \leq 0.05$). Cdk5 downregulation is shown (*t*-test, SEM, $*p \leq 0.001$). $n = 3$. nt: non-targeting siRNA. (B) Effect of Cdk5 inhibition by roscovitine on DII4-induced expression of Notch downstream target genes Hey1, Hey2 and NRARP is shown (One-Way ANOVA, Tukey, SEM, $*p \leq 0.05$). $n = 6$. (C) Effect of Cdk5 inhibition by roscovitine on Notch reporter gene activation is shown (ANOVA on Ranks, Student-Newman-Keuls, SEM, $*p \leq 0.05$). $n = 3$. (D) Expression of the Notch downstream target genes Hey1 and Hey2 in blood vessel endothelial cells (BECs) from E16.5 control and Cdk5^{fl/fl}Tie2Cre embryos is shown (*t*-test, SEM, $*p \leq 0.001$). Expression of Notch target genes was induced by plating of BECs onto DII4. Cdk5 downregulation is shown (*t*-test, SEM, $*p \leq 0.001$). $n = 3$. (E) Expression of the Notch downstream target genes Hey1 (*t*-test, SEM, $*p = 0.003$) and Hey2 (*t*-test, $*p = 0.012$) in tumors from control versus Cdk5^{fl/fl}VECCre mice is shown. Expression of VE-Cadherin (VEC) is shown. Hey1 and Hey2 mRNA levels were normalized to VEC to compensate for the hypervascularization. $n = 4$.

effect of anti-VEGF treatment on Lewis lung carcinoma (LLC) growth in endothelial-specific Cdk5 knockout mice. The LLC model has been described to be resistant to conventional anti-angiogenic therapy [43]. As expected, the anti-VEGF antibody B20-4.1.1 did not reduce LLC tumor growth in control mice. However, in endothelial Cdk5 knockout mice anti-VEGF treatment diminished tumor growth (Figure 8). Thus, Cdk5 inhibition enhanced sensitivity of tumors to anti-VEGF treatment.

DISCUSSION

Substantial advances in understanding of angiogenesis have been made with regard to the regulation and targeting of growth factor receptors such as the

VEGF-Receptor [1, 44, 45]. However, the inhibition of growth factors is not effective in all cancers [46]. Therefore, it is essential to further understand how the tumor vasculature can be effectively targeted in order to develop new anti-angiogenic therapies. However, the knowledge about intracellular processes that mediate neovascularization is still limited.

Here, we show that endothelial Cdk5 contributes to blood vessel development and tumor angiogenesis. In doing so, this work provides the first evidence for an *in vivo* role of Cdk5 in blood vessel formation. There have been various reports including ours, describing functions of Cdk5 in endothelial cells: in detail, endothelial Cdk5 was implicated in endothelial senescence [47], in neovascularization after ischemic stroke [48], and in

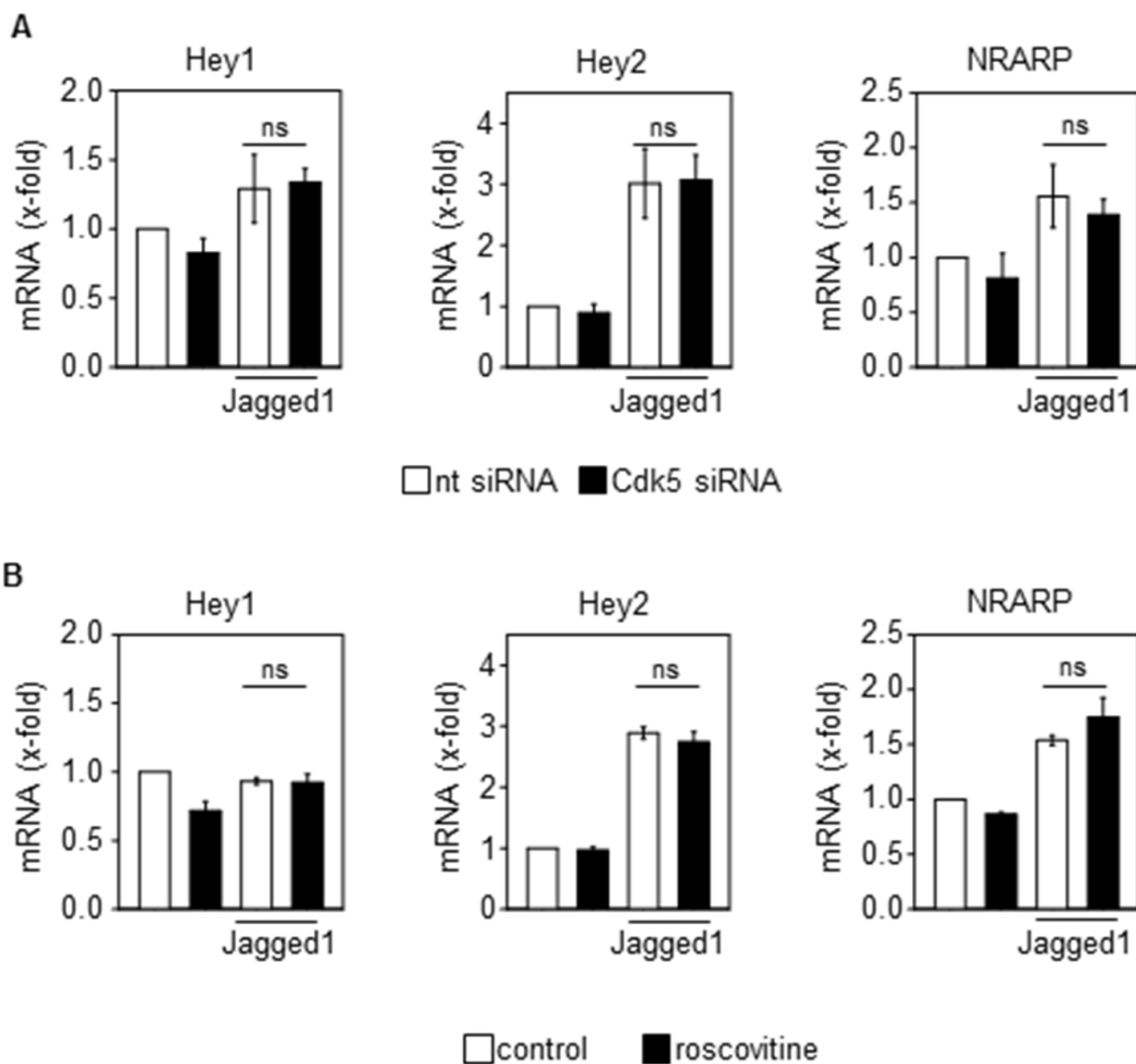


Figure 4: Cdk5 does not regulate the Jagged1-induced activation of the Notch pathway. (A) Effect of Cdk5 siRNA on Jagged1-induced expression of Notch downstream target genes Hey1, Hey2 and NRARP in HUVECs is shown (One-Way ANOVA, Tukey, SEM, ns: not significant). $n = 3$. nt: non-targeting siRNA. (B) Effect of Cdk5 inhibition by roscovitine (10 μ M, 48 h) on Jagged1-induced expression of Notch downstream target genes Hey1, Hey2 and NRARP is shown (One-Way ANOVA, Tukey, SEM, ns: not significant). $n = 3$.

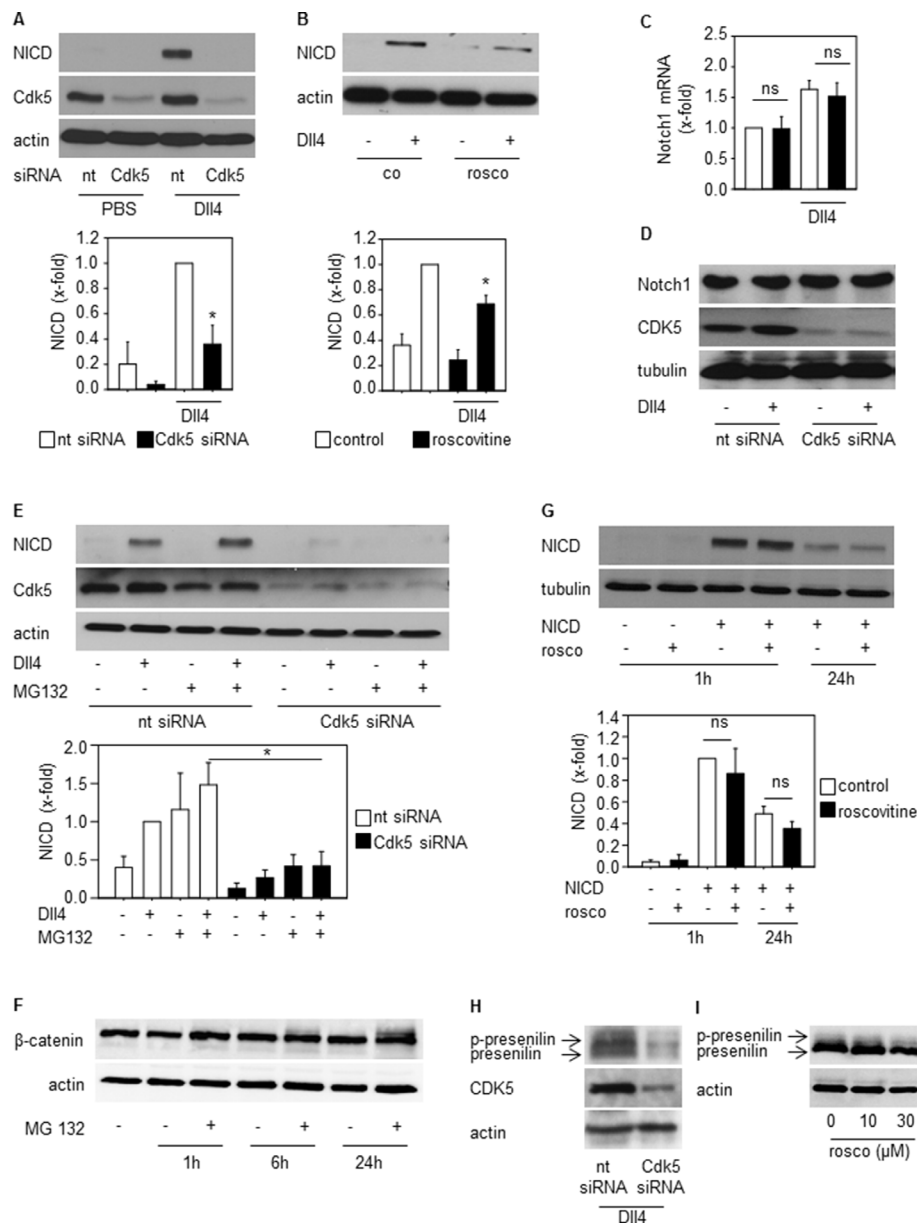


Figure 5: Cdk5 regulates NICD generation. (A) Immunoblots from HUVECs transfected with nt (non-targeting) and Cdk5 siRNA and plated onto PBS- or DLL4-coated dishes probed with anti-NICD, anti-Cdk5, and anti-actin antibodies are shown. $n = 3$. The bar graph displays the quantification of the NICD immunoblot normed to the loading control (One Way ANOVA, Tukey, SEM, $*p \leq 0.05$). (B) Immunoblots from HUVECs untreated (co) or treated with roscovitine (rosco, 10 μM), plated onto PBS- or DLL4-coated dishes and probed with anti-NICD and anti-actin antibodies are shown. $n = 3$. The bar graph displays the quantification of the NICD immunoblot normed to the loading control (One Way ANOVA, Tukey, SEM, $*p \leq 0.05$). (C) Expression of Notch1 receptor mRNA of HUVECs transfected with nt (non-targeting) or Cdk5 siRNA is shown. One-Way ANOVA, Tukey, $n = 3$. (D) Immunoblots from HUVECs transfected with nt (non-targeting) or Cdk5 siRNA and probed with anti-Notch, anti-Cdk5, and anti-tubulin antibodies are shown. $n = 3$. (E) Immunoblots of HUVECs silenced with nt (non-targeting) or Cdk5 siRNA and treated with MG132 for 24 h before plating onto DLL4 and probed with anti-NICD, anti-Cdk5 and anti-actin antibodies are shown. $n = 3$. The bar graph displays the quantification of the NICD immunoblot normed to the loading control (One Way ANOVA, Tukey, SEM, $*p \leq 0.05$). (F) Immunoblots of HUVECs treated with MG132 for the indicated timepoints and probed with anti- β -catenin and anti-actin antibodies are shown. $n = 2$. The bar graph displays the quantification of the NICD immunoblot normed to the loading control (One Way ANOVA, Tukey, SEM, $*p \leq 0.05$). (G) Immunoblots of HUVECs overexpressing NICD or empty vector treated with/without roscovitine for the indicated times and probed with anti-NICD and anti-tubulin antibodies are shown. $n = 3$. (H) Immunoblots of HUVECs transfected with nt (non-targeting) or Cdk5 siRNA plated onto DLL4 and probed with anti-presenilin, anti-Cdk5, and anti-actin antibodies are shown. Phosphorylated and total presenilin is denoted by the upper and lower band and marked by arrows. $n = 3$. (I) Immunoblots of HUVECs treated with/without roscovitine at indicated concentrations plated onto DLL4 and probed with anti-presenilin and anti-actin antibodies are shown. Phosphorylated and total presenilin is denoted by the upper and lower band and marked by arrows. $n = 3$.

diseases associated with NO dysfunction [49, 50]. Our former studies demonstrated that small molecule Cdk5 inhibitors exert anti-angiogenic effects and that Cdk5 is implicated in endothelial cell migration by regulating the small GTPase Rac1 which was restricted to *in vitro* assays. However, the specific *in vivo* role of Cdk5 in the blood vessel endothelium by genetic knockdown models has not been addressed to date. Of note, as we started to analyze the *in vivo* function of Cdk5 in the endothelium, we

observed no changes in arterial-venous cell specification and blood vessel morphology by Cdk5 knockdown in the endothelium [33]. In fact, we found that Cdk5 is essential for lymphatic vessel development and valve formation by phosphorylating the transcription factor Foxc2 [33]. Our present study though elucidates a crucial role of Cdk5 in blood vessel patterning.

With respect to the mechanisms and potential targets of Cdk5 action in blood vessels, rather the Dll4/

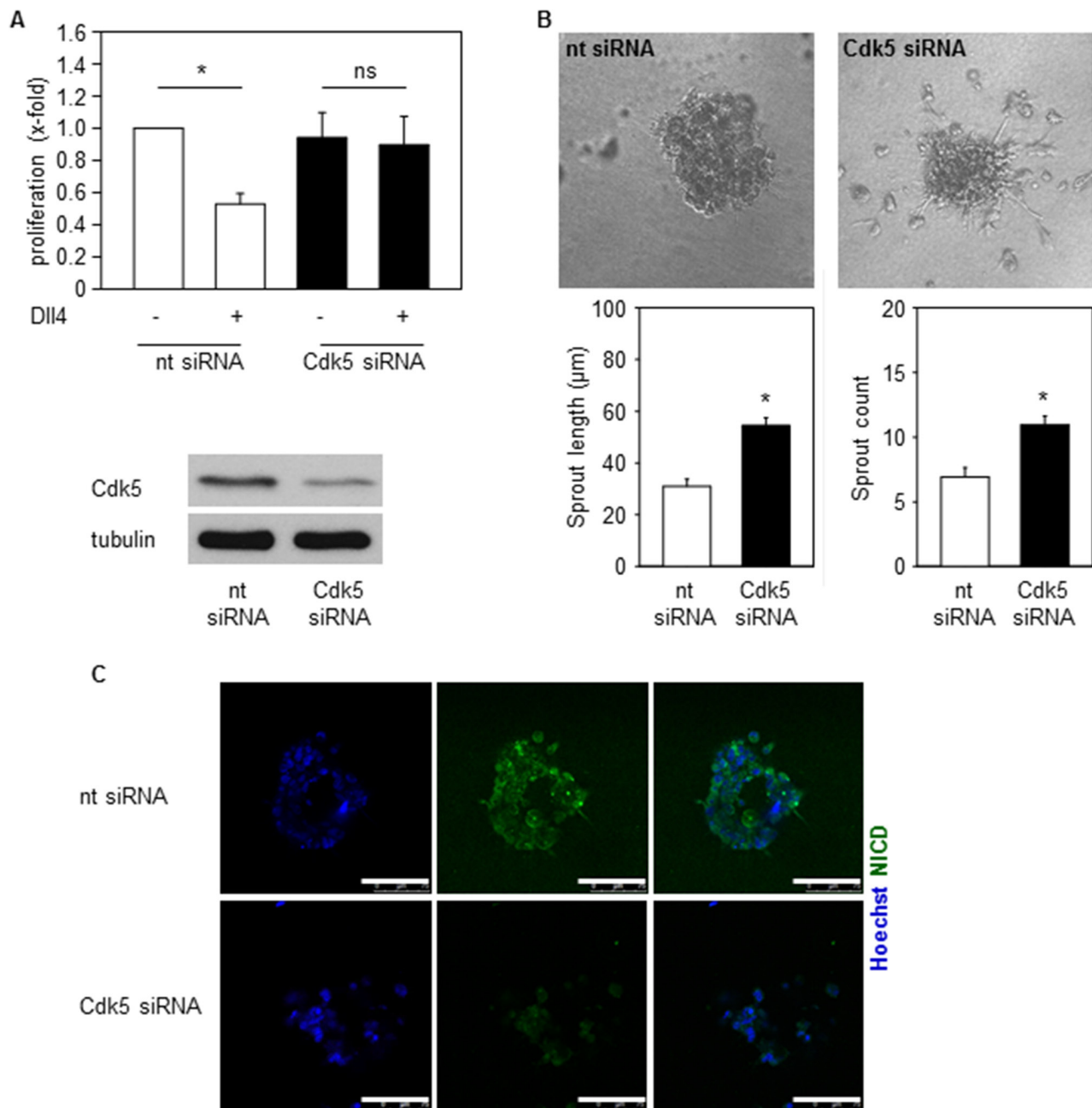


Figure 6: Cdk5 regulates Notch pathway dependent endothelial functions. (A) Proliferation of HUVECs transfected with nt (non-targeting) or Cdk5 siRNA and plated onto PBS or Dll4 is shown. One-Way ANOVA, Tukey, SEM $*p \leq 0.05$. $n = 4$. (B) Spheroids generated from HUVECs transfected with nt (non-targeting) or Cdk5 siRNA embedded into Dll4 containing gels are shown. Quantifications of sprout length and number of sprouts are displayed. *T*-test, SEM, $*p \leq 0.001$. Number of evaluated spheroids: non-targeting siRNA $n = 21$, Cdk5 siRNA $n = 26$. (C) Immunostainings of spheroids generated from nt (non-targeting) or Cdk5 siRNA transfected HUVECs for NICD (green) and Hoechst 33342 (blue) are shown. Scale bar 100 μm. $n = 3$.

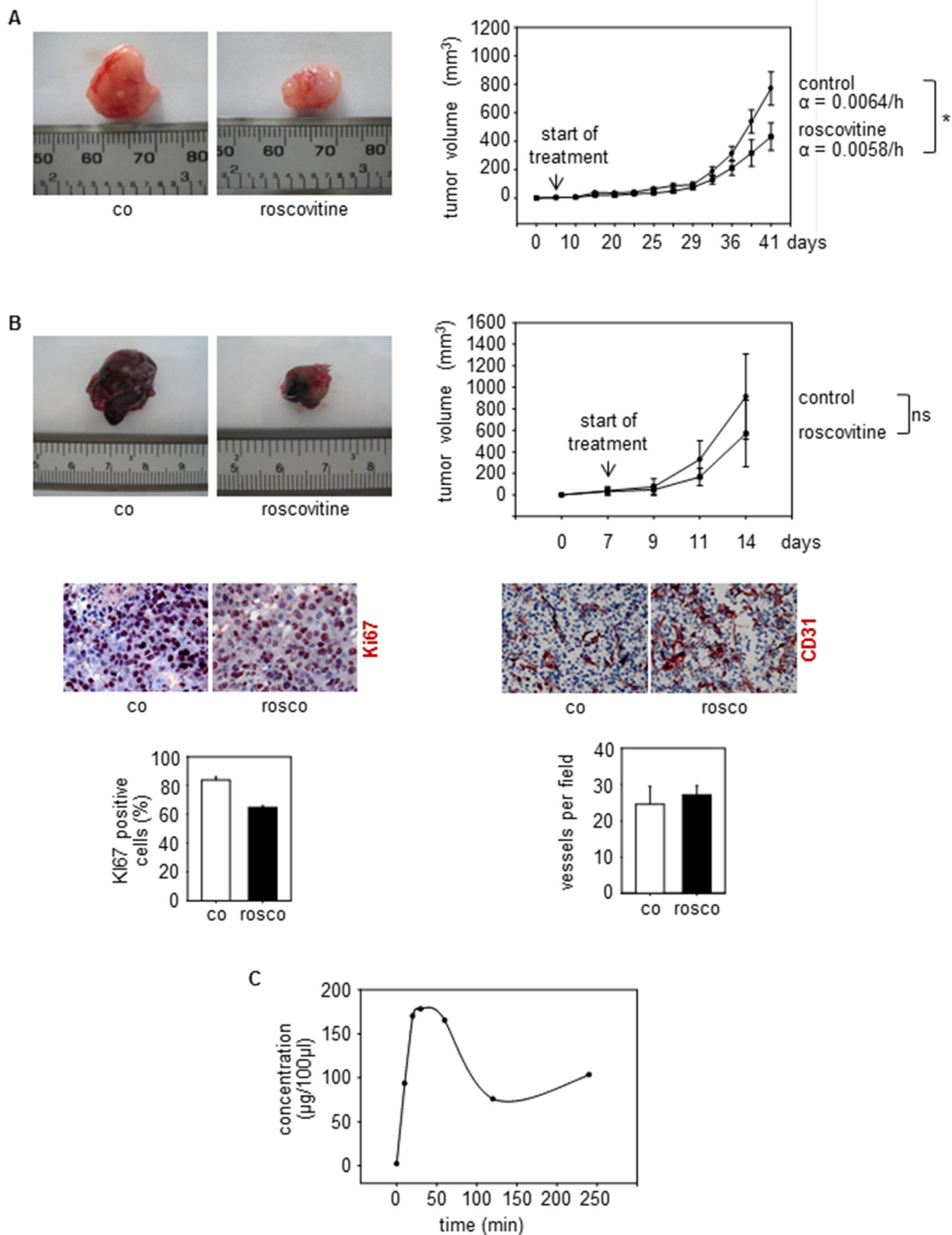


Figure 7: Cdk5 inhibition reduces tumor growth. (A) U87 tumors from mice treated with solvent (co) or roscovitine (rosco) is shown. $n = 5$. The graph shows tumor growth over time. Growth rate α of tumors is indicated ($*p = 3 \times 10^{-7}$). (B) B16F1 tumors from $Cdk5^{fl/fl}VECCre$ mice treated with solvent (co) or roscovitine (rosco) is shown. The bar graph shows tumor growth over time (t -test, ns: not significant, $n = 3$). Staining of tumors $Cdk5^{fl/fl}VECCre$ mice for Ki67 (red, upper panel) and CD31 (red, lower panel) is shown ($n = 2$). The bar graphs display respective quantifications. (C) Pharmacokinetics of Roscovitine in mice is shown. The graph displays the concentration (μg per $100 \mu\text{l}$) of Roscovitine in blood of mice after i.p. injection at the indicated timepoints. $n = 3$ mice per timepoint.

Notch system was indicated to be important, as suggested by the reminiscent phenotype of Cdk5 knockout mice to angiogenesis observed by Dll4/Notch blockade. Similar to the genetic or pharmacologic inhibition of endothelial Cdk5, the disruption of Dll4/Notch signaling results in increased vessel sprouting during development [3]. Dll4/Notch signaling regulates tip and stalk cell specification during vascular morphogenesis. Dll4 is induced in endothelial tip cells and activates Notch in adjacent stalk cells which represses the tip cell phenotype. Inhibition of the Notch pathway results in increased vessel sprouting and branching due to excessive tip cell formation and endothelial cell proliferation. Moreover, in line with our results showing dysfunction of tumor vessels in endothelial Cdk5 knockout mice, preclinical models have demonstrated that blockade of Dll4/Notch signaling results in increased vessel sprouting and branching in tumors and impairs tumor growth by promoting non-productive angiogenesis [6, 7]. With respect to the target of Cdk5 within the Dll4/Notch signaling hub our work points to an alteration of presenilin/ γ -secretase and therefore the regulation of NICD generation by endothelial Cdk5. In neurons presenilin/ γ -secretase was identified as Cdk5 target before [51]. Presenilin comprises the catalytic component of the γ -secretase multiprotein complex that is essential for Notch receptor processing and NICD generation [35].

Therapeutic targeting of the Dll4/Notch pathway has evolved as an attractive anti-angiogenic strategy as the

adaptive ability of neoplastic cells to become anti-VEGF resistant has arisen as a major obstacle to anti-angiogenic therapies [2] and can be caused by compensation of alternative angiogenesis mechanisms such as the Dll4/Notch pathway [5, 8, 9]. Potentiated Notch signaling due to either loss of a negative regulator or increased expression of the Notch activating ligand Dll4 in the tumor vasculature correlates with tumorigenesis and therapeutic resistance [4, 5, 10, 52, 53]. In breast cancer, high Dll4 expression by intratumoral endothelial cells was elucidated as an adverse prognostic factor of patient survival [54]. In line, strong expression of Dll4 in ovarian cancer was associated with poor patient prognosis whereas low Dll4 expression correlated with responsiveness to anti-VEGF therapy [8]. Recently, it was shown that the modulation of Dll4/Notch by the extracellular matrix (ECM) protein fibulin-3 promotes angiogenesis in high-grade gliomas [42]. However, whereas Dll4 expression in tumors consistently affected the vascular phenotype, tumor growth was increased only in some tumors, probably due to differences in the vasculature and/or levels of endogenous components of the Dll4/Notch pathway [4, 6]. In line, our study shows that Cdk5 inhibition alone inhibited B16F1 melanoma growth but not LLC tumor growth. Importantly, Dll4/Notch blockade has been shown to inhibit the growth of anti-VEGF resistant tumors and even enhance the sensitivity of tumors to anti-VEGF treatment [5, 8, 9]. Consequently, various approaches have been developed to target the Dll4/Notch pathway including

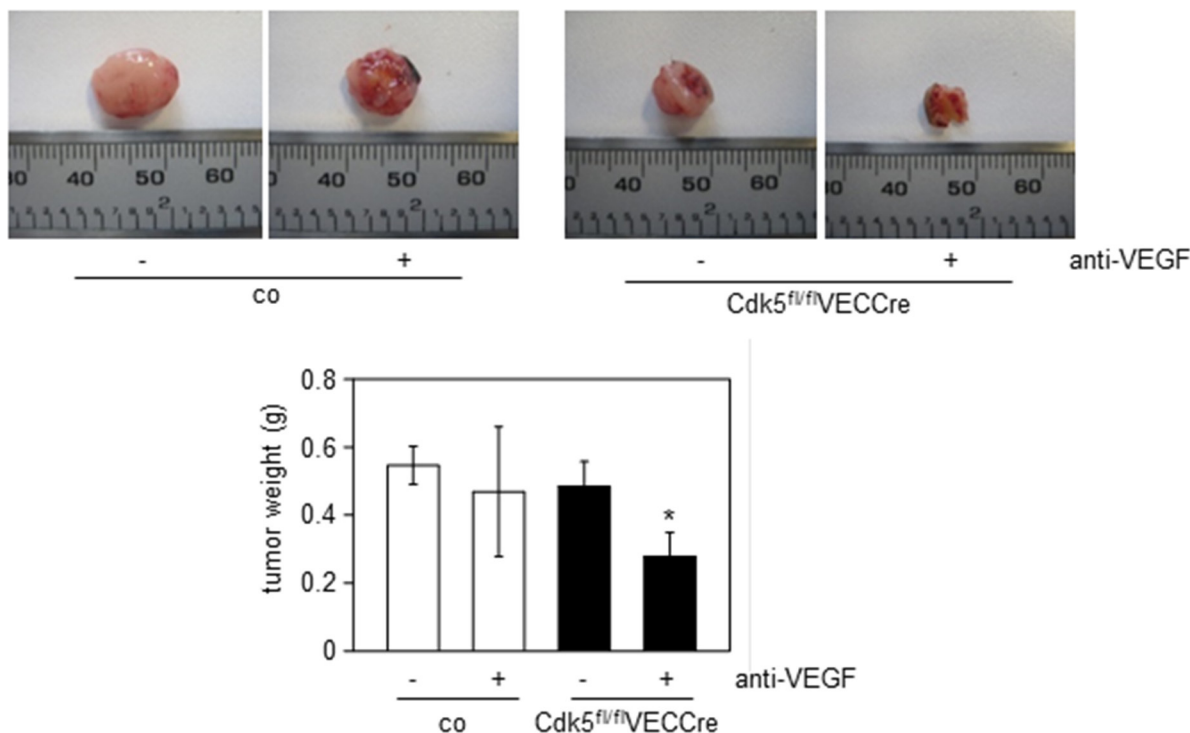


Figure 8: Cdk5 inhibition sensitizes to anti-angiogenic treatment. LLC tumors from control (co) or Cdk5^{fl/fl}VECCre mice treated with solvent or the anti-VEGF antibody B20-4.1.1 are shown. Quantification of tumor weight is indicated. ANOVA on Ranks, Dunn's Method, SEM, * $p \leq 0.05$. control/solvent $n = 10$, control/anti-VEGF $n = 9$, Cdk5^{fl/fl}VECCre/solvent $n = 9$, Cdk5^{fl/fl}VECCre/anti-VEGF $n = 8$.

anti-Dll4 antibodies, Dll4-Fc and Notch-Fc decoys, DNA vaccination, anti-Notch antibodies, as well as γ -secretase inhibitors and anti-Dll4/Notch therapy is currently evaluated in clinical trials for cancer therapy [9]. Still, the molecular basis of this sensitizing effect has not been well explained [9]. Here we show that Cdk5 inhibition within the neovascular endothelium of burgeoning tumors can sensitize them for more effective anti-angiogenic treatment. This may be of particular relevance to tumors such as lewis lung carcinoma (LLC) which have been described to be resistant to anti-angiogenic treatment [43]. Thus, the control of Notch signaling by Cdk5 in the neovascularizing endothelium is proposed as an additional target for tumor treatment although up to now, absolutely selective inhibition specifically of Cdk5 is not possible as the currently available Cdk5 inhibitors interfere with other Cdks like Cdk1, Cdk2, Cdk7, and Cdk9 as well. Nevertheless, inhibition by small molecules inhibiting Cdk5 and additionally Cdk1, Cdk2, Cdk7, and Cdk9 have shown promising effects in cancer/angiogenesis [18, 30, 31, 55, 56]. In fact, as inhibition of several kinases can address different functions in endothelial as well as in tumor cells, and therefore interfere with tumor growth and progression in a multifaceted mode of action, this might be beneficial in terms of therapeutic efficiency.

In sum, the present study elucidates an essential *in vivo* role of Cdk5 in tumor angiogenesis suggesting Cdk5 inhibition as a novel approach for anti-angiogenic treatment.

MATERIALS AND METHODS

Animal experiments

All animal experiments were performed with approval by the District Government of Upper Bavaria in accordance with the German animal welfare and institutional guidelines.

Endothelial-specific Cdk5 knockout mice

Generation, breeding, and genotyping of endothelial-specific Cdk5 knockout mice was previously described [33]. Floxed Cdk5 mice were described [57]. Tie2Cre mice were from Jackson Laboratory (B6.Cg-Tg(Tek-cre)12Flv/J, 004128). Tamoxifen-inducible Cdh5(PAC)-CreERT2 mice were described [34]. Endothelial Cdk5 knockdown in pups was achieved by tamoxifen injection at day 1 – day 3 (50 μ g/day i.p., Sigma Aldrich). Cdk5 knockdown was proved at day 6 (Supplementary Figure 1A). For deletion of Cdk5 in adult mice, tamoxifen (0.5 mg/day i.p.) was injected at 5 consecutive days. Cdk5 knockdown was proved two weeks and four weeks after treatment with tamoxifen (Supplementary Figure 1B).

Tumor models

B16F1 melanoma cells (1×10^6 cells in 100 μ l PBS) were subcutaneously injected into the flanks of 8 week old Cdk5^{fl/fl}VECCre and control mice at day 15 after tamoxifen injection when Cdk5 was downregulated. Tumor growth was observed for 14 days (until d30). Tumor volume was evaluated every 2nd day ($\pi/6 \times l \times w \times h$). Tumor weight was evaluated. In case of therapy with roscovitine, mice were intraperitoneally treated with roscovitine (150 mg/kg, 3 \times per week) starting from day 7 after tumor cell injection, when tumors had established. The tumor volume was evaluated three times per week. Mice were sacrificed at day 14 and the tumor weight was determined.

U87 glioblastoma cells [4, 5] were subcutaneously injected (5×10^6 cells in 100 μ l PBS:Matrigel 1:1) into the flanks of 6 week old female Balb/c nude mice (Harlan). Mice were treated intraperitoneally (i.p.) with roscovitine (150 mg/kg, 3 \times per week) starting at day 7 after tumor cell implantation when tumors had established and the tumor volume was evaluated twice per week. Mice were sacrificed at day 42. Tumor volume was modelled using an exponential growth model where the tumor volume at a given time t ($N(t)$) is a function of the starting volume $N(0)$, the time of growth t and of a growth rate α : $N(t) = N(0) \cdot \exp^{\alpha \cdot t}$. Modeling was performed using non-linear mixed effects modeling with the software NONMEM 7.3. [58].

LLC cells (2×10^6 cells in 100 μ l PBS) cells were subcutaneously injected into the flanks of 8 week old Cdk5^{fl/fl}VECCre and control mice at day 15 after tamoxifen injection when Cdk5 was downregulated. Starting at d3 after tumor cell implantation, mice were treated with anti-VEGF antibody (B20–4.1.1, Genentech, 5 mg/kg 2 \times / week, i.p.) or solvent (PBS) respectively. Mice were sacrificed at day 18 and tumor weight was evaluated.

Pharmacokinetics

Plasma concentrations of roscovitine were determined by HPLC-DAD. Mice were treated with roscovitine and blood was collected after 10, 20, 30, 60, 120, and 240 min. For each time point, blood of three mice was pooled.

100 μ l mice blood were mixed with 200 μ l acetonitrile, vortexed (1 min), centrifuged (5 min, 10,000 g, RT) and the supernatant was analyzed by HPLC-DAD using an Agilent Series 1100 HPLC system (Waldbronn, Germany) consisting of a quaternary pump system (G1311 A QuatPump), an autosampler (G1329 A ALS), a column oven (G1316 A ColComp) and a UV-DAD detector (G1315 A DAD). Chromatographic separation was carried out with an Agilent poroshell 120 EC-C18 (100 \times 3.0 mm, i.d. 2.7 μ m) column (Waldbronn, Germany) and a mobile phase of acetonitrile and water (0.1% phosphoric acid, 1.0% tetrahydrofuran) 15:85 (v/v). The total run time was

7 min with an isocratic flow rate at 1.0 ml/min, and an injection volume of 10 μ l. The column oven was set at 50°C. The UV detection wave-length was set at 292 nm. Data analysis and instrument control was carried out with Agilent ChemStation® software Rev. B04.02. The average retention time of roscovitine was 3.1 min. The concentration of roscovitine was determined according to an external standard calibration.

Retina preparation and staining

Retina preparation and staining was performed according to Pitulescu et al. [59]. Briefly, eyes were removed, fixed in PFA 4% (2 h, RT) and retinae were prepared. After blocking (2 h, RT), retinae were stained for isolectin B4 (IB4, Alexa 488 conjugated, Millipore), and BrdU staining was performed. Nuclei were labeled with Hoechst33342. Pictures were taken with a Zeiss LSM 510 META confocal microscope. The area covered by ECs, the numbers of branch points per field, number of BrdU positive cells per field, and of sprouts per 1,000 μ m vessel length were calculated by using Image J.

Immunohistochemistry

Paraffin sections: Tumors were removed, fixed with PFA 4% for 24 h, left in PFA 1%, embedded into paraffin and sections (5 μ m) were prepared.

Cryosections: Tumors were removed and frozen into TissueTek. 10 μ m sections were prepared and fixed with formalin 4% (10 min, RT).

Stainings: Sections were blocked (1% BSA/PBS), incubated with primary antibodies (CD31, 553370, BD Pharmingen; endomucin, sc-65495 Santa Cruz; α -SMA C6198, Sigma) for 2 h, at RT or o/n at 4°C, washed, incubated with AlexaFluor-labeled secondary antibodies (45 min, RT, Life Technologies) and Hoechst 33342 (5 μ g/ml) and mounted (Fluorsave Reagent, Calbiochem). Pictures were taken with a Zeiss LSM 510 META confocal microscope.

For evaluations of stainings, ImageJ and the particle counter plugin were used. Vessel number was determined by counting the number of vessels per mm². Vessel size was determined by evaluating the area covered by vessels divided by the number of vessels per μ m². For the quantification of smooth muscle cell coverage of vessels, tumor sections were stained for CD31 and α -smooth muscle cell actin (α -SMA). Vessels with and without α SMA-staining were counted.

Whole mount staining of embryonic skin and yolk sacs

Tissues were removed, fixed (formalin 4%, 30 min, RT), washed, blocked (1 h, RT, 0.5% TritonX, 2%

BSA/PBS), incubated with anti-CD31 primary antibodies (553370, BD Pharmingen) (o/n, 4°C), washed, incubated with AlexaFluor-labeled secondary antibodies (2 h, RT), and mounted. Numbers of branch points per field were calculated by using Image J and the particle counter plugin.

Tumor vessel perfusion

At day 15 after tumor cell inoculation, mice were intravenously injected (tail vein) with FITC-Lectin (150 μ g, 1 mg/ml, Sigma Aldrich). After circulation of FITC-Lectin for 5 min, mice were sacrificed and tumors were removed. Staining was performed according to the description under immunohistochemistry. Vessels with and without FITC-Lectin labeling were counted by using ImageJ and the particle counter plugin.

Cells

HUVECs were cultivated as described [32] with Endothelial Cell Growth Medium (ECGM, Promocell) containing 10% FCS. Embryonic blood vessel endothelial cells (BECs) and liver sinusoidal endothelial cells LSECs were isolated and cultivated as described [33]. For experiments with Dll4, plates were coated with Dll4 (5 μ g/ml; 1 h RT or o/n 4°C; human Dll4 for HUVECs and mouse Dll4 for mouse BECs, both R & D Systems 1506-D4 and 1389-D4). Plates were washed once with PBS before cells were plated. For proteasome inhibition experiments, MG132 (1 μ M, Enzo Life Sciences) stimulation was started 1 h before re-plating of HUVECs onto Dll4. HUVECs were plated onto Dll4 for 1 h or 24 h. BECs were plated onto Dll4 for 24 h.

For experiments with Jagged1, plates were coated with Jagged1 (10 μ g/ml; 1 h RT; R & D Systems 1277-JG). Plates were washed once with PBS before cells were plated. HUVECs were treated with roscovitine (10 μ M) or nt (non-targeting) or Cdk5 siRNA and plated onto Dll4 for 48 h.

Transfection of cells

HUVECs were transfected using Targefect (Targeting Systems; El Cajon, California) according to the manufacturer's protocol. DNA, Transfection Media, Targefect and Virofect Enhancer were mixed and incubated for 25 min. The transfection complex was added to the cells for 2 h. Fresh HUVEC medium was added to the cells for 24 h. NICD plasmid was from addgene (26892). The siRNAs were from Thermo Scientific/Dharmacon: nt siRNA D-001810-01; Cdk5 siRNA J-003239-09 and J-003239-10. For the experiments involving Cdk5 siRNA, a mix of both siRNAs was used.

Proliferation

HUVECs were transfected with nt or Cdk5 siRNA (Thermo Scientific). 24 h after transfection, cells (1500 cells per 96-well) were seeded onto PBS or Dll4 coated plates. Initial cell number was determined after 1 h. Proliferation was measured after 72 h via crystal violet staining.

Spheroids

HUVECs were transfected with nt or Cdk5 siRNA. Spheroids were generated via the hanging drop method as described [37]. Briefly, a suspension of HUVECs and 20% Methocel was mixed and 20 μ l drops were seeded onto a petri dish and incubated upside down over night. Spheroids were embedded into HUVEC growth medium containing 5% Minimal Essential Eagle's Medium (Sigma), 5% Bicarbonate, 60% collagen and Dll4 (5 μ g/ml). The collagen pellets were covered with ECGM containing 20% FCS. Pictures were taken on day 0, 1, 2 and 3. Sprout length and number of sprouts were determined.

For spheroid staining, embedded spheroids were fixed with 4% PFA, permeabilized with 0, 2% Triton X and blocked with 1% BSA in PBS for 3 days. Primary antibody (NICD 4147, Cell Signalling) was incubated for 3 days and secondary antibody (AlexaFluor 488, Life Technologies) for further 3 days. Nuclei were stained with Hoechst 33342 (0, 5 μ g/ml, 40 min, RT). Pictures were taken at the Leica SP8 SMD confocal microscope.

Immunoblotting

Immunoblotting was described previously [33]. The following primary antibodies were used: actin (MAB 150 1R, Chemicon), Cdk5 (AHZ0492, Life Technologies), NICD (4147 Cell Signalling), presenilin (5643, Cell Signaling).

RT-PCR

mRNA was isolated using the Qiagen RNeasy Mini Kit. For reverse transcription the High-Capacity cDNA Reverse Transcription Kit (Applied Biosystems) was used. RT-PCR was performed with the 7300 Real Time PCR System. The following Taqman gene expression assays were used: Cdk5 Hs00358991_g1 and Mm01134945_g1, Hey1 Hs00232618_m1 and Mm00468865_m1, Hey2 Hs00232622_m1 and Mm00469280_m1, NRARP Hs01104102_s1 and Mm00482529_s1, VE-cadherin Mm00486938_m1 (Applied Biosystems). GAPDH was used as housekeeper.

Statistics

All experiments were performed at least three times (biological replicates) Respective tests, *p*-values and exact numbers of independently performed experiments are indicated in the respective figure legends. Graph data represent means \pm SEM. Statistical analysis was performed using SigmaStat Version 3.1.

ACKNOWLEDGMENTS

We thank Paul Greengard (Rockefeller University) for providing the floxed Cdk5 mice. We thank Adrian Harris (Oxford University Department of Oncology, Weatherall Institute of Molecular Medicine, John Radcliffe Hospital, Oxford) for providing U87 glioblastoma cells. We thank Genentech for providing the anti-VEGF antibody B20-4.1.1. We thank Helene Maby-El Hajjami (University of Lausanne) for the LEC/BEC isolation protocol. We thank Kerstin Loske for mouse genotyping. The animal facility of the Department of Pharmacy, Ludwig-Maximilians-University Munich is gratefully acknowledged. This work was supported by German Research Foundation (ZA 186/4-1).

FUNDINGS

This work was supported by German Research Foundation (ZA 186/4-1). Siwei Zhang was supported by the LMU - China Scholarship Council.

CONFLICTS OF INTEREST

None.

REFERENCES

1. Ellis LM, Hicklin DJ. VEGF-targeted therapy: mechanisms of anti-tumour activity. *Nat Rev Cancer*. 2008; 8:579-591.
2. Bergers G, Hanahan D. Modes of resistance to anti-angiogenic therapy. *Nat Rev Cancer*. 2008; 8:592-603.
3. Hellstrom M, Phng LK, Hofmann JJ, Wallgard E, Coultas L, Lindblom P, Alva J, Nilsson AK, Karlsson L, Gaiano N, Yoon K, Rossant J, Iruela-Arispe ML, et al. Dll4 signalling through Notch1 regulates formation of tip cells during angiogenesis. *Nature*. 2007; 445:776-780.
4. Li JL, Sainson RC, Shi W, Leek R, Harrington LS, Preusser M, Biswas S, Turley H, Heikamp E, Hainfellner JA, Harris AL. Delta-like 4 Notch ligand regulates tumor angiogenesis, improves tumor vascular function, and promotes tumor growth *in vivo*. *Cancer Res*. 2007; 67:11244-11253.
5. Holopainen T, Bry M, Alitalo K, Saaristo A. Perspectives on lymphangiogenesis and angiogenesis in cancer. *J Surg Oncol*. 2011; 103:484-488.

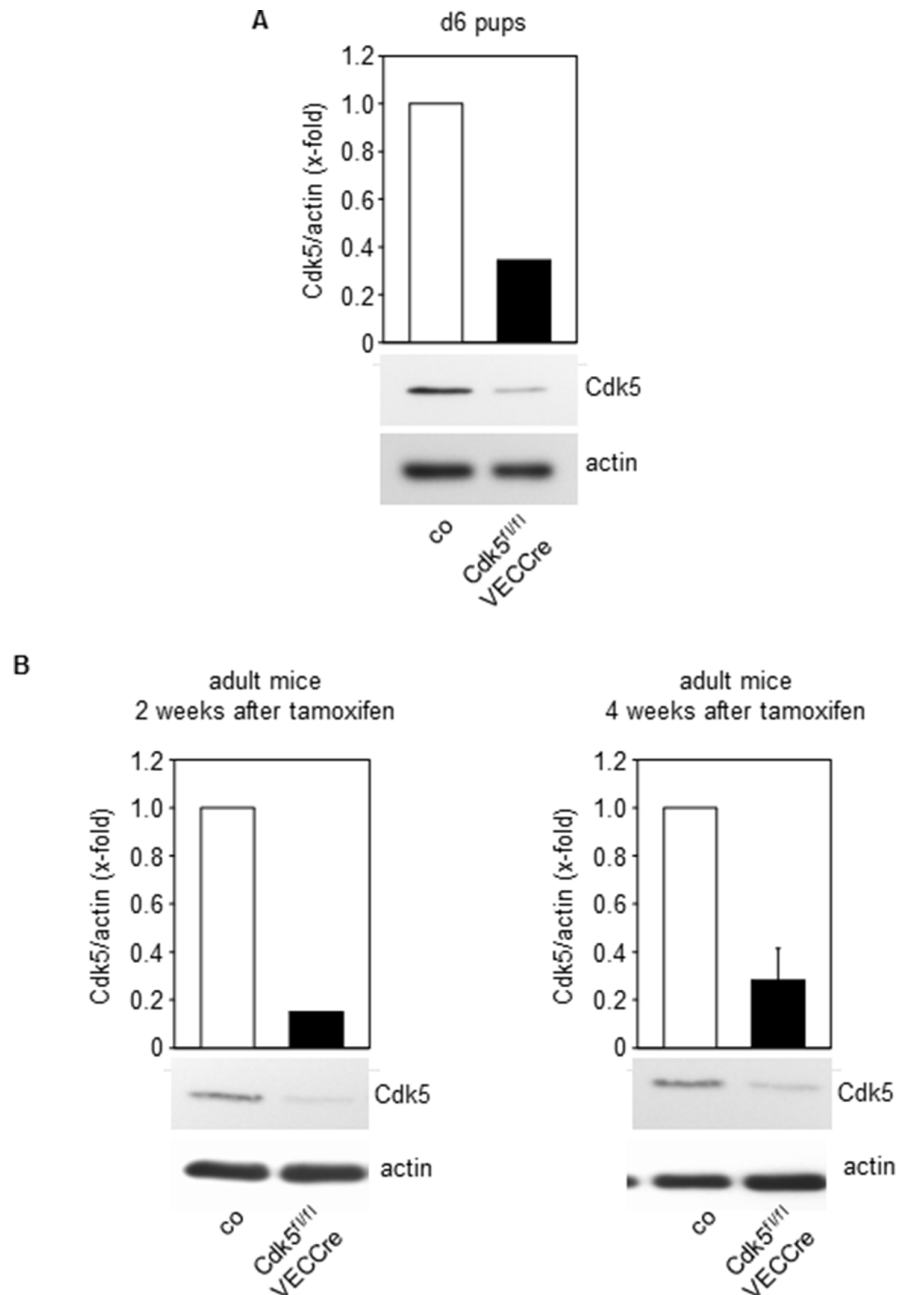
6. Noguera-Troise I, Daly C, Papadopoulos NJ, Coetzee S, Boland P, Gale NW, Lin HC, Yancopoulos GD, Thurston G. Blockade of Dll4 inhibits tumour growth by promoting non-productive angiogenesis. *Nature*. 2006; 444:1032–1037.
7. Ridgway J, Zhang G, Wu Y, Stawicki S, Liang WC, Chantry Y, Kowalski J, Watts RJ, Callahan C, Kasman I, Singh M, Chien M, Tan C, et al. Inhibition of Dll4 signalling inhibits tumour growth by deregulating angiogenesis. *Nature*. 2006; 444:1083–1087.
8. Hu W, Lu C, Dong HH, Huang J, Shen DY, Stone RL, Nick AM, Shahzad MM, Mora E, Jennings NB, Lee SJ, Roh JW, Matsuo K, et al. Biological roles of the Delta family Notch ligand Dll4 in tumor and endothelial cells in ovarian cancer. *Cancer Res*. 2011; 71:6030–6039.
9. Kuhnert F, Kirshner JR, Thurston G. Dll4-Notch signaling as a therapeutic target in tumor angiogenesis. *Vasc Cell*. 2011; 3:20.
10. Ranganathan P, Weaver KL, Capobianco AJ. Notch signalling in solid tumours: a little bit of everything but not all the time. *Nat Rev Cancer*. 2011; 11:338–351.
11. Dhavan R, Tsai LH. A decade of CDK5. *Nat Rev Mol Cell Biol*. 2001; 2:749–759.
12. Barnett DG, Bibb JA. The role of Cdk5 in cognition and neuropsychiatric and neurological pathology. *Brain Res Bull*. 2011; 85:9–13.
13. Cheung ZH, Ip NY. Cdk5: a multifaceted kinase in neurodegenerative diseases. *Trends Cell Biol*. 2012; 22:169–175.
14. Liebl J, Furst R, Vollmar AM, Zahler S. Twice switched at birth: cell cycle-independent roles of the “neuron-specific” cyclin-dependent kinase 5 (Cdk5) in non-neuronal cells. *Cell Signal*. 2011; 23:1698–1707.
15. Contreras-Vallejos E, Utreras E, Gonzalez-Billault C. Going out of the brain: non-nervous system physiological and pathological functions of Cdk5. *Cell Signal*. 2012; 24:44–52.
16. Rosales JL, Lee KY. Extraneuronal roles of cyclin-dependent kinase 5. *Bioessays*. 2006; 28:1023–1034.
17. Feldmann G, Mishra A, Hong SM, Bisht S, Strock CJ, Ball DW, Goggins M, Maitra A, Nelkin BD. Inhibiting the cyclin-dependent kinase CDK5 blocks pancreatic cancer formation and progression through the suppression of Ras-Ral signaling. *Cancer Res*. 2010; 70:4460–4469.
18. Feldmann G, Mishra A, Bisht S, Karikari C, Garrido-Laguna I, Rasheed Z, Ottenhof NA, Dadon T, Alvarez H, Fendrich V, Rajeshkumar NV, Matsui W, Brossart P, et al. Cyclin-dependent kinase inhibitor Dinaciclib (SCH727965) inhibits pancreatic cancer growth and progression in murine xenograft models. *Cancer Biol Ther*. 2011; 12:598–609.
19. Eggers JP, Grandgenett PM, Collisson EC, Lewallen ME, Tremayne J, Singh PK, Swanson BJ, Andersen JM, Caffrey TC, High RR, Ouellette M, Hollingsworth MA. Cyclin-dependent kinase 5 is amplified and overexpressed in pancreatic cancer and activated by mutant K-Ras. *Clin Cancer Res*. 2011; 17:6140–6150.
20. Strock CJ, Park JI, Nakakura EK, Bova GS, Isaacs JT, Ball DW, Nelkin BD. Cyclin-dependent kinase 5 activity controls cell motility and metastatic potential of prostate cancer cells. *Cancer Res*. 2006; 66:7509–7515.
21. Jin JK, Tien PC, Cheng CJ, Song JH, Huang C, Lin SH, Gallick GE. Talin1 phosphorylation activates beta1 integrins: a novel mechanism to promote prostate cancer bone metastasis. *Oncogene*. 2015; 34:1811–21.
22. Pozo K, Castro-Rivera E, Tan C, Plattner F, Schwach G, Siegl V, Meyer D, Guo A, Gundara J, Mettlach G, Richer E, Guevara JA, Ning L, et al. The role of Cdk5 in neuroendocrine thyroid cancer. *Cancer Cell*. 2013; 24:499–511.
23. Pozo K, Hillmann A, Augustyn A, Plattner F, Hai T, Singh T, Ramezani S, Sun X, Pfragner R, Minna JD, Cote GJ, Chen H, Bibb JA, et al. Differential expression of cell cycle regulators in CDK5-dependent medullary thyroid carcinoma tumorigenesis. *Oncotarget*. 2015; 6:12080–12093. doi: 10.18632/oncotarget.3813.
24. Liu R, Tian B, Gearing M, Hunter S, Ye K, Mao Z. Cdk5-mediated regulation of the PIKE-A-Akt pathway and glioblastoma cell invasion. *Proc Natl Acad Sci U S A*. 2008; 105:7570–7575.
25. Xie W, Wang H, He Y, Li D, Gong L, Zhang Y. CDK5 and its activator P35 in normal pituitary and in pituitary adenomas: relationship to VEGF expression. *International journal of biological sciences*. 2014; 10:192–199.
26. Liang Q, Li L, Zhang J, Lei Y, Wang L, Liu DX, Feng J, Hou P, Yao R, Zhang Y, Huang B, Lu J. CDK5 is essential for TGF-beta1-induced epithelial-mesenchymal transition and breast cancer progression. *Sci Rep*. 2013; 3:2932.
27. Demelash A, Rudrabhatla P, Pant HC, Wang X, Amin ND, McWhite CD, Naizhen X, Linnoila RI. Achaete-scute homologue-1 (ASH1) stimulates migration of lung cancer cells through Cdk5/p35 pathway. *Mol Biol Cell*. 2012; 23:2856–2866.
28. Chen XX, Xie FF, Zhu XJ, Lin F, Pan SS, Gong LH, Qiu JG, Zhang WJ, Jiang QW, Mei XL, Xue YQ, Qin WM, Shi Z, et al. Cyclin-dependent kinase inhibitor dinaciclib potently synergizes with cisplatin in preclinical models of ovarian cancer. *Oncotarget*. 2015. doi: 10.18632/oncotarget.3717.
29. Ehrlich SM, Liebl J, Ardelt MA, Lehr T, De Toni EN, Mayr D, Brandl L, Kirchner T, Zahler S, Gerbes AL, Vollmar AM. Targeting cyclin dependent kinase 5 in hepatocellular carcinoma - A novel therapeutic approach. *J Hepatol*. 2015; 63:102–13.
30. Liebl J, Krystof V, Vereb G, Takacs L, Strnad M, Pechan P, Havlicek L, Zatloukal M, Furst R, Vollmar AM, Zahler S. Anti-angiogenic effects of purine inhibitors of cyclin dependent kinases. *Angiogenesis*. 2011; 14:281–291.
31. Weitensteiner SB, Liebl J, Krystof V, Havlicek L, Gucky T, Strnad M, Furst R, Vollmar AM, Zahler S. Trisubstituted pyrazolopyrimidines as novel angiogenesis inhibitors. *PLoS One*. 2013; 8:e54607.

32. Liebl J, Weitensteiner SB, Vereb G, Takacs L, Furst R, Vollmar AM, Zahler S. Cyclin-dependent kinase 5 regulates endothelial cell migration and angiogenesis. *J Biol Chem.* 2010; 285:35932–35943.
33. Liebl J, Zhang S, Moser M, Agalarov Y, Demir CS, Hager B, Bibb JA, Adams RH, Kiefer F, Miura N, Petrova TV, Vollmar AM, Zahler S. Cdk5 controls lymphatic vessel development and function by phosphorylation of Foxc2. *Nat Commun.* 2015; 6:7274.
34. Wang Y, Nakayama M, Pitulescu ME, Schmidt TS, Bochenek ML, Sakakibara A, Adams S, Davy A, Deutsch U, Luthi U, Barberis A, Benjamin LE, Makinen T, et al. Ephrin-B2 controls VEGF-induced angiogenesis and lymphangiogenesis. *Nature.* 2010; 465:483–486.
35. Kopan R, Ilagan MX. The canonical Notch signaling pathway: unfolding the activation mechanism. *Cell.* 2009; 137:216–233.
36. Aberle H, Bauer A, Stappert J, Kispert A, Kemler R. beta-catenin is a target for the ubiquitin-proteasome pathway. *EMBO J.* 1997; 16:3797–3804.
37. Guarani V, Deflorian G, Franco CA, Kruger M, Phng LK, Bentley K, Toussaint L, Dequiedt F, Mostoslavsky R, Schmidt MH, Zimmermann B, Brandes RP, Mione M, et al. Acetylation-dependent regulation of endothelial Notch signalling by the SIRT1 deacetylase. *Nature.* 2011; 473:234–238.
38. Benedito R, Roca C, Sorensen I, Adams S, Gossler A, Fruttiger M, Adams RH. The notch ligands Dll4 and Jagged1 have opposing effects on angiogenesis. *Cell.* 2009; 137:1124–1135.
39. Bach S, Knockaert M, Reinhardt J, Lozach O, Schmitt S, Baratte B, Koken M, Coburn SP, Tang L, Jiang T, Liang DC, Galons H, Dierick JF, et al. Roscovitine targets, protein kinases and pyridoxal kinase. *J Biol Chem.* 2005; 280:31208–31219.
40. Gray N, Detivaud L, Doerig C, Meijer L. ATP-site directed inhibitors of cyclin-dependent kinases. *Current medicinal chemistry.* 1999; 6:859–875.
41. Delehouze C, Godl K, Loac N, Bruyere C, Desban N, Oumata N, Galons H, Roumeliotis TI, Giannopoulou EG, Grenet J, Twitchell D, Lahti J, Mouchet N, et al. CDK/CK1 inhibitors roscovitine and CR8 downregulate amplified MYCN in neuroblastoma cells. *Oncogene.* 2014; 33:5675–5687.
42. Nandhu MS, Hu B, Cole SE, Erdreich-Epstein A, Rodriguez-Gil DJ, Viapiano MS. Novel paracrine modulation of Notch-DLL4 signaling by fibulin-3 promotes angiogenesis in high-grade gliomas. *Cancer Res.* 2014; 74:5435–5448.
43. Bais C, Wu X, Yao J, Yang S, Crawford Y, McCutcheon K, Tan C, Kolumam G, Vernes JM, Eastham-Anderson J, Haughney P, Kowanetz M, Hagenbeek T, et al. PlGF blockade does not inhibit angiogenesis during primary tumor growth. *Cell.* 2010; 141:166–177.
44. Levitzki A. Tyrosine kinase inhibitors: views of selectivity, sensitivity, and clinical performance. *Annu Rev Pharmacol Toxicol.* 2013; 53:161–185.
45. Adams RH, Alitalo K. Molecular regulation of angiogenesis and lymphangiogenesis. *Nat Rev Mol Cell Biol.* 2007; 8:464–478.
46. Gacche RN, Meshram RJ. Angiogenic factors as potential drug target: efficacy and limitations of anti-angiogenic therapy. *Biochimica et biophysica acta.* 2014; 1846:161–179.
47. Bai B, Liang Y, Xu C, Lee MY, Xu A, Wu D, Vanhoutte PM, Wang Y. Cyclin-dependent kinase 5-mediated hyperphosphorylation of sirtuin-1 contributes to the development of endothelial senescence and atherosclerosis. *Circulation.* 2012; 126:729–740.
48. Slevin M, Krupinski J. Cyclin-dependent kinase-5 targeting for ischaemic stroke. *Curr Opin Pharmacol.* 2009; 9:119–124.
49. Cho DH, Seo J, Park JH, Jo C, Choi YJ, Soh JW, Jo I. Cyclin-dependent kinase 5 phosphorylates endothelial nitric oxide synthase at serine 116. *Hypertension.* 2010; 55:345–352.
50. Lee CH, Wei YW, Huang YT, Lin YT, Lee YC, Lee KH, Lu PJ. CDK5 phosphorylates eNOS at Ser-113 and regulates NO production. *J Cell Biochem.* 2010; 110:112–117.
51. Lau KF, Howlett DR, Kesavapany S, Standen CL, Dingwall C, McLoughlin DM, Miller CC. Cyclin-dependent kinase-5/p35 phosphorylates Presenilin 1 to regulate carboxy-terminal fragment stability. *Mol Cell Neurosci.* 2002; 20:13–20.
52. Kang M, Jiang B, Xu B, Lu W, Guo Q, Xie Q, Zhang B, Dong X, Chen D, Wu Y. Delta like ligand 4 induces impaired chemo-drug delivery and enhanced chemoresistance in pancreatic cancer. *Cancer Lett.* 2013; 330:11–21.
53. Jubb AM, Browning L, Campo L, Turley H, Steers G, Thurston G, Harris AL, Anson O. Expression of vascular Notch ligands Delta-like 4 and Jagged-1 in glioblastoma. *Histopathology.* 2012; 60:740–747.
54. Jubb AM, Soilleux EJ, Turley H, Steers G, Parker A, Low I, Blades J, Li JL, Allen P, Leek R, Noguera-Troise I, Gatter KC, Thurston G, et al. Expression of vascular notch ligand delta-like 4 and inflammatory markers in breast cancer. *Am J Pathol.* 2010; 176:2019–2028.
55. Zhu YX, Tiedemann R, Shi CX, Yin H, Schmidt JE, Bruins LA, Keats JJ, Braggio E, Sereduk C, Mousses S, Stewart AK. RNAi screen of the druggable genome identifies modulators of proteasome inhibitor sensitivity in myeloma including CDK5. *Blood.* 2011; 117:3847–3857.
56. Haider C, Grubinger M, Reznickova E, Weiss TS, Rotheneder H, Miklos W, Berger W, Jorda R, Zatloukal M, Gucky T, Strnad M, Krystof V, Mikulits W. Novel inhibitors of cyclin-dependent kinases combat hepatocellular carcinoma without inducing chemoresistance. *Mol Cancer Ther.* 2013; 12:1947–1957.
57. Hawasli AH, Benavides DR, Nguyen C, Kansy JW, Hayashi K, Chambon P, Greengard P, Powell CM, Cooper DC, Bibb JA. Cyclin-dependent kinase 5 governs learning and

- synaptic plasticity via control of NMDAR degradation. *Nat Neurosci.* 2007; 10:880–886.
58. Beal S, Sheiner, L.B., Boeckmann, A., & Bauer, R.J. *NONMEM User's Guides.* (1989–2009). Icon Development Solutions, Ellicott City, MD, USA,. 2009.
59. Pitulescu ME, Schmidt I, Benedito R, Adams RH. Inducible gene targeting in the neonatal vasculature and analysis of retinal angiogenesis in mice. *Nat Protoc.* 2010; 5:1518–1534.

Inhibition of endothelial Cdk5 reduces tumor growth by promoting non-productive angiogenesis

Supplementary Materials



Supplementary Figure S1: Cdk5 Knockdown in inducible Cdk5^{fl/fl}VECCre mice. (A) Immunoblots and quantitative evaluation of liver sinusoidal endothelial cells (LSECs) of d6 pups with control and Cdk5^{fl/fl}VECCre genotype that were injected with tamoxifen (50 μ g / day i.p.) from day 1 to day 3 for Cdk5 and actin (loading control) is shown (B) Western blots and quantitative evaluations of liver sinusoidal endothelial cells (LSECs) of adult mice with control and Cdk5^{fl/fl}VECCre genotype that were injected with tamoxifen (0.5 mg / day i.p.) for five consecutive days two weeks and four weeks after tamoxifen injection for Cdk5 and actin (loading control) are shown.

6.4 Danksagung

Mein allergrößter Dank geht an Frau Prof. Dr. Vollmar. Durch die Möglichkeit an zwei interessanten und herausfordernden Projekten promovieren zu dürfen, habe ich sehr viel gelernt. Ihre große Begeisterung für die Naturwissenschaft und Ihr stetig wähernder Enthusiasmus haben mich stets beeindruckt und motiviert. Sie sind für mich ein Vorbild sowohl in fachlichen wie auch persönlichen Belangen.

Zudem möchte ich Herrn Prof. Dr. Zahler für die kritischen und konstruktiven Diskussionen danken. Vielen Dank dafür, dass Sie sich immer mit viel Mühe und Muße um jegliche analytische Probleme gekümmert haben. Danke auch, dass Sie sich meiner Doktorarbeit als Zweitprüfer angenommen haben.

Herrn Prof. Dr. Wahl-Schott und Herrn Prof. Dr. Wagner danke ich dafür, dass sie sich mit meiner Arbeit als Dritt- und Viertprüfer auseinander gesetzt haben. Auch Herrn Prof. Dr. Bracher und Herrn PD Dr. Michalakis und möchte ich als Fünft- und Sechstprüfer für ihr Interesse an meiner Arbeit danken.

Liebe Hanna, an dich geht ein ganz besonderes Dankeschön! Vielen Dank für die hervorragende Betreuung in den letzten Jahren. Deine Tür stand immer offen, sowohl für wissenschaftliche Diskussionen vermeintlich unlösbarer Probleme aber auch für persönliche Gespräche.

Es ist nicht selbstverständlich, dass man mit so vielen netten Kollegen und in einer so guten Atmosphäre arbeiten darf. Ich bin stets gerne in die Uni gekommen wodurch die letzten Jahre wie im Flug vergingen. Vielen Dank an die ehemaligen und aktuellen Mitglieder des AK Vollmar.